DEVELOPMENT AND VERIFICATION OF A CENTRIFUGAL COMPRESSOR TEST BENCH FOR MICRO GAS TURBINES (MGTs)

by
Muaz Ahmad Jan

Thesis presented in partial fulfilment of the requirements for the degree of Master of Engineering (Mechanical) in the Faculty of Engineering at Stellenbosch University

Supervisor: Prof. S.J. van der Spuy

March 2020

Declaration

By submitting this thesis electronically, I declare that the entirety of the work contained therein is my own, original work, that I am the sole author thereof (save to the extent explicitly otherwise stated), that reproduction and publication thereof by Stellenbosch University will not infringe any third party rights and that I have not previously in its entirety or in part submitted it for obtaining any qualification.

Date: March 2020

Abstract

Development and Verification of a Centrifugal Compressor Test Bench for Micro Gas Turbines (MGTs)

M.A. Jan

Department of Mechanical and Mechatronic Engineering,
University of Stellenbosch,
Private Bag X1, Matieland 7602, South Africa.

Thesis: M. Eng. (Mech)

March 2020

In recent times the demand for Micro Gas Turbines (MGTs) with power levels below 10 kW has increased. Despite MGTs being a potential replacement of internal combustion (IC) engines, they are prone to aerodynamic and machine design problems. To address the design problems there has been a considerable amount of research dedicated to the development of centrifugal compressors stages for MGT applications. This project sets out to develop and verify a centrifugal compressor test bench in order to characterize new designs of centrifugal compressors.

A fully automated test bench was designed and commissioned which used a complete turbocharger unit to drive the compressor. The turbocharger turbine was driven by supplying compressed air at ambient temperature. The test bench was equipped with the necessary instrumentation which were required to obtain performance test measurements. The experimental data was then processed to evaluate the total to static (t-s) pressure ratio, and total to total (t-t) temperature ratio and the efficiency of the compressor. Numerous successful tests were conducted at speeds of 60 000, 80 000, and 100 000 rpm and shown to be repeatable.

A 1D flow analysis was performed with the help of the Flownex® Simulation Environment (SE) in order to simulate the centrifugal compressor test bench. The results from the simulations correlated well with the experimental results, with a difference of between 0 to 6 % for the mass flow rates and 0 to 6.5 % for the turbine inlet pressure. This model will assist in designing further modifications that may be implemented on the test bench. Such a modification may include the installation of a heating system in order to increase the energy content of the air that is used to drive the turbine.

Uittreksel

Ontwikkeling en Verifikasie van ’n Sentrifugaal Kompressor Toetsbank vir Mikrogasturbines (MGTs)

M.A. Jan

Departement Meganiese en Megatroniese Ingenieurswese,
Universiteit van Stellenbosch,
Privaatsak X1, Matieland 7602, Suid Afrika.

Tesis: M. Ing. (Meg)

Maart 2020

Die aanvraag na mikrogasturbines (MGTs) met drywingsvlakke onder 10 kW, vir beide burgerlike en militêre toepassings, het onlangs toegeneem. MGTs het die potensiaal om binnebrandenjins te vervang, maar is geneig tot aërodinamiese en masjienontwerps probleme. Om die ontwerps probleme aan te spreek, is daar ‘n aansienlike hoeveelheid navorsing gewy aan die ontwikkeling van sentrifugaal kompressor stadiums vir MGT toepassings. Die doel van hierdie tesis is om ’n sentrifugaal kompressor toetsbank te ontwikkel en verifieër vir die karakterisering van nuwe sentrifugaal kompressors.

’n Volledige outomatiese toetsbank was ontwerp en in gebruik geneem. Die toetsbank maak gebruik van ’n volledige turboaanjaer eenheid om die kompressor aan te dryf. Die turboaanjaer word gedryf deur saamgeperste lug wat verskaf word teen omgewingstemperatuur. Die toetsbank is toegerus met die nodige instrumentasie wat vereis word om die prestasietoetsmetings uit te voer. Die eksperimentele data is verwerk om die totale tot statiese (t-s) drukverhouding, totale tot totale (t-t) temperatuurverhouding en die benuttingsgraad van die kompressor te verkry. Talle suksesvolle en herhaalbare toetse was uitgevoer teen omwentelingsnelhede van 60 000, 80 000 en 100 000 opm.

’n 1D Vloeianalise, wat gebruik maak van die Flownex® Simulasie-omgewing (SE), is uitgevoer om die sentrifugaal kompressor toetsbank te simuleer. Die resultate van die simulasies het goed ooreen gestem met die eksperimentele resultate. Die verskil in massavloeitempo en die turbine-inlaatdruk was 0 tot 6 % en 0 tot 6.5 %, onderskeidelik. Die model kan dus gebruik word om toekomstige verbeterings vir die toetsbank te ontwerp en te implementer. Een so ’n moontlikheid kan die installasie van ’n verhitting stelsel wees wat die energieinhoud van die lug wat die turbine aan dryf verhoog.

Acknowledgements

I would like to extend and express my profound gratitude to the following:

- I give thanks to Allah Almighty, who has been my strength pillar and guidance throughout the duration of my thesis.
- To my parents who supported me emotionally, financially and supported me throughout this journey. I will forever be grateful for their love and support.
- To my supervisor Prof. S.J van der Spuy for his endless support, guidance and uplifting spirit that kept me persevering in order to complete my thesis.
- To CSIR for providing the funding for past three years.
- To the Mechanical and Mechatronic engineering department for providing the funding for the project.
- To all personnel from the Mechanical and Mechatronic workshop who helped and assisted me in manufacturing and the assembling of the test bench.
- To the supporting staff of Flownex® especially Ms. Nicole Leeb for her endless support regarding the simulation of the test bench.
- To the sales and technical staff of SAMSON to provide assistance and service regarding the commissioning of the control valve.
- Lastly, I'd like to extend gratitude to the following friends: Ms. Humaira Fataar, Mr. Brian Ssebabi, and Mr. Ziyauddin Panchbhaya for their assistance and input.

Dedications

To my mom and dad…

Table of Contents

List of Figures

List of Tables

Nomenclature

Symbols

A	Area	$[\mathrm{m}^2]$
A_c	Cross section area	$[\mathrm{m}^2]$
b	Blade height	[mm]
C_d	Coefficient of discharge	$[-]$
c_p	Specific heat	$[\mathrm{J/kg \cdot K}]$
c	Absolute velocity	[m/s]
D	Inner diameter of pipe	[m]
d	Throat diameter	[m]
Δp	Change in pressure	[Pa]
E	Longitudinal joint factor	$[-]$
F	Fluctuation of measured quantity	$[-]$
	Design factor	$[-]$
h	Enthalpy	[J/kg]
K	Dynamic correction factor	$[-]$
K_v	Valve coefficient	$[\mathrm{m}^3/\sqrt{\mathrm{bar}}\,.\,\mathrm{h}\,]$
L	Length	[m]
$\dot{m}$	Mass flow rate	[kg/s]
M	Molar mass	[kg/mol]
	Number of data sets	$[-]$
Ma	Mach number	$[-]$
N	Number of samples	$[-]$
	Rotational Speed	[rpm]
p	Pressure	[Pa]
Q	Volume Flowrate	$[\mathrm{m}^3/\mathrm{s}]$
R	Gas constant	$[\mathrm{J/kg \cdot K}]$

Re_D	Reynolds number	$[-]$
r	Radius	$[\mathrm{mm}]$
S	Specific minimum yield strength	$[\mathrm{MPa}]$
$\langle S_{\bar{x}} \rangle$	Pooled standard deviation of the means	$[-]$
T	Temperature	$[\mathrm{K}]$
	Temperature de-rating factor	$[-]$
t	Thickness	$[\mathrm{mm}]$
U	Tangential velocity	$[\mathrm{m/s}]$
V	Velocity	$[\mathrm{m/s}]$
	Voltage input	$[\mathrm{V}]$
w	Relative velocity	$[\mathrm{m/s}]$
x	Measured quantity	$[-]$
x'	True mean value	$[-]$
$\bar{x}$	Mean of the samples	$[-]$
y	Throttling valve opening percentage	$[\%]$

Greek Symbols

α	Flow coefficient	$[\mathrm{m}^2]$
β	Relative flow angle	$[\mathrm{m}^2]$
	Diameter ratio	$[-]$
γ	Specific heat ratio	$[-]$
ϵ	Expansion factor	$[-]$
η	Efficiency	$[-]$
μ	Dynamic viscosity	$[\mathrm{kg/m \cdot s}]$
ν	Kinematic viscosity	$[\mathrm{m}^2/\mathrm{s}]$
ρ	Density	$[\mathrm{kg/m}^3]$
σ	Slip factor	$[-]$
ω	Rotational speed	$[\mathrm{rad/s}]$

Π	Pressure ratio	$[-]$

Subscripts

0	Compressor inlet
1	Impeller outlet
2	Diffuser outlet
3	Compressor outlet
amb	Ambient condition
bm	Bellmouth
c	Compressor
op	Orifice plate
t	Turbine
$t-t$	Total-to-total
$t-s$	Total-to-static
s	Static thermodynamic condition

Superscripts

$'$	Blade angle
$-$	Mean value
$\cdot$	Time rate of change

Acronyms

AC	Alternating Current
AMB	Active Magnetic Bearing
ASME	American Society of Mechanical Engineers
ASTM	American Society for Testing and Materials
BMT	Baird Micro Turbine
BS	British Standard

CSIR	Council for Scientific and Industrial Research
CV	Control Valve
DAQ	Data Acquisition
DC	Direct Current
IC	Internal Combustion
KT	Kanontonnel
MGT	Micro Gas Turbine
PTC	Performance Test Code
SEP	Standard Engineering Practice
UAV	Unmanned Aerial Vehicle

1 Introduction

1.1 Background

In recent times, the demand for micro gas turbines (MGTs) with a power output level below 10 kW has increased in both civilian and military applications (Aus der Wiesche, 2012). Its high energy density potential and extensive power range make it suitable for a variety of applications in power generation, automotive and aerospace industry (van den Braembussche, 2005; Jain *et al.*, 2015; Pilavachi, 2002). A notable application for the MGT is its use for the propulsion of unmanned aerial vehicles (UAVs) due to its high thrust-to-weight ratio (Benini & Giacometti, 2007).

In the last decade, Stellenbosch University has dedicated numerous research projects to the development of centrifugal compressor stages for MGTs. In order to complete the development process, the experimental validation of the newly developed compressor stages is required. The Department of Mechanical and Mechatronic Engineering has a simple test bench designed by Struwig (2014) which has been used for the experimental validation. However, this test bench has few limitations which are discussed in Section 1.2. This project is set out to develop and verify a centrifugal compressor test bench which can be used to characterize newly developed components by generating compressor maps. It must be noted that the new test bench will use the test bench designed by Struwig (2014) as a baseline.

1.2 Motivation

Literature suggests that the gas turbine for which the power output ranges from 15 kW to 300 kW is considered “micro” (Antônio *et al.*, 2014; Jain *et al.*, 2015). Despite MGTs being a potential replacement of IC engines, they are known to pose aerodynamic and machine design challenges. These challenges are inherent in the scaling down of gas turbine engines which results in poor performance of the MGTs. According to van den Braembussche (2005), the main factors contributing to the poor performance of MGTs are:

- The large change in the engine's characteristic Reynolds number.
- Significant heat transfer between hot and cold components, which is negligible in large machines.
- Geometrical restrictions related to material and manufacturing of small gas turbine components.

1.2.1 Reynolds Number

The ratio between the inertial and viscous forces in a flow field is represented by its characteristic Reynolds number (Dixon & Hall, 2014). It is a key parameter when considering the effects of scaling on a micro engine. Since Reynolds number scales linearly with the length scale of the turbine (for the same fluid properties), it is significantly lower in magnitude for a MGT, when compared to a conventional engine. At a low Reynolds number, the behaviour of the boundary layers on the surfaces of the turbomachines have a significant effect on the efficiency of the engine (Simon & Jiang, 2003). Under these conditions, the flow is more prone to separation which results in higher coefficients of friction which can lead to significant losses and lower efficiencies.

1.2.2 Heat Transfer

In small turbomachines, internal heat transfer has a significant impact on their performance (Van den Braembussche, 2005). The surface-to-volume ratio inherently increases when reducing the size of the machine, which results in higher heat transfer between hot and cold components. This is usually negligible in large machines. However, thermal losses encountered in micro turbomachines make the use of insulation between hot and cold components essential.

1.2.3 Geometrical Restrictions

Geometrical scaling results in a larger relative tip clearance for the micro turbomachines which results in greater losses. According to van den Braembussche (2005), exact geometrical scaling is not always possible because of its associated

limitations. For example, scaling the blade thickness proportional to the impeller diameter will lead to thin blades which are prone to mechanical failure. Furthermore, it is difficult to achieve similar tolerance and smoothness on the blades of small turbomachines, compared to large turbomachines. For this purpose, advanced manufacturing techniques have to be exploited, which are proven to be costly.

To tackle some of the issues mentioned above and improving the overall efficiency of the MGTs several research projects have been initiated at Stellenbosch University. Van der Merwe (2012) designed the impeller of a centrifugal compressor using a mean-line calculation code in order to deliver a specific level of performance. Krige's (2013) research project included the design of a radial diffuser which was then assembled on to the Baird Micro Turbine (BMT 120 KS) and tested. Diener (2016) designed a mixed-flow compressor impeller for a MGT that was specified to deliver 600 N thrust. This was followed by the design of a cross-over diffuser for a mixed flow compressor impeller (Kock, 2017).

Figure 1.1: Centrifugal compressor test bench

The aforementioned research requires a centrifugal compressor test bench on which these designs can be tested. Previously, a test bench (Figure 1.1) was designed by Struwig (2014) which was utilized by numerous researchers including Swanepoel (2018), who tested the mixed flow compressor impeller and cross-over diffuser. The test bench was located in the Gas Dynamics Laboratory of the Department of Mechanical and Mechatronic Engineering which houses several other experimental setups. The location of the test bench within the proximity of other experimental test stands, limits the extent to which compressors can be tested, mainly due to safety concerns. These limitations include:

- The laboratory where the test bench is located is over-crowded with various test setups.
- The speed control of the test bench is not equipped with a feedback control which increases the difficulty of the operation of the test bench.
- The mass flow rate of the compressor is manually controlled which makes it difficult to achieve repeatable results.
- The operator is not provided with a safe space from which to operate the experiments.
- The laboratory has inadequate ventilation which is not suitable for high-temperature exhaust.

By addressing these limitations and safety concerns, the current test setup can be utilized for a variety of experiments. It is currently used only for the testing of compressors. It can however be expanded in future to test combustors or both compressors and combustors in conjunction. This will increase the range of compressors that can be tested.

1.3 Objectives

The objective of this project is to design and build a centrifugal compressor test bench. The setup must be capable of accurately measuring the performance of centrifugal compressors. Secondary objectives are as follows:

- Perform a theoretical analysis of the test facility.
- Design and build a compressor test bench.
    - Install the necessary equipment and controls to make it fully automated.
    - Install suitable instrumentation and a data acquisition system to acquire measurements.
    - Characterize any auxiliary systems or components that will be used in the test bench, i.e. high-pressure air supply.
    - Formulate a suitable test procedure which ensures the safety of the operator.
- Evaluate the performance of the test rig. The evaluation will consider the modularity, durability, stability, and repeatability of the measurements, and safety of operation.
- Validate the operation of the test bench by performing a one-dimensional (1D) flow analysis on the test bench with the help of Flownex® Simulation Environment software.
    - The model must represent the actual test bench with its true dimension.
    - The operation of the model must be similar to the actual test bench.

2 Literature Study

This chapter discusses the operation of centrifugal compressors in order to gain a better understanding of their performance and operating principles. An overview of academic research projects which were undertaken to investigate the performance of centrifugal compressors is presented. Furthermore, the test facilities used for these projects are discussed in this chapter.

2.1 Centrifugal Compressor

A brief description of the centrifugal compressor's operation is given in this section with reference to Dixon & Hall (2014), Aungier (2000), and Whitfield & Baines (1990). Turbomachines such as fans, pumps, and compressors increase the pressure of working fluids. Compressors and fans are used to increase the pressure of flowing gas, whereas pumps increase the pressure of flowing liquids. The pressure increase in the gas caused by fans is usually so small that the gas is considered incompressible. In contrast, a compressor is a pressure-increasing machine where the density ratio across it is ≥ 1.05 i.e. the gas is compressible (Dixon & Hall, 2014).

2.1.1 Operation of a Centrifugal Compressor

A centrifugal compressor in its most basic form consists of a stationary volute shaped casing, which encapsulates a rotating impeller, followed by a diffuser (Figure 2.1). The air enters the impeller through the eye and the rotating impeller imparts energy into the fluid. The diffuser then converts that kinetic energy into pressure energy. The diffusion process can be assisted by the addition of stationary vanes, in which case it is known as a vanned diffuser. Lastly, the volute collects and transfers the fluid to the exit cone. In MGT applications, the volute is replaced by a radial-to-axial bend, followed by a set of de-swirler vanes that prepare the fluid for the downstream combustor.

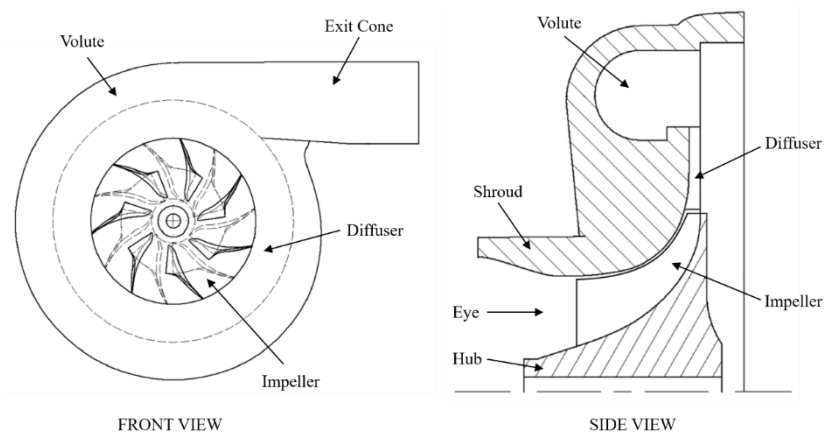

Figure 2.1: Front and side view of a single-stage compressor (adapted from Aungier (2000))

The flow through a centrifugal compressor is described with the help of the inlet and outlet velocity vector diagrams shown in Figure 2.2. Assuming no pre-whirl is applied, the air is drawn into the eye of the impeller in an axial direction with an absolute velocity of c_1. The flow encounters the impeller rotating with a tangential velocity U_1. Consequently, at the entry to the impeller, the flow has a relative velocity w_1 at a relative flow angle β_1. The fluid then advances into the inducer section where energy is transmitted to the fluid. The rotating impeller increases the angular momentum of the fluid by whirling it outwards, thereby increasing its energy level. Both the static pressure and velocity of the air increases as the fluid moves from the radius r_1 to r_2. The fluid then exits the impeller with an absolute velocity of c_2.

The relative flow leaving the impeller is not perfectly guided by the finite number of vanes, therefore, it does not exit the impeller with the same angle as outlet blade angle. This effect is known as slip, which results in the reduction of the tangential component of absolute velocity $c_{\theta 2}$. To account for the actual relative flow leaving the impeller, a slip factor (σ) is introduced. The slip factor is a measure of the fluid slip in the impeller of a compressor. The actual tangential velocity can now be defined as $c_{\theta 2} = \sigma c'_{\theta 2}$, where $c'_{\theta 2}$ is the hypothetical tangential velocity. The slip factor can be reduced by

increasing the number of vanes, which results in an increase in the solidity of the impeller eye i.e. a decrease in the effective flow area (Saravanamuttoo *et al.*, 2017). In the case of radial impellers, the hypothetical tangential velocity $c'_{\theta 2}$ is equal to the absolute blade tip velocity U_2 due to the fact that the relative velocity w_2 is at an angle β_2. Traditionally, high-speed impellers are designed with radial blades that have an outlet blade angle of zero. In modern designs, the blades at the exit are typically backswept by -30° to -40° (Japikse & Baines, 1994).

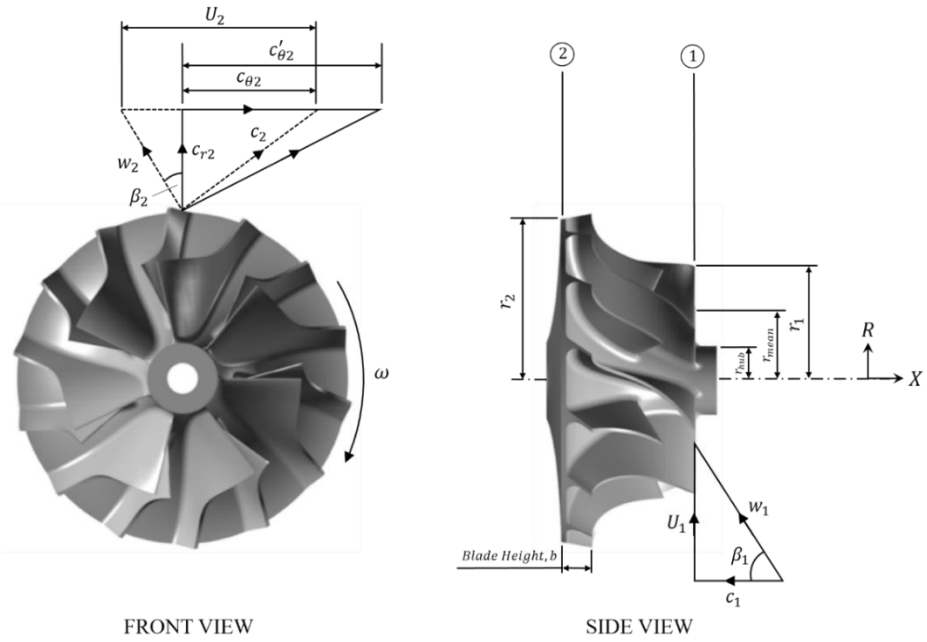

Figure 2.2: Velocity vector diagram of a centrifugal compressor

After exiting the impeller, the air enters the vaned and/or vaneless diffuser where the kinetic energy of the fluid is converted into pressure energy. This is where the remainder of the static pressure rise is obtained by reducing the velocity of the air. Compressors are usually designed in a manner that about half of the pressure rise occurs in the impeller and half in the diffuser (Saravanamuttoo *et al.*, 2017). The fluid then enters the volute, which collects and transfers the air to the downstream pipe via an exit cone.

2.1.2 Performance of a Centrifugal Compressor

The thermodynamic properties of the working fluid best describe the performance of the centrifugal compressor. Thermodynamic analysis can be done by tracing the compression cycle on the Mollier (h-s) diagram (Figure 2.3). The analysis starts with the use of Euler's turbomachinery equation (Equation 2.1) which is derived from the conservation of angular momentum and the first law of thermodynamics, with the assumption that the flow is steady and adiabatic.

$$\Delta W_c = h_{t2} - h_{t1} = U_2 c_{\theta 2} - U_1 c_{\theta 1} \Rightarrow \Delta h_t = \Delta(U c_\theta) \tag{2.1}$$

For the analysis, it is further assumed that the air enters the impeller eye in the axial direction. Hence, initially, the air has zero angular momentum. At the inlet of the compressor, the air is at atmospheric conditions with a total enthalpy of,

$$h_{t0} = h_{s0} + \frac{{c_0}^2}{2} \tag{2.2}$$

where h_{s0} is the static enthalpy and c_0 the absolute inlet velocity.

Upon entrance to the leading edge of the impeller, the air is accelerated from c_0 to c_1, which results in a drop of static pressure from p_{t0} to p_{s1}. Since no shaft work is done at this point Equation 2.1 implies that $h_{t0} = h_{t1}$,

$$h_{s0} + \frac{{c_0}^2}{2} = h_{s1} + \frac{{c_1}^2}{2} \tag{2.3}$$

The impeller does work on the flow going through it, which results in a rise of static pressure and temperature. The rise in static conditions is due to the conservation of rothalpy across the impeller. Rothalpy is defined as an invariant property that is obtained when the Euler turbomachinery equation is applied along a streamline (Japikse & Baines, 1994) and is given by Equation 2.4.

$$I = h_{0,rel} - \frac{1}{2}U^2 \tag{2.4}$$

where $h_{0,rel}$ is relative stagnation enthalpy and it is defined as

$$h_{0,rel} = h + \frac{1}{2}w^2 \tag{2.5}$$

Conservation of rothalpy implies that $I_1 = I_2$ therefore,

$$h_{s2} - h_{s1} = \frac{1}{2}\left({U_2}^2 - {U_1}^2\right) + \frac{1}{2}\left({w_2}^2 - {w_1}^2\right) \tag{2.6}$$

It follows from Equation 2.1 that the specific work done on the fluid is equal to the rise in stagnation enthalpy. With the assumption of zero angular momentum $c_{\theta 1} = 0$, Equation 2.1 reduces to,

$$\Delta W_c = U_2 c_{\theta 2} \tag{2.7}$$

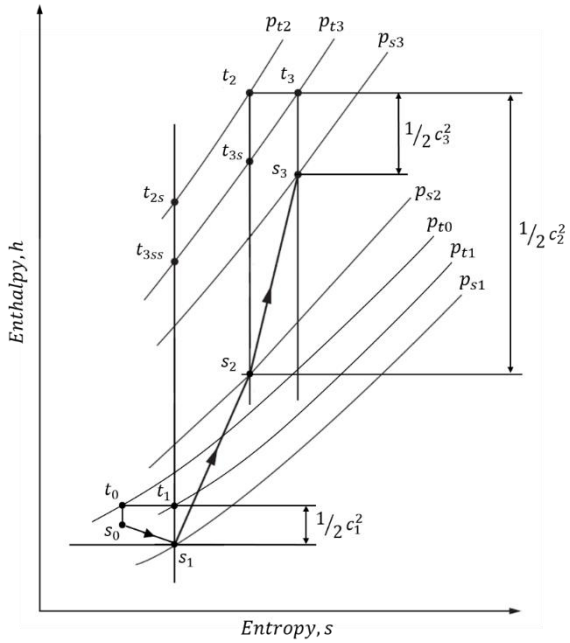

Figure 2.3: Mollier diagram for compressor stage (Dixon & Hall, 2014)

As fluid flows through the diffuser its velocity decreases from c_2 to c_3 which in turn increases the static pressure from p_{s2} to p_{s3}. This reduction in velocity is due to the increase in radius and cross-sectional area. Inside the diffuser, there is no work done on the fluid which implies that the stagnation enthalpy remains constant, $h_{t2} = h_{t3}$. However, it must be noted that the process is irreversible due to friction, with a total pressure loss from p_{t2} to p_{t3}.

The performance of the compressor can be defined in terms of the total-to-total pressure ratio (Π_{t-t}) and the isentropic efficiency (η_{t-t}) using the aforementioned thermodynamic quantities. The total-to-total isentropic efficiency of the compressor is defined as the ratio of change in isentropic enthalpy ($h_{t3ss} - h_{t1}$) to the actual change in enthalpy ($h_{t3} - h_{t1}$). It can be simplified to,

$$\eta_{t-t} = \frac{h_{t3ss} - h_{t1}}{h_{t3} - h_{t1}} = \frac{c_p T_{t1}\left[\left({}^{T_{t3ss}}/_{T_{t1}}\right) - 1\right]}{U_2\, c_{\theta 2}} \tag{2.8}$$

Using the isentropic relationship, the pressure ratio across the compressor is,

$$\frac{p_{t3}}{p_{t1}} = \left(\frac{T_{t3ss}}{T_{t1}}\right)^{\frac{\gamma}{\gamma-1}} \tag{2.9}$$

Rearranging Equation 2.9 and substituting into Equation 2.8 results in the total-to-total pressure ratio

$$\Pi_{t-t} = \left[1 + \frac{\eta_{t-t} U_2 c_{\theta 2}}{c_p T_{t1}}\right]^{\frac{\gamma}{\gamma-1}} \tag{2.10}$$

The performance of the compressor cannot simply be presented by plotting curves of the delivery pressure and temperature versus mass flow for various rotational speeds. These characteristics depend on variables such as the entry pressure and temperature conditions and the physical properties of the working fluid. Therefore, the performance of the compressor is described in terms of the following parameters:

- Corrected mass flow, $\dot{m}\sqrt{T_{t1}}/p_{t1}$
- Corrected rotational speed, $N/\sqrt{T_{t1}}$
- Total-to-total pressure ratio, Π_{t-t}
- Total-to-total isentropic efficiency, η_{t-t}

The corrected mass flow and rotational speed are normalized to the ambient pressure and temperature using dimensional analysis. Generally, total-to-total isentropic efficiency and pressure ratio is plotted versus corrected mass flow on a fixed corrected

speed line. These curves are commonly known as the compressor performance map or characteristic curves (Figure 2.4).

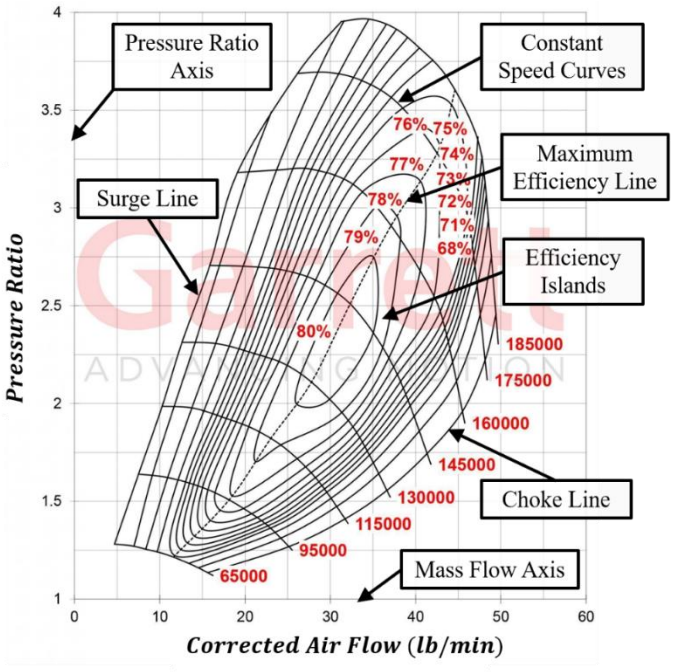

Figure 2.4: Performance map of a turbocharger compressor (Garrett, 2019)

2.1.3 Phenomena Associated with a Compressor

Surge is likely to occur when the mass flow is reduced while maintaining a constant rotational speed. This phenomenon is described with the aid of a theoretical characteristic of the centrifugal compressor shown in Figure 2.5. Suppose that the compressor is operating at point D which has a positive slope. A decrease in mass flow will cause a drop in the delivery pressure. If the air pressure further downstream of the compressor does not drop quickly enough, the air will flow back in the direction of the resultant pressure gradient towards the compressor outlet (Saravanamuttoo *et al.*, 2017). This causes the pressure ratio to drop quickly. In the meantime, the pressure further downstream of the compressor also drops. This allows the compressors to pick up again and repeat the cycle of events at a high frequency.

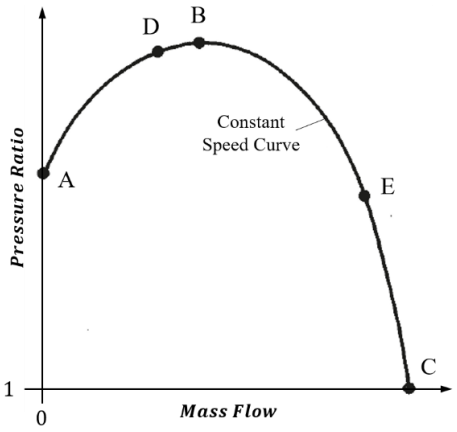

Figure 2.5: Theoretical characteristic (Saravanamuttoo *et al.*, 2017)

It must be noted that the surge does not immediately occur when the operating point is moved to the left of B. However, the operating points between A and B are inherently unstable. Surge is often preceded by an aerodynamic effect known as rotating stall which occurs because of non-uniformity in the flow or geometry of channels between the vanes and blades (Saravanamuttoo *et al.*, 2017). Surge is associated with a sudden drop in delivery pressure, extreme aerodynamic pulsation, mechanical vibration, and an increase in noise levels.

Prolonged operation in the surge region can lead to catastrophic mechanical failure. All compressor performance maps (Figure 2.4) have a feature known as a surge line, which limits the stable operation. Compressor turndown and surge margin are the two methods provided by Brun & Nored (2006) to determine the safe operating range for a compressor. The allowable operating range in terms of flow rate (Q) is known as turndown of a centrifugal compressor. It ranges between the design point and the surge line at any given speed for a fixed pressure ratio. The turndown (TD) can be determined using Equation 2.11.

$$TD\% = 100 \times \left| \frac{Q_{design} - Q_{surge}}{Q_{design}} \right|_{Head=Constant} \tag{2.11}$$

The surge margin (SM) indicates how close the compressor design point is to surge at a fixed speed, and is determined by Equation 2.12.

$$SM\% = 100 \times \left| \frac{Q_{design} - Q_{surge}}{Q_{design}} \right|_{Speed=Constant} \quad (2.12)$$

Another phenomenon linked to the centrifugal compressor is known as choking, which usually occurs either at the inlet, inside the impeller, or inside the diffuser. This occurs when the local velocity inside the compressor reaches sonic conditions (Ma = 1) (Saravanamuttoo *et al.*, 2017). This implies that the mass flow cannot be increased further either by reducing the backpressure.

2.2 Centrifugal Compressor Test Facilities

Numerous centrifugal compressor test benches were investigated. It was observed that the method used to drive a centrifugal compressor dictates the configuration of the test bench. Common methods used to drive the compressors were identified to be either using an electric motor, as a complete micro gas turbine (MGT), or as a complete turbocharger unit.

2.2.1 Test Bench Driven by Electric Motor

Numerous centrifugal compressor test benches are driven by electric motors. These test benches are being used in research to understand phenomena such as rotating stall and surge, along with investigating flow structures and loss mechanisms in the volute. The motors used by the abovementioned test benches are rated between 45 to 1 350 kW, driving an impeller of diameter 270 to 400 mm at a maximum speed which ranges between 13 500 to 29 160 rpm (Bianchini *et al.*, 2015; Hagelstein *et al.*, 2000; Lim, *et al.*, 2011).

The objective of the test bench designed by Bianchini *et al.* (2015) was to examine the operation of a centrifugal compressor at a minimum flow limit in order to investigate rotating stall. The proposed design of the test rig was to test industrial size impellers (diameters up to 0.4 m) at a maximum inlet Mach number of 0.7. The test rig consists

of a 45 kW electric motor with high-velocity belt and pulley system, high-frequency torque meter and main rotor train to drive an impeller at a maximum speed of 13 500 rpm.

The test bench designed by Lim *et al.* (2011) was also used to investigate surge in centrifugal compressors. He utilized a new method for surge control. The method used an active magnetic bearing (AMB) to actuate the impeller in the axial direction with a maximum end-to-end displacement of 0.5 mm, thereby increasing or decreasing tip clearance of the impeller, which in turn controls the onset of surge. The configuration of the test bench was such that the compressor was directly coupled to a 125 kW high-speed induction motor to drive the impeller at a maximum speed of 23 000 rpm. It was equipped with National Instruments™ high-speed modules in conjunction with the LabVIEW™ software as a data acquisition system.

Hagelstein *et al.* (2000) carried out an investigation of a volute with a rectangular cross-section to study the flow structures and loss mechanisms in the volute. The test bench used for this study comprised of a 1.35 MW DC motor coupled to a gearbox with a gear ratio of 1:16.2. This was used to drive the compressor with an impeller of 400 mm diameter at a maximum speed of 29 160 rpm.

It must be noted that all of the abovementioned test benches drive an industrial size impeller at relatively low speeds compared to the operating speeds of the micro gas turbines. In fact, extensive research done by Chernov (2013) indicates that the highest speed for a test bench with an electric motor as a driver is 35 200 rpm.

2.2.2 Test Bench Driven as a Complete MGT

There are several test benches designed by Krige (2013), Aus der Wiesche (2012), and Benini & Giacometti (2007) amongst others, which investigate the overall performance of MGTs.

The objective of the research conducted by Benini & Giacometti (2007) was to design and develop a low-cost MGT with a thrust of 200 N for educational purposes. The

overall performance of the design was then tested on the test bench. The test bench utilized an electric motor for start-up. It accelerated the core-assembly to approximately 10 000 rpm. Thereafter, natural gas was used for combustion which ramps the engine up to its minimum idle speed of 20 000 rpm. This was followed by a changeover to kerosene to achieve its maximum speed of 60 000 rpm. The test bench was equipped with a synchronized control valve, lubrication system for the bearings, ignition unit, and the necessary instrumentation.

Similarly, Aus der Wiesche (2012) developed a test bench to investigate the overall performance of a turbo-shaft MGT. Its operation was validated by using a commercial turbo-shaft engine with shaft power of 1 to 7 kW. The test bench was equipped with an engine, gearbox, engine control unit, fuel tank and cooling water system along with the thermal brake system. All of these components were mounted on a table to make it portable. The necessary instrumentation was installed to measure quantities such as temperature, pressure, torque, and thrust. The shaft power was measured using thermal measurements taken at the brake.

Krige (2013) developed a test bench to evaluate the performance of the BMT 120 KS micro gas turbine. The test bench consisted of two “beds” which were two U-shaped aluminum frames. The base bed was rigid as it was bolted onto a table which was fixed to the ground. The runner bed was secured with ball bearings placed on the vertical walls which allowed movement in the horizontal direction. This assisted in measurement of the thrust of the engine. All the measurements were obtained and logged using HBM Spider data loggers.

2.2.3 Test Bench Driven as a Complete Turbocharger

Test benches designed by Esper *et al.*, (2017), Struwig (2014), Olivero (2012), Venson *et al.*, (2008), and Galindo *et al.*, (2006) were used for the generation of performance maps for centrifugal compressor. All of the test benches except those by Olivero (2012)

and Struwig (2014) used a heating system to increase turbine inlet temperature, which ranges from 220℃ to 830℃.

Esper *et al.* (2017) used compressed air at a maximum pressure of 6 bar to drive the turbine of the turbocharger with a maximum mass flow rate of 6 kg/s. A 10.5 MW natural gas (NG) fired preheater was used to vary the turbine inlet temperature from 220 ℃ up to 500 ℃. An additional electrical preheater was installed to provide steady-state parameters, as the temperature gradients caused by the NG fired preheater were too wide for steady operation. A control valve was used to regulate the mass flow rate through the turbine. The compressor received air at ambient conditions which was then discharged into an exhaust pipe. The mass flow through the compressor was regulated by a throttling valve. Orifice plates were used to measure the mass flow rate through both the turbine and compressor.

The test bench used by Venson *et al.* (2008) had a mass flow rate of 0.02 to 0.30 kg/s. It utilized a tubular combustion chamber which was fired by liquid petroleum gas (LPG) to drive the turbine of the turbocharger. The exhaust gasses were supplied to the turbine at a pressure of 300 kPa and temperature which could be varied up to 730 ℃. A radial compressor is used to provide the initial air to the turbine before the combustion process. Galindo *et al.* (2006) used the exhaust from a 6 cylinder 250 kW diesel engine to drive the turbine. The mass flow rate of the exhaust gas was 0.5 kg/s at a maximum temperature of 750℃.

Olivero (2012) used two oil-free screw compressors to provide compressed air at 8 bar and ambient temperature to two buffer tanks with a combined capacity of 9 m^3. These compressors had a total combined mass flow rate of ~1.28 kg/s (6.06 m^3/min). The compressed air was then supplied to the turbine via a control valve at 3 bar. The rotational speed of the compressor was regulated with the help of a turbine control valve which controlled the flow through the turbine. The flow rate through the compressor was varied with the help of a throttling valve which was located

downstream of the compressor. This test bench was able to drive the compressor with an impeller diameter of 20 mm at a maximum speed of 220 000 rpm.

Similarly, the test bench designed by Struwig (2014) used compressed air at 10 bar which was supplied by two receiver tanks with a combined capacity of 88 m^3. A manual control valve was used to control the supply of the air to the test bench. The air was fed into the turbine via a control valve which was used to regulate the flow, thereby regulating the speed of the compressor. The compressor received air at ambient conditions and discharged it via a throttling valve. This valve was used to regulate the mass flow rate through the valve and was operated manually. The compressor with an impeller diameter of 81 mm was successfully tested at a maximum speed of 100 000 rpm.

2.3 Chapter Summary

In summary, considering the test benches detailed in the literature study, a test bench driven as a complete turbocharger was considered to be the best choice for the application in question. The test bench designed by Struwig (2014) is therefore taken as a baseline for the new test bench. The pipe sections from this test bench can be incorporated into the new test bench. Furthermore, the test bench is fully equipped with a suitable data acquisition system (DAQ). This system was used for the new test bench, hence reducing the overall cost.

3 Compressor Test Bench Setup

This chapter describes the mechanical design of the test facility. It focuses on the hardware, such as the design of the pipeline system, selection of valves, test sections and operation of the lubrication system. It discusses the data acquisition system (DAQ) and the installation of instruments on the test bench, along with a description regarding the automation of the test bench. As mentioned in Section 2.3 the test bench designed by Struwig (2014) was used as a baseline for this design and as far as possible, sections of the old test bench were re-used.

3.1 Introduction

The centrifugal compressor test bench was assembled and installed in Room 255 of the Department of Mechanical and Mechatronic Engineering at Stellenbosch University. The laboratory is commonly referred to as the “Kanontonnel” (KT). A general layout of the test bench is illustrated in Figure 3.1. The test bench was designed according to the ASME PTC 10 Performance Test Code on Compressors and Exhausters (ASME, 1997) and followed the methodology presented by Struwig (2014). The results from research detailed in Section 2.2 motivated the use of compressed air to drive the test bench. Furthermore, the compressed air system was readily available to the test facility.

Figure 3.1: General layout of the centrifugal compressor test bench

3.2 Mechanical Design

According to SANS 347:2012, a pressure vessel is defined as an enclosure which contains fluid at a pressure of 50 kPa or greater. The compressed air was supplied to the test bench at a pressure of 1 MPa, therefore the pipeline system which transferred the compressed air was considered to be a pressure vessel. According to Table 1 in SANS 347:2012, pipe sections that convey a non-dangerous gas should be evaluated according to Figure 7 of SANS 347:2012. The regulations stipulate that, if the design point lies on the borderline between two categories, it is considered to be from the category below the line. By inspection of Figure 7 from SANS 347:2012, it can be seen that the maximum pipe diameter at the operating pressure is 100 mm, in order for the design to stay within standard engineering practice (SEP) category. This implies that pipes with a diameter of 100 mm and smaller can be used for the test bench, provided that they are evaluated for service using standard engineering practice (Appendix F).

3.2.1 Pipeline System

The test facility's pipeline system was divided into two parts. The first part was the connection from the compressed air tank to the test bench and the second part was the test bench itself. These parts were joined by a threaded ball valve which acted as a primary valve for the test bench. The piping for the test facility was classified as a gas transportation and distribution piping system according to ASME B31.1-2001. As a result, the pipeline system had to be designed in accordance with ASME B31.8-2003.

In order for the pipe to be selected for the pipeline system, the minimum wall thickness had to be determined. It was calculated using Equation 3.1 from ASME B31.8-2003.

$$P = \frac{2St}{D} FET \tag{3.1}$$

where P is the design pressure, S is the minimum yield strength of the pipe material, t is the pipe thickness, and D is the outside diameter of the pipe. The design factor F, longitudinal joint factor E, and the temperature de-rating factor T were obtained from

the relevant tables in ASME B31.8-2003. The detailed calculation of the minimum wall thickness of the pipe can be found in Appendix B.1.

The minimum wall thickness required for the pipe was calculated to be 0.34 mm. Therefore, ASTM A106 Grade B – Seamless, 100 mm – Schedule 40 was chosen as a specification for the pipe. This pipe had a wall thickness of 6.02 mm, which was greater than the minimum requirement.

An 80 mm diameter pipe was required to place a control valve on the test bench. Similarly, the required minimum wall thickness was determined to be 0.26 mm. The ASTM A106 Grade B – Seamless, 80 mm – Schedule 40 pipe, which had a thickness of 5.49 mm was chosen for this section of the test bench.

For the pipe fittings, the ASTM A234 Grade WPB Seamless, 100 mm – Schedule 40 specification was chosen for the elbows and T-piece which had a thickness of 6.02 mm. The flanges used for the design were ASTM/ASME A105 Class 150 Slip-on – 100 mm and BS4504 Slip-on – 80 mm. All the pipes and fittings were supplied by MACSTEEL, whose products were designed in accordance with the respective design codes.

3.2.1.1 Compressed Air Supply Connection

The first part of the pipeline system connected the compressed air tank to the test bench. This part consisted of a combined pipe length of 12 m, one T-piece, three 90° elbows, and the main shut-off valve. The dimensions of the compressed air supply connection are shown in Appendix E (Figure E.3). The horizontal pipe section was supported by four supports, whereas the vertical pipe section only required one support.

The pipe section was connected to the T-piece, which was welded to the outlet pipe of the tank. A shut-off valve was placed between the T-piece and the pipe section. This valve isolated the test facility from the compressed air tank. The other end of the pipe section went through the wall into the laboratory and was connected to a threaded ball valve.

3.2.1.2 Test Bench

The second part of the pipeline system was the test bench itself. This part was divided into six subassemblies which are referred to as sections (Figure 3.2). Each section and its components are described below and it should be noted that all pipe diameters were 100 mm, except where otherwise stated:

1. Section A formed part of the compressed air supply connection which was protruding out of the wall. A manually operated threaded ball valve was connected to this section. This acted as the primary valve of the test bench.
2. Section B consisted of an orifice plate, along with an upstream pipe length of 3000 mm and a downstream length of 1500 mm.
3. Section C consisted of a pipe with a length of 413 mm which was connected to two 90° elbows. This section elevates the test section by 796 mm.
4. Section D consisted of an automated butterfly valve with an upstream and downstream pipe length of 225 mm. This valve was the secondary valve on the test bench.
5. Section E consisted of an automated globe valve which was connected to an 80 mm diameter up- and downstream pipe section. Each of these pipe sections comprised of a 100x80 mm reducer and a pipe with a length of 400 mm. The globe valve acted as a control valve for the test bench.
6. Section F consisted of a pipe length of 900 mm which was connected to an adapter.

The adapter mentioned in point 6 above was used to accommodate the turbine inlet which was rectangular in shape. It comprised of a 100x80 mm reducer, an 80 mm diameter pipe section, a circular to rectangular cross-section reducer (lofted piece), and the turbine inlet flange. The circular to rectangular cross-section reducer was a sheet metal component that was bent to the required size and shape (Figure 3.3). It was welded onto an 80 mm pipe in order to convert the pipe's circular cross-section to a

rectangular cross-section. The rectangular side of the reducer was welded onto the turbine inlet flange.

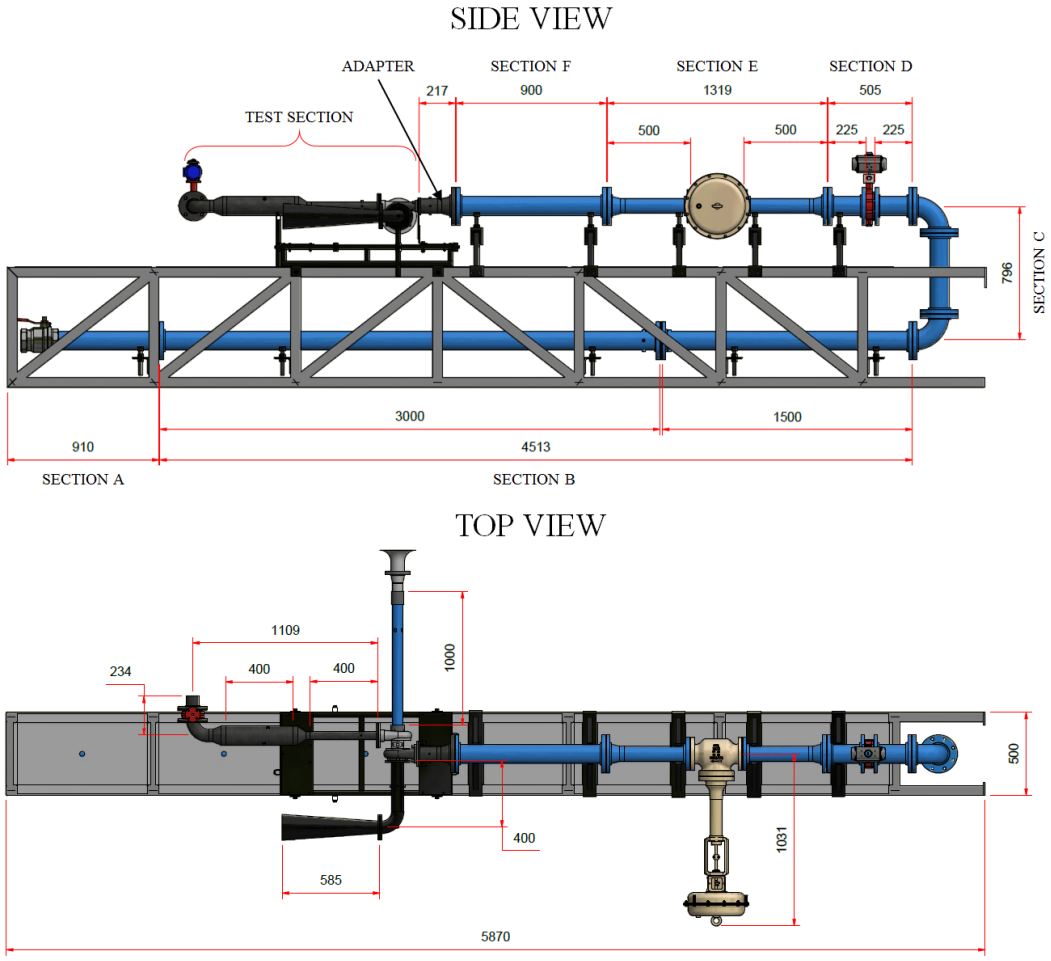

Figure 3.2: Side and top view of the centrifugal compressor test bench

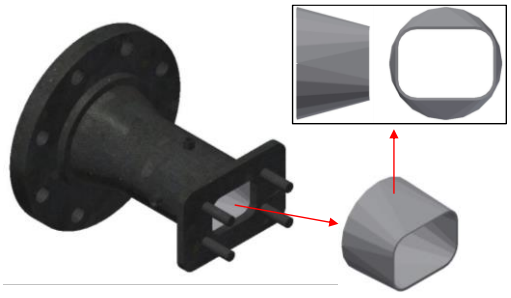

Figure 3.3: Circular to rectangular cross-section reducer

3.2.2 Test Section

The test section comprised of a BorgWarner KKK K27 turbocharger, piping installed at the inlet and outlet of the turbocharger and the supporting frame. The selection of the turbocharger was done by Struwig (2014) using specifications provided by the CSIR. According to his calculations, the power delivered by the turbine correspond to that absorbed by a compressor with an outlet diameter of 74 mm and the K27 compressor had the closest diameter of 81 mm. It is important to note that the actual turbocharger used for the new test bench is a different machine than the one used by Struwig (2014). The serial numbers for both the compressor and turbine of the turbocharger are listed in Table 3.1.

Table 3.1: KKK K27 turbocharger specification

	Serial No.
Turbine	5327 101 6574F
Compressor	5327 101 5280

The pipe sections used for the test section were re-used from the setup of Struwig (2014). The pipeline system described in the previous section was directly connected to the inlet of the turbine. At the outlet of the turbine, a 60 mm diameter pipe section with a length of 280 mm along with a 90° elbow was attached. It was followed by a diffuser which was 570 mm in length and had an upstream and downstream diameter of 69 mm and 146 mm respectively.

The compressor section draws in air through a class 9 polyvinyl chloride (PVC) pipe with a length of 1000 mm and a wall thickness of 2.70 mm. At the inlet of the PVC pipe, a bellmouth was attached along with protecting mesh. The discharge pipe section consisted of a Schedule 40 pipe which was 40 mm in diameter and had a length of 200 mm. A 40 mm diameter pipe was used in order to keep the discharge pipe diameter the same as the outlet diameter of the compressor. The pipe diameter was then

increased to 100 mm with the use of a 40x100 mm reducer. This change in diameter was required for the installation of thermocouples. The 100 mm diameter pipe section had a length of 400 mm followed by a 100x80 mm reducer and a 90° elbow. A butterfly valve was attached downstream of the elbow, which acted as a throttling valve to vary the mass flow rate through the compressor. The butterfly valve replaced the hand-operated globe valve used by Struwig (2014).

3.2.3 Valves

There were five valves used to maintain safe operation and to achieve controllability of the test bench. This section briefly describes the function of each valve along with its location and specifications.

3.2.3.1 Main Shut-off Valve

The main shut-off valve was located at the outlet of the compressed air supply tank. It was a manual DN100 slim butterfly valve with a pressure rating of 1 600 kPa. The main purpose of this valve was to isolate the test facility from the tank.

3.2.3.2 Primary Valve

The primary valve was a threaded ball valve that connected the compressed air supply pipeline to the test bench. The main shut-off valve was situated outside the laboratory, therefore this valve acted as a primary valve for the test bench. It was a manual DN100 valve with a pressure rating of 1 400 kPa which supplied the air to the test bench.

3.2.3.3 Secondary Valve

The secondary valve was a DN100 slim butterfly valve coupled with an Air Torque (AT) double-acting pneumatic actuator (Figure 3.4). It was located upstream of the control valve and had a pressure rating of 1 600 kPa, whereas the pneumatic actuator had a pressure rating of 800 kPa. The pneumatic actuator was operated with the use of an AIRMATE WP solenoid valve which had a spring return setting.

Air at 450 kPa was supplied to the solenoid valve with the help of a SAMSON Type 4708-45 supply pressure regulator. The solenoid valve allowed the air into the

actuator when switched on and released the air when switched off. This valve acted as a safety valve for the test bench. In case of an unforeseen event, the operator could simply close the valve with the use of an emergency switch, which stops the supply of air to the test section.

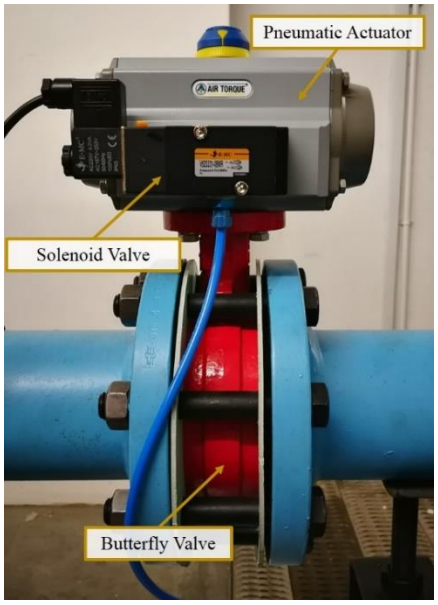

Figure 3.4: Secondary valve

3.2.3.4 Control Valve

The control valve (CV) shown in (Figure 3.5) was a SAMSON Type 3251 DN80 globe valve coupled with a pneumatic actuator. The pressure and temperature rating of the valve was 4 000 kPa and 500 °C respectively. Keeping in mind the installation of a heating system in the future, a control valve with high temperature rating was chosen. The valve has an equal percentage characteristic with a rated travel of 30 mm and a maximum valve flow coefficient (K_v) of 100 m^3/h. The sizing of the valve was done by SAMSON Controls (PTY) LTD in accordance with IEC 60534.

An electro-pneumatic positioner Type 3730-1 was mounted onto the actuator which controlled its travel, hence controlling the globe valve percentage opening. The valve could be operated manually with the use of a switch on the positioner. The main

purpose of this valve was to control the speed of the turbocharger. This was done with the use of a TROVIS 6493 compact controller, which was used to automate the control valve. A detailed description of the controlling procedure is given in Section 3.4.1.

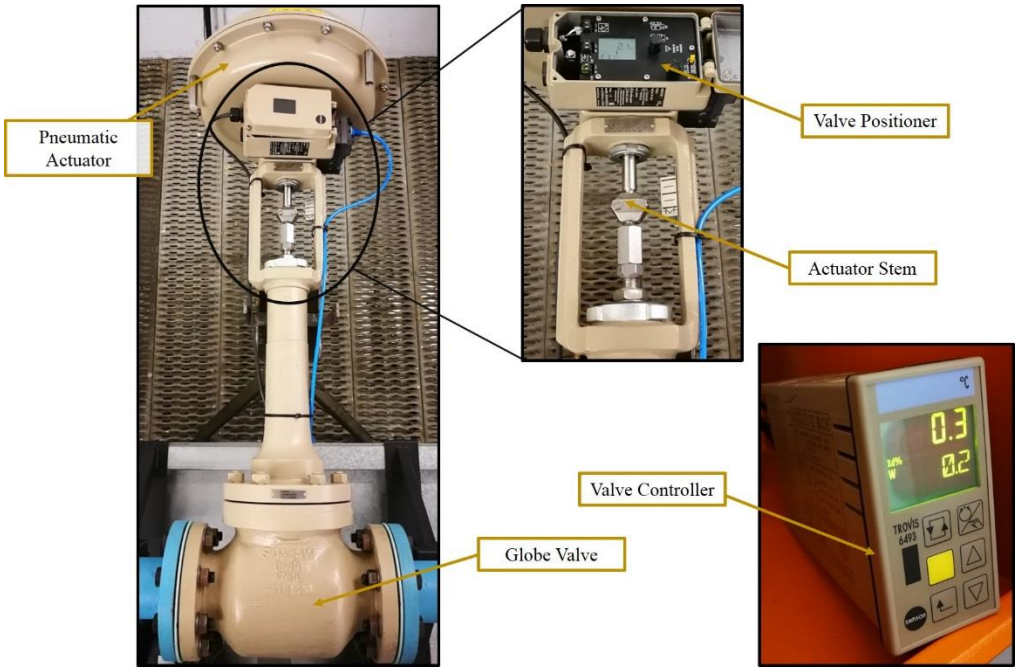

Figure 3.5: Control valve with the pneumatic actuator, positioner, and the controller

3.2.3.5 Throttling Valve

The throttling valve was a DN80 slim butterfly valve that was placed at the discharge of the compressor pipeline. The assembly of the throttling valve is shown in (Figure 3.6). The valve was coupled to an AOX-008 electric actuator which had a travel range of 0° to 90° and it was controlled by the attached ZXQ-E1 positioner. This valve was used to control the flow through the compressor by throttling the discharged air. The control procedure is described in Section 3.4.2.

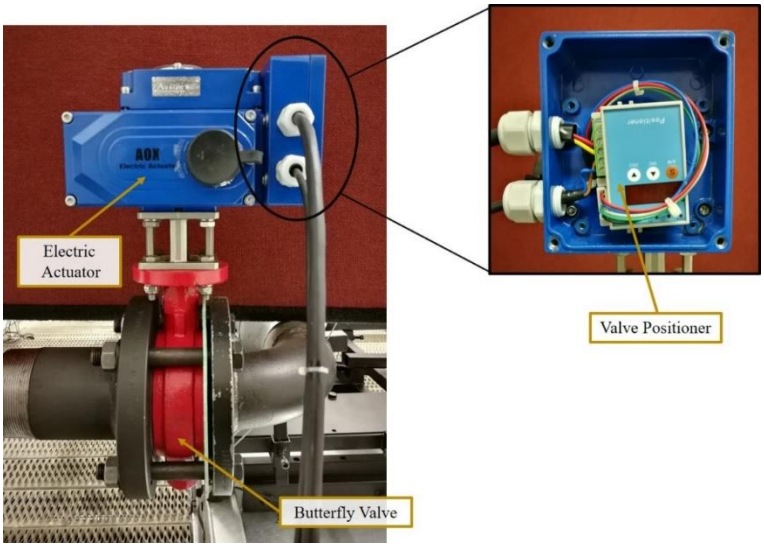

Figure 3.6: Throttling valve with the electric actuator and the positioner

3.2.4 Lubrication System

The lubrication system formed an essential part of the operation of the test bench. The bearing housing of a turbocharger consisted of an axial thrust bearing and two radial journal bearings, which required lubrication for smooth operation. The lubrication system used for the test bench was the same as that used by Struwig (2014) shown in Figure 3.7. It was originally designed by Nieuwoudt (1987).

Upon switching on the lubrication system, the temperature was set with the use of a thermostat, while the bypass valve was closed. It ensured that the turbocharger was bypassed and the oil circulated within the lubrication system. This was done to preheat the oil before it was delivered to the turbocharger. When the oil reached the set temperature, the bypass valve was opened to circulate the oil through the turbocharger bearings. The temperature was monitored with the help of two thermocouples at the inlet and outlet of the reservoir.

The lubrication system allowed the user to maintain the inlet pressure and the flow rate of the oil. This was done by adjusting the pressure and volume control knobs on the lubrication system (Figure 3.7). The inlet pressure of the oil was measured using two

pressure gauges and a pressure transducer. One pressure gauge was mounted on the lubrication system and the second pressure gauge was mounted close to the inlet of the turbocharger. This was done to measure the true oil inlet pressure after pipe losses. A pressure transducer was attached at the same point as the second pressure gauge to provide real-time feedback to the user through the graphical user interface (GUI).

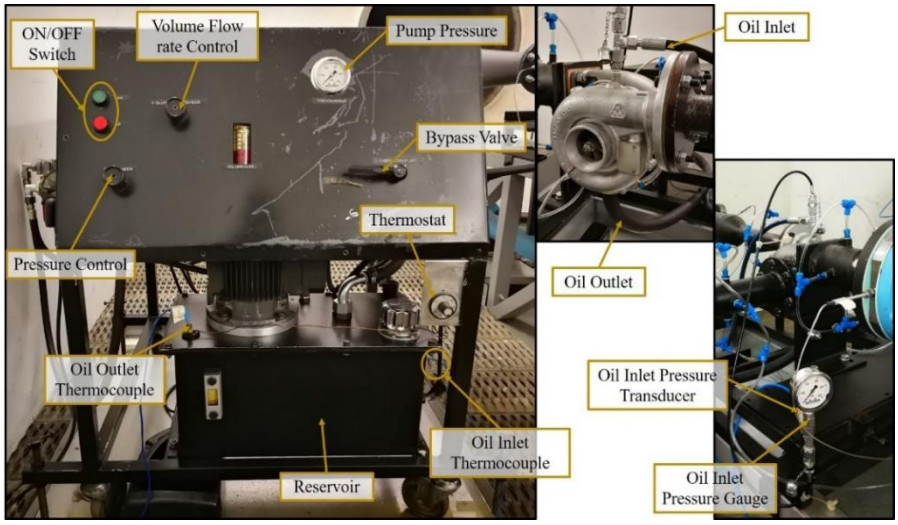

Figure 3.7: Lubrication System

There was no pressure measurement required at the outlet of the turbocharger bearing housing as oil simply flowed back to the reservoir under gravity. The operating requirements for the turbocharger oil system could not be obtained from the supplier. Therefore, before performing tests, the turbocharger was tested on a CIMAT Turbo Test Pro Flow Bench at Turbo Exchange in Cape Town. This provided the optimal oil pressure and temperature for the turbocharger's bearing housing. These operating conditions are listed in Table 3.2. The oil used for the lubrication was 15W40 motor oil.

Table 3.2: Optimal oil operating conditions for the turbocharger

Temperature	40 – 45 °C
Pressure	400 – 450 kPa

3.3 Instrumentation

The instrumentation and data acquisition (DAQ) system used on the test bench is described in this section. It explains the implementation of the instruments, along with the position of installation and procedure of acquiring data. It must be noted that the test section consists of a turbine and a centrifugal compressor. Therefore, instruments are divided into two groups, each of which is dedicated to taking measurements of the above specified components. The placement of all the instruments is shown in Figure 3.8.

Important parameters such as mass flow rates, speed, static temperature, and static pressure need to be measured to describe the performance of the centrifugal compressor. This section describes the instrumentation used and the placement thereof to obtain the necessary measurements. Furthermore, it discusses in detail the post-processing method followed in order to calculate the total-static (t-s) pressure ratio, efficiency, and power of the centrifugal compressor and the radial turbine.

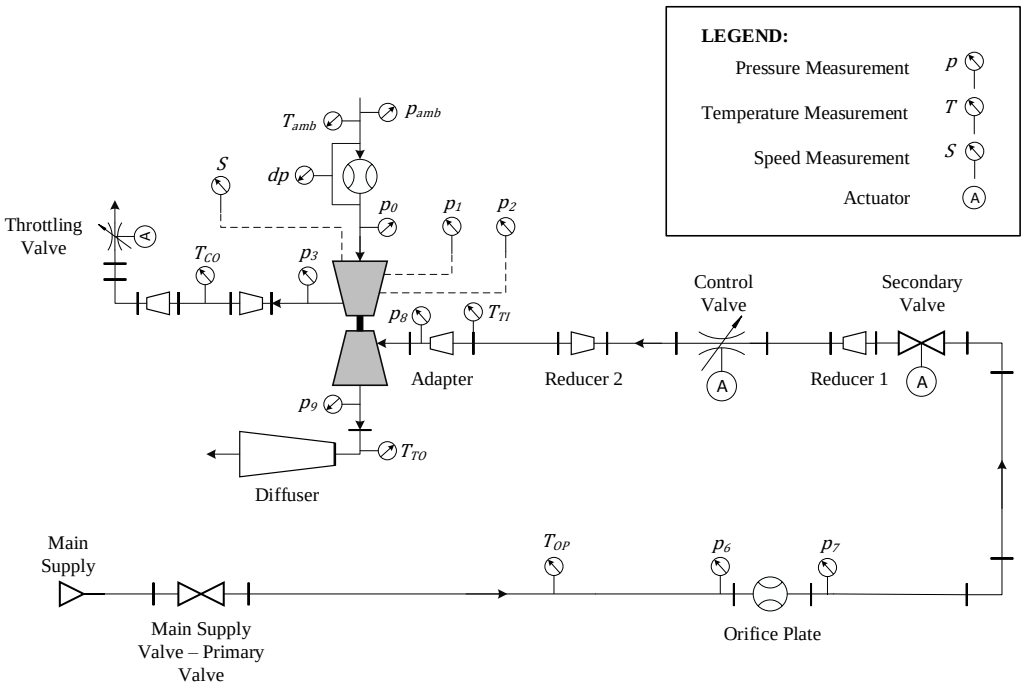

Figure 3.8: Placement of instrumentation

3.3.1 Temperature Measurement

There were fourteen J-type thermocouples installed in the test facility. The thermocouples were manufactured by Temperature Control Pty (Ltd). These thermocouples were used to measure the temperature at five different locations (Figure 3.8). Six of the thermocouples were placed on the turbine side and eight on the compressor side. Two additional K-type thermocouples were used to measure the inlet and outlet temperature of the oil, which was previously discussed in Section 3.2.4.

On the turbine side, six thermocouples were used to measure the temperature at the following locations:

1. Upstream of the orifice plate, T_{OP}
2. Inlet of the turbine, T_{TI}
3. Outlet of the turbine, T_{TO}

At the turbine inlet, four thermocouples were used, whereas at the other two locations only one thermocouple was deemed sufficient.

ASME PTC 10 (1997) specifies that at each of the temperature measuring stations four thermocouples, spaced 90° apart must be used as shown in Figure 3.9 a. On the compressor side, eight thermocouples were used to measure the temperature at the following locations:

1. Inlet of the bellmouth, T_{amb}
2. Outlet of the compressor, T_{CO}

To measure the inlet total temperature of the bellmouth, thermocouples were fixed to the safety grid at the bellmouth inlet. Thermocouples protruded into the safety grid such that the length of the thermocouple reached the throat diameter of the bellmouth.

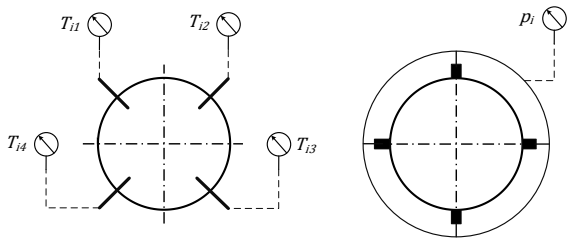

(a) (b)

Figure 3.9: Positioning of (a) Thermocouples (b) Pressure Transducer

It is important to understand the use of thermometry in high-velocity air streams. If an ideal shaped temperature measuring probe is stationary in a moving ideal gas, it must sense the total temperature as it brings the gas to a halt. This is only true if the process of decelerating the gas to stagnation point is isentropic and there is no heat transfer between the gas and the probe.

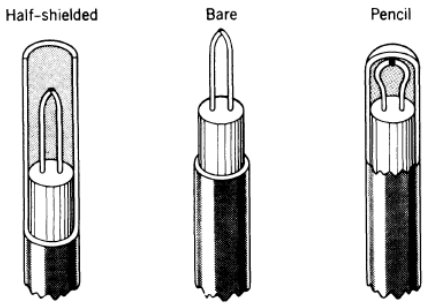

Figure 3.10: Three types of thermocouple probes (Benedict, 1977)

However, these assumptions are not valid in the context of practical thermometry, where a real probe is immersed in a real moving gas. This is because the process is diabatic as radiation occurs between the probe and its surrounding and conductive heat transfer takes place along the stem of the probe. The real probe is also not able to stop the gas isentropically (Benedict, 1977). Thus, to correct the measurement of a probe that measures temperature in a real flowing gas, a dynamic correction factor K is introduced and presented in Equation 3.2.

$$T_P = T + KT_v \tag{3.2}$$

where T_P represents the temperature sensed by the stationary real probe and T_v is the dynamic temperature. The total temperature (T_0) can be defined as Equation 3.3.

$$T_0 = T_P + (1 - K)\frac{c^2}{2c_p} \tag{3.3}$$

Benedict (1977) presented experimental results to determine the value of *K* for the three types of thermocouple probes shown in Figure 3.10. The pencil type was most sensitive whereas the half-shielded type was least sensitive to radiation, Mach and Reynolds effects. The value of the dynamic factor ranged between 0 and 0.82 for the pencil type and for the half-shielded type it was approximately 0.96 (Benedict, 1977). All the thermocouple probes used were of the pencil type, except the ones at the compressor outlet which were of the half-shielded type. This is because high temperatures are only experienced at the outlet of the compressor and half-shielded type is least sensitive to radiation (Benedict, 1977). Calibration curves for all the thermocouples are presented in Appendix A.1.

3.3.2 Pressure Measurement

There were eleven pressure transducers installed in the test facility to measure static and differential pressure at different locations. Four of these transducers were placed on the turbine side and five on the compressor side. The other two pressure transducers were used to measure ambient pressure and oil pressure. In order to measure pressure at the turbine and compressor side, each pressure station consisted of four pressure taps which were spaced 90° apart, as shown in Figure 3.9 b.

On the turbine side, four HBM P8AP absolute pressure transducers were installed to measure static pressure at four different locations. These transducers were positioned at the following locations (Figure 3.8) which were perpendicular to the flow direction:

1. Upstream of the orifice plate, p_6
2. Downstream of the orifice plate, p_7
3. Inlet of the turbine, p_8

4. Outlet of the turbine, p_9

The placement of the transducers across the orifice plate was in accordance with the British Standard (BS) 1042 (BSI, 1992). These transducers were rated at 2 MPa, whereas the other two transducers were rated at 1 MPa. The reason for this difference in transducer rating is due to the fact that the supply pressure could vary up to 1.4 MPa. In case of an increase in supply pressure, the transducers must still be able to measure the pressure across the orifice plate.

At the compressor side, five pressure transducers were installed. Four of which were HBM P8AP absolute pressure transducers and one which was an Endress+Hauser PMD70 differential pressure transducer. ASME PTC 10 – 1997 specifies the location of the pressure measurements on the compressor, which are as follows:

1. Across the bellmouth, dp
2. Upstream of the compressor inlet, p_0
3. Outlet of the impeller, p_1
4. Outlet of the vaneless diffuser, p_2
5. Downstream of the compressor outlet, p_3

The operating range for the HBM P8AP is 1 MPa, whereas the Endress+Hasuer PMD70 can measure up to 3 kPa differential pressure. In order to obtain the pressure at the impeller and diffuser outlet, pressure taps were manufactured and press-fitted into the backplate of the compressor. These pressure taps were made out of brass with a diameter of 1.5 mm (Struwig, 2014).

The two transducers that were used to measure ambient and oil pressure are also HBM P8AP absolute pressure transducers with a maximum operating range of 1 MPa. The location of the oil pressure transducer is discussed in Section 3.2.4.

The HBM P8AP absolute pressure transducer is a strain gauge (SG) based pressure transducer with a nominal sensitivity of 2 mV/V. Hence, it required a measuring amplifier to provide the SGs with the excitation voltage. For this purpose, all the HBM P8AP absolute pressure transducers were used in conjunction with an HBM AE301 strain gauge measuring amplifier. These amplifiers have a maximum voltage output of ± 10 V. Calibration curves for all the pressure transducers are presented in Appendix A.2.

3.3.3 Flow rate Measurement

The mass flow rate was measured at the turbine side ($\dot{m}_T$) and the compressor side ($\dot{m}_C$) with the help of an orifice plate and bellmouth respectively.

3.3.3.1 Turbine Side

In order to obtain the flow rate through the turbine and compressor, the relationship between velocity and the pressure difference along the flow path was exploited. This principle is commonly used in obstruction flow meters and the governing equation to obtain the mass flow rate is presented in Equation 3.4.

$$\dot{m} = C_d E \epsilon \frac{\pi}{4} d^2 \sqrt{2 \Delta p \rho_1} \tag{3.4}$$

From Equation 3.4 it can be seen that parameters such as the obstruction throat diameter d, pressure difference Δp across the obstruction, and the upstream density of the fluid, ρ_1 is required to measure the flow rate. C_d is the discharge coefficient, E is the velocity of approach factor, and ϵ is the expansibility factor. These factors can be calculated using the geometric parameters along with the fluid properties.

A concentric square-edge orifice plate was used to measure the flow through the turbine. The design and the installation of the orifice plate were in accordance with the BS 1042 (BSI, 1992). A D and $D/2$ configuration for the pressure taps was used where D was the upstream internal pipe diameter. The upstream temperature was measured using a thermocouple which was installed upstream of the orifice plate.

To increase the modularity of the test rig, two orifice plates were designed. These two plates had different operating ranges; one was to measure low flow rates of 0.5 kg/s and the second was to measure a maximum flow rate of 1 kg/s. A maximum pressure of 1 MPa and design pressure drop of 20 kPa were considered for the design. This resulted in diameter ratios (β) of 0.376 and 0.532 for 0.5 kg/s and 1 kg/s respectively. The sample calculation for the design of the orifice plates is shown in Appendix B.2.

3.3.3.2 Compressor Side

The flow rate through the compressor was measured at the suction side of the compressor with the use of the bellmouth. As mentioned previously, four thermocouples and a differential pressure transducer were installed to measure the inlet temperature and a pressure difference across the bellmouth. Another pressure transducer was used to measure ambient pressure. Using all these measured parameters along with the bellmouth's throat diameter ($d = 77.50$ mm), the flow rate through the compressor was calculated. Details regarding the calibration of the bellmouth can be found in Struwig (2014). The calculation of the mass flow rates was an iterative process and is briefly discussed in Section 4.2.2.

3.3.4 Speed Measurement

Generally, proximity, magnetic or inductive sensors are used to measure rotational speed. For the facility, a turboSPEED DZ140 sensor from MICRO-EPSILON was used to measure the speed of the compressor. It is a fast proximity sensor that exploits the eddy current measuring principle to measure the speed (Micro-Epsilon, 2016). The sensor worked in conjunction with its controller. The controller allowed the user to set the mode of measurement and the number of blades. Considering these settings, the speed was identified by the controller and it outputs an analog voltage signal (0-5V). This voltage can be converted to revolutions per minute (rpm) with the use of a linear curve shown in Figure 3.11.

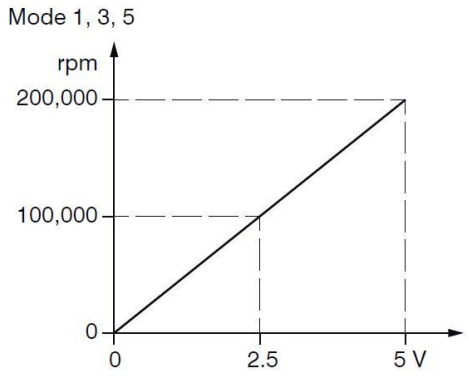

Figure 3.11: Linear relation between voltage and rpm (Micro-Epsilon, 2014)

A hole with M5 thread was tapped at a 45° angle from the axial direction of the compressor housing inlet as shown in Figure 3.12 a. The sensor was mounted such that it sees all the blades of the compressor, including the rotor splitter blades. The setting on the controller was set at mode 1 which represented a maximum speed of 200 000 rpm at high sensitivity and the number of blades was set to 14 as shown in Figure 3.12 b.

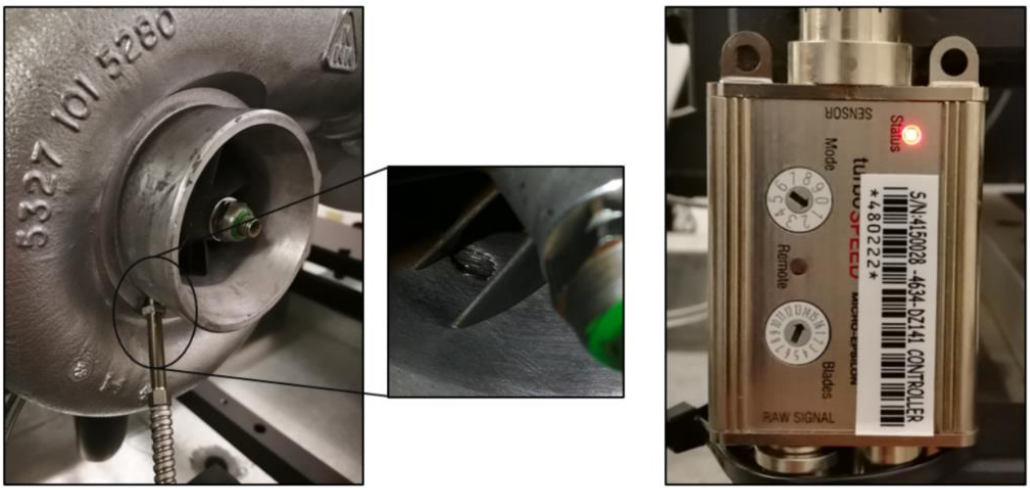

(a) (b)

Figure 3.12: (a) Positioning of the speed sensor (b) Controller of the speed sensor

3.4 Test Bench Control

3.4.1 Speed Control

The control of the shaft's rotational speed was performed using a turboSPEED DZ140 sensor, a SAMSON Type 3251 valve, Type 3730-1 electro-pneumatic positioner, and a TROVIS 6493 compact controller. The operation of each component is described in this section.

The SAMSON Type 3251 globe valve was coupled to a pneumatic actuator. An electro-pneumatic positioner type 3730-1 was used to change the valve position. This regulated the flow rate into the turbine, thereby controlling the shaft speed of the turbocharger. The TROVIS 6493 compact controller was used to automate the control valve and can also be used as a PID controller.

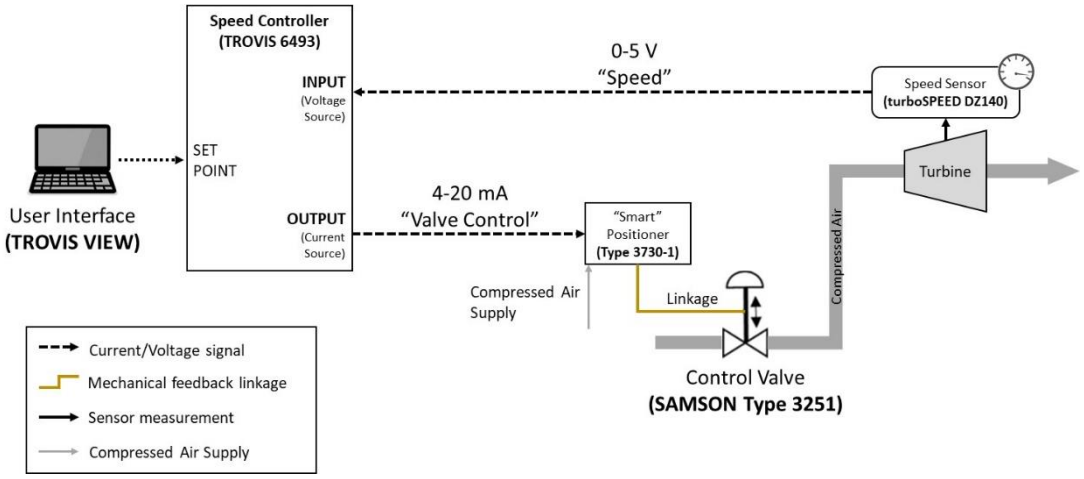

Figure 3.13: Speed control loop

The speed control loop of the test rig is shown in Figure 3.13. The output of the speed sensor was an analog signal of 0 to 5 V to the controller. The controller then compared the signal with the setpoint defined by the user. If the input signal was less than the setpoint, the controller sent an output signal to the positioner which opened/closed the valve until it reached the setpoint. TROVIS 6493 was used as a PI controller as only

proportional and integral parameters were adjusted to achieve fine control of the speed of the turbocharger. The control parameters for the controller are listed in Table 3.3.

Table 3.3: Control parameters for TROVIS 6493

Parameters	Value
Proportional (P)	2.7
Integral (I)	7.0

3.4.2 Flow rate Control

A National Instruments™ (NI) CompactRIO (cRIO) was used as the data acquisition (DAQ) system for the test bench and is discussed in detail in the subsequent section. It was not only used to acquire data, but also used as a controller for the throttling valve. The positioner of the AOX electric actuator required a 4-20 mA signal to fully open and close the throttling valve. This was done by using a NI-9263 output module and an ACDC voltage to current converter.

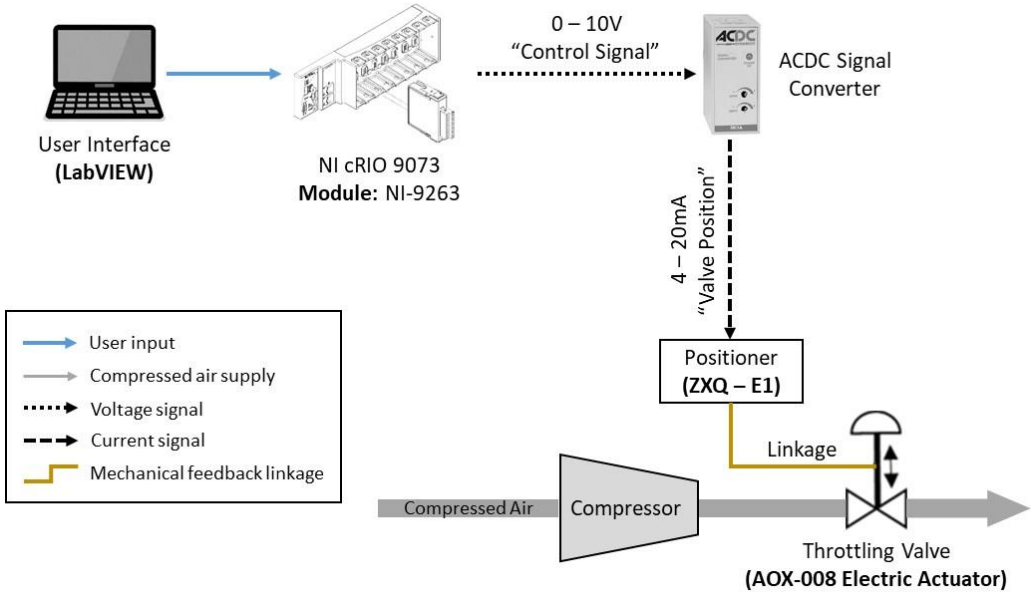

Figure 3.14: Throttling valve control - Signal flow diagram

The operation of this control is explained with the aid of the signal flow diagram illustrated in Figure 3.14. An output signal of 0 to 10 V was sent from the NI-9263 module to the ACDC signal converter. The converter converted the voltage to 4-20 mA which was then fed to the positioner of the AOX electric actuator which in turn opened or closed the valve. Preliminary tests were done on the throttling valve to obtain an equation (Equation 3.5) which related the voltage (x) to the percentage opening of the valve (y).

$$y = 11.394x - 4.5048 \tag{3.5}$$

3.5 Data Acquisition System

The National Instruments^{TM} (NI) CompactRIO (cRIO – 9073) in conjunction with Laboratory Virtual Instrument Engineering Workbench (LabVIEW^{TM}) was used as a Data acquisition system (DAQ) for the test facility. This DAQ was similar to the one used by Struwig (2014). However, there were some modifications required to account for a few new transducers installed in the test facility. This section briefly describes the procedure of acquiring data using the installed transducers and DAQ. The data acquisition hardware, along with the control equipment were mounted in an instrumentation cabinet and it can be seen in Figure 3.15. This completely isolates the equipment from the test bench.

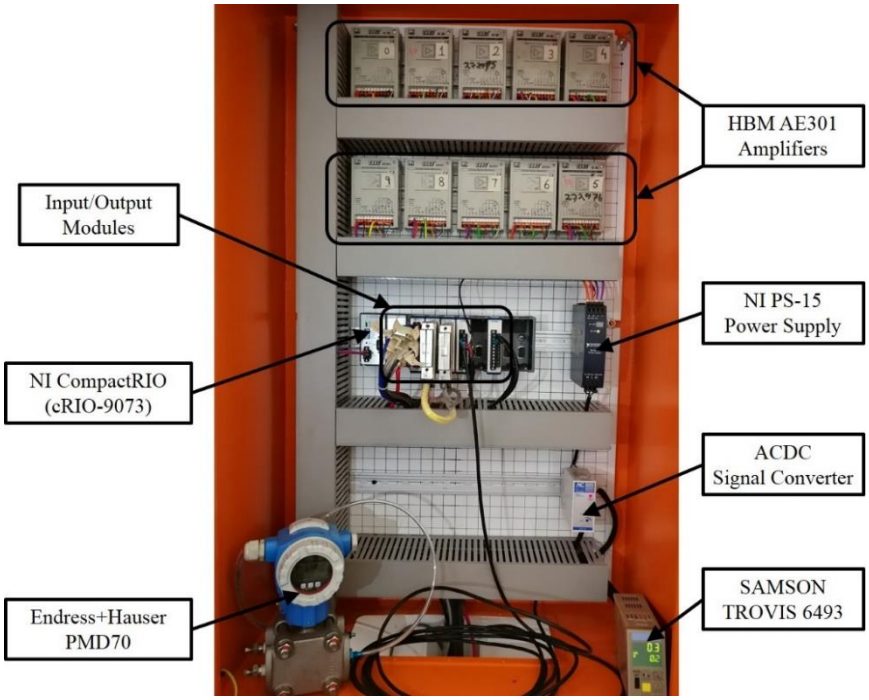

Figure 3.15: Hardware of the data acquisition system

The cRIO-9073 consisted of a real-time controller and a reconfigurable field-programmable gate array (FPGA) chassis which provided eight slots for input/output (I/O) modules. A user-defined FPGA was used to obtain the data from I/O modules. This data was then transferred to the controller through a local peripheral component interconnect (PCI) bus with the use of built-in communication functions. The cRIO-9073 had a processing speed of 266 MHz and required a power supply which ranged from 19 – 30 V. The power supply, a (NI PS-15), 24 VDC, 5 A, was used to power the cRIO. All the transducers were connected to the following I/O modules to sample the data:

1. NI-9213, a 16-channel thermocouple module
2. NI-9207, a 16-channel analog input (AI) module with 8-channel current (±20 mA) input and 8-channel voltage (±10 V) input module
3. NI-9215, a 4-channel analog input (AI) module
4. NI-9263, a 4-channel analog output (AO) module

3.5.1 Program Operation

LabVIEW™ is a graphical programming language that was used to create a graphical user interface (GUI). It uses dataflow programming, where the execution is determined by the flow of data (NI, 2003). The GUI is known as the front panel which is controlled by the code which is a graphical representation of functions. The operation of the LabVIEW™ program used for the test bench is discussed in detail by Struwig (2014). The GUI for the test bench is shown in Figure 3.16.

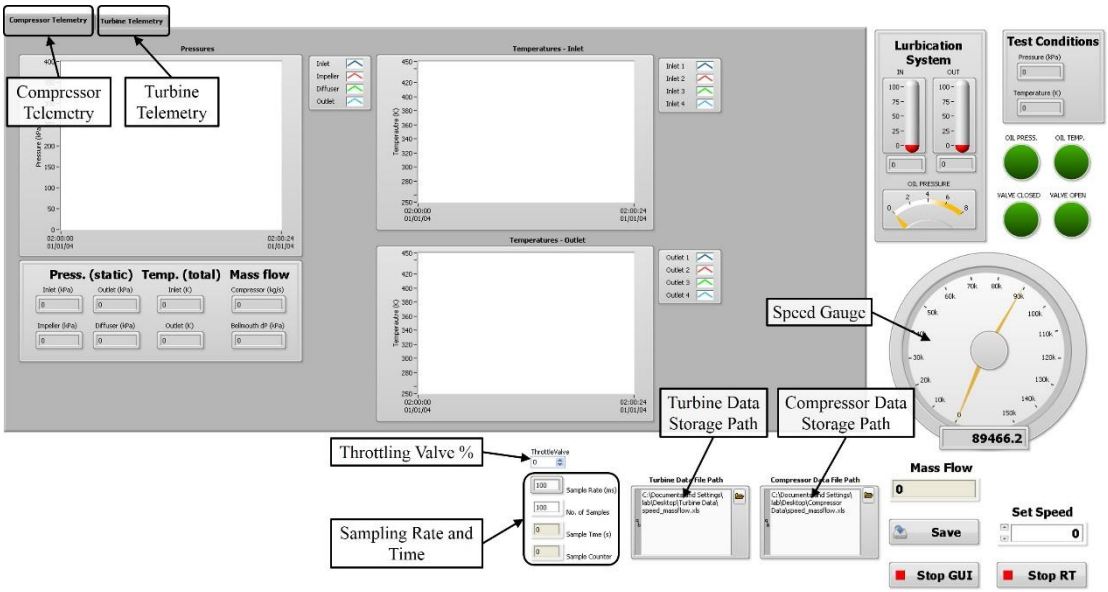

Figure 3.16: Graphical User Interface (GUI) for data acquisition

The GUI allowed the user to see the stabilization of measurements in the shape of graphs in the compressor and turbine telemetry tabs, while speed could be noted from the speed gauge. The operating conditions of the tests and the lubrication system were displayed on the top right corner of the GUI. Warnings were given to the operator if the optimal conditions for lubrication oil were not reached. The GUI allowed the user to change the percentage opening of the throttling valve to acquire the desired compressor mass flow rate. Furthermore, the sampling rate and the number of samples for the test could also be altered, and data for the compressor and turbine was stored in separate files in Microsoft Excel™ .xls format.

3.5.2 Temperature Measurement

The thermocouples used in the facility were connected to the NI-9213 module to sample the temperature measurement. NI-9213 module was slotted into the first channel of the cRIO chassis. It was a 16-channel thermocouple module that could be used for all temperature ranges defined by different types of thermocouples. For the test facility, there were fourteen J-type and 2 T-type thermocouples used. The raw temperature data obtained by the module was in μV which had to be converted to Kelvin. This conversion was done in LabVIEW, which provided the polynomial functions to convert the thermocouple's voltage to temperature (Appendix C.1).

The NI-9213 module consisted of 2 additional channels which were a cold-junction compensation (CJC) channel and an autozero channel. These channels were solely dedicated to improving the accuracy of temperature measurements. Heat dissipated by adjacent modules or nearby heat sources can result in a temperature change of the module terminals (NI, 2009). This could lead to errors in thermocouple measurement. The built-in CJC compensates for this error. The autozero channel eliminates all the offset errors which might have been present at the start of each scan.

3.5.3 Pressure Measurement

Two NI-9207 modules were used, which were slotted in channels 2 and 3 of the cRIO. All the absolute HBM pressure transducers were connected to the module slotted in channel 2. The Endress+Hasuer PMD70 differential transducer was connected to the module slotted in channel 3. The HBM P8AP pressure transducers were coupled to HBM AE301 strain gauge measuring amplifiers. The measuring amplifiers were calibrated to provide a 0-10 V full-scale output for each pressure measurement. The equations obtained for the calibration curves were then used to convert the measured voltage signal to pressure. This conversion was done in LabVIEW (Appendix C.2).

3.5.4 Speed Measurement

The speed sensor was connected to the NI-9215 module in order to sample the speed measurement. This module was slotted in channel 4 of the cRIO. NI-9215 is a high-speed sampling module with a sampling rate of 100 kHz per channel. The speed sensor outputs a 0-5 V signal which was obtained by channel 1 of this module. The voltage (V) was then converted to speed (N) with the use of Equation 3.6 which was obtained from Figure 3.11. This conversion was done in LabVIEW (Appendix C.3).

$$N = 40\,000V \tag{3.6}$$

3.5.5 Flow rate Measurement

Based on the explanation in Section 3.4.2, the NI-9263 output module which was slotted into channel 6 of the cRIO was used to control the percentage opening of the throttling valve. This resulted in control of the mass flow rate through the compressor.

4 Experimental Testing

Tests were performed to investigate the operation and stability of the test bench, as well as the reliability of the test results. This chapter describes the test methods followed, along with the post-processing of the acquired data from the tests.

4.1 Test Method

The compressed air was supplied from a compressed air tank. This implied that the tests encountered time constraints as the compressed air depleted during the tests and had to be refilled. Refilling the tank made it difficult to obtain constant operating conditions for each test run. For this reason, numerous tests were performed to exhibit the functionality of the test bench at different operating conditions.

Tests were divided into three different categories. The first category of tests was performed without the attachment of the turbocharger to the test bench, which was further divided into two different sets of tests. The second and third category of tests involved the complete test bench with the turbocharger installed. This section discusses the methodology followed for each category and its respective set of tests. It further discusses the complications encountered during the testing phase of the project.

4.1.1 Test without Turbocharger

The test without the turbocharger was needed in order to acquire the range of mass flow rates which could be achieved on the test bench. This also assisted in validating the numerical model and fine tuning it so that the model best represented the actual test bench. These tests were performed by simply opening the control valve (CV) in percentage increments of five. It was realized that it would not be possible to get the full range of the mass flow rate in one continuous test. Therefore, the test was subdivided into two parts, first of which was a discontinuous test and the second one was a continuous test with a CV opening of 5-100% and 40-90% respectively.

4.1.1.1 Control Valve Opening (5 – 100%)

This was the discontinuous test and was conducted by opening the CV from 5 to 100 %. The test comprised of three ranges, namely 5-50 %, 55-80 %, and 85-100 %. After covering every range, or when the upstream pressure of the orifice plate reached 600 kPa, the test was discontinued for the compressed air tank to be replenished. The replenishment took approximately 30 to 40 minutes after each test.

The test was conducted by opening the CV to a certain percentage and operating the test bench at this configuration for approximately 1 to 2 minutes for the measurements to stabilize. Once stability was reached, the two sets of data were recorded with a sampling rate of 10 S/s for a duration of 10 s. The recorded data comprised of the temperature and pressure measurements at the orifice plate and the turbine inlet from where the compressed air was discharged into the atmosphere.

4.1.1.2 Control Valve Opening (40 – 90%)

This test was performed by opening the CV from 40 to 90 %. The test was conducted twice, once by opening the valve from 40-90 % which is referred to as “Up” and secondly in closing the valve from 90-40 %, which is referred to as “Down”. The test methodology, sampling rate, and the data obtained were similar to the CV opening 50 - 100 % test.

4.1.2 Test with Turbocharger

This category includes the preliminary and final tests which are discussed below.

4.1.2.1 Preliminary Tests

ASME (1997) states that the preliminary test had to be performed before final testing could commence. The purpose of this test was to verify the operating range of the test bench and the stability of the measurements. With regards to measurement stability, Brun & Nored (2006) suggested that the compressor needed to be operated at least 30 minutes prior to the test. This duration was required to achieve a complete heat soak and for the temperature probes to reach equilibrium. Moreover, an interval of

10 minutes between each measurement was considered to be acceptable if the variation between the measurements adhered to the range provided by ASME (1997) and Brun & Nored (2006) (Table 4.1).

Table 4.1: Stability criteria for compressor measurements (Adapted from ASME (1997) and Brun & Nored)

Parameters	ASME	Brun & Nored
Inlet temperature	0.5 %	± 1 ℃
Outlet temperature	0.5 %	± 1 ℃
Inlet pressure	2.0 %	± 1 % of average value
Outlet pressure	2.0 %	± 1 ℃ of average value
Speed	0.5 %	± 10 rpm
Mass flow rate	0.5 %	± 1 % of average value

There were three preliminary tests performed at three operating speeds namely, 60 000, 80 000 and 100 000 rpm. It was noted that the operating time of 30 minutes prior to the test was not feasible as the capacity of the compressed air tank limited the operation. For the same reason, a 10-minute time interval between each measurement was not attainable. However, from the preliminary tests, it was noted that the stability of the readings could be obtained with a time interval ranging from 2 to 4 minutes.

The preliminary tests assisted in estimating the operating time, which was inherently different for each speed. According to ASME (1997) at least five test points were required to complete a performance curve. During the preliminary test, it was noticed that six test points per speed were easily attainable. These test points were evenly spaced from choke to the onset of the surge.

Furthermore, the throttling valve position corresponding to the respective compressor mass flow rate was noted. This helped in reaching the intended test point quickly during the final tests, allowing more time for the measurements to stabilize. Additionally, a

detailed operating procedure for the operation of the test bench was compiled, which is presented in Appendix D. This operating procedure was strictly followed for the final tests.

4.1.2.2 Final Tests

Final tests were conducted to obtain the performance curves for the centrifugal compressor. These tests were conducted by following the procedure compiled from the preliminary tests (Appendix D). There were two sets of tests conducted to analyze the stability and the repeatability of the measurements. The data was sampled at a rate of 10 S/s for a duration of 10 seconds.

The stability of the measurements was tested by acquiring four sets of data with 100 samples each for every test point. The repeatability of the measurements was tested by operating the test bench at a specific speed thrice, consecutively. After each test run, the test bench was allowed to cool down for at least 1.5 hours and operated at a different speed. The post-processing of the data to generate the performance curves of the centrifugal compressor, along with the stability analysis are presented in subsequent sections.

4.2 Data Reduction and Post-processing

After all the necessary measurements were acquired, the processing of the data could be initiated. This processing was done with the use of a code written in MATLAB. Post-processing of the data involved the correction of measured values using calibration curves, statistical analysis of the corrected measurements and finally the computation of the centrifugal compressor's and turbine's performance parameters. This section explains the procedure followed in the post-processing of the data.

4.2.1 Statistical Analysis

Figliola & Beasley (2015) states that a better statistical estimation is achieved by conducting repeated tests and obtaining pooled data where M is the repeated number of tests and N is the number of samples. As mentioned in Section 4.1.2 three sets of

data were obtained (M = 3) with each data set including 100 samples (N = 100). In order to obtain a single value that best represents the average and the variation in the measured data, the statistical approach described by Figliola & Beasley (2015) was utilized. The true mean value (x') of a measured variable is defined by Equation 4.1.

$$x' = \bar{x} \pm t_{v,P}\langle S_{\bar{x}} \rangle \quad (P\%) \tag{4.1}$$

where $\bar{x}$ is the mean of the samples and $\pm t_{v,P}\langle S_{\bar{x}} \rangle$ represents the confidence interval about the mean value at the assigned probability ($P\%$). Furthermore, the pooled mean and pooled standard deviation of the mean are defined as Equation 4.2 and 4.3 respectively.

$$\bar{x} = \frac{1}{MN}\sum_{j=1}^{M}\sum_{i=1}^{N} x_{ij} \tag{4.2}$$

$$\langle S_{\bar{x}} \rangle = \frac{\sqrt{\frac{1}{M-1}\sum_{j=1}^{M}(\bar{x}_j - \langle \bar{x} \rangle)^2}}{\sqrt{M}} \tag{4.3}$$

The calculation of the compressor performance was carried out using the pooled average of each measured quantity. The average of the pooled averages was used for the temperature measurements since there were four measurements obtained at each temperature measuring station.

In order to evaluate the stability of the compressor's operation, the fluctuation of the measurements was calculated when operating at steady conditions. ASME (1997) provided an equation to compute these fluctuations. It was defined as the difference between the maximum and minimum test sample divided by the sample average (Equation 4.4).

$$\Delta F = \frac{100(x_{max} - x_{min})}{\frac{1}{N}\sum_{i=1}^{N} x_i} \tag{4.4}$$

Fluctuations of three test points namely surge, best efficiency and choke were then compared with the permissible fluctuations provided in Table 4.1. The results of the comparison are shown in Section 6.1.

4.2.2 Compressor Performance

The performance of the compressor was defined by the parameters such as total-static pressure ratio, total-total efficiency, and corrected mass flow rate. The computation of these parameters is explained with the help of a schematic of the compressor side shown in Figure 4.1.

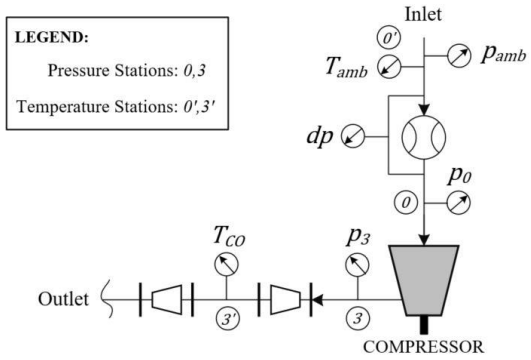

Figure 4.1: Compressor side – Pressure and temperature stations

At the inlet of the compressor, ambient temperature and pressure values (T_{amb}, p_{amb}) were used to calculate the density of the air (ρ_{amb}). The air density was then used along with the differential pressure across the bellmouth (Δp_{bm}) to calculate the velocity through the bellmouth (V_{bm}) with the help of Equation 4.5. This velocity could be used to calculate the Reynolds number (Re_{bm}).

$$V_{bm} = \sqrt{\frac{2\Delta p_{bm}}{\rho_{amb}(1-\beta^4)}} \tag{4.5}$$

It is important to note that the value of β approaches zero ($D \gg d$) for the bellmouth. Following this, the discharge coefficient of the bellmouth ($C_{d,bm}$) was calculated with

the help of Equation 4.6. This equation was obtained from the bellmouth calibration performed by Struwig (2014).

$$C_{d,bm} = e^{\frac{-1500}{Re_{bm}}} \tag{4.6}$$

The mass flow rate through the compressor can now be calculated using Equation 3.4. The total pressure at the compressor inlet was computed using Equation 4.7.

$$p_{t0} = p_{s0} + \rho_{amb} \frac{{V_{bm}}^2}{2} \tag{4.7}$$

In order to compute the total conditions at the outlet of the compressor, a method presented in ASME PTC-10 was utilized. This method is an iterative method that treats air as an ideal gas and it is explained with the help of the flow diagram shown in Figure 4.2. It must be noted that the effects of humidity, as well as dry and wet bulb temperature, were not considered.

The method initially sets the static outlet temperature (T_{s3}) equal to the measured temperature (T_{CO}). This was used to compute the static properties of the air such as the specific heat ($c_{p,3}$), specific heat ratio (γ_3), and the density (ρ_3). These properties along with the diameter of the outlet pipe were then used to compute the outlet velocity (V_3) and corresponding Mach number (Ma_3). The velocity was then used to compute the total temperature at the outlet (T_{t3}) using Equation 3.3. The Mach number along with the total temperature was used to compute the new static temperature ($T_{s3,new}$) using Equation 4.8.

$$T_{s3,new} = \frac{T_{t3}}{1 + \left(\frac{\gamma_3 - 1}{2}\right) {Ma_3}^2} \tag{4.8}$$

It is important to note that the compressibility of the flow for Ma $>$ 0.3 was taken into consideration with the help of the criteria presented in the literature (Çengel & Cimbala, 2008). In the case of the Mach number exceeding 0.3, an average of the total and static

temperature was used to compute specific heat at a constant pressure using Equation 4.9.

$$\bar{c_p} = 28.11 + 0.1967 \times 10^{-2}T + 0.4802 \times 10^{-5}T^2 - 1.966 \times 10^{-9}T^3 \quad (4.9)$$

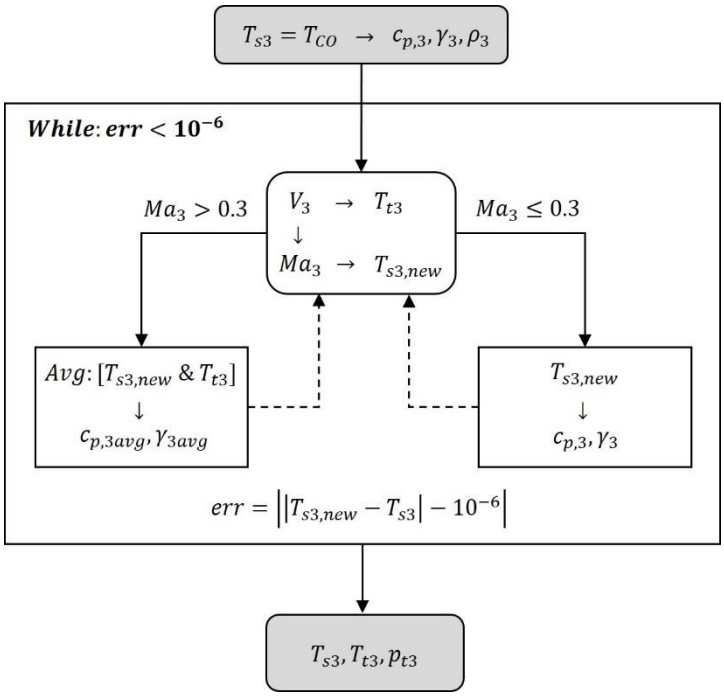

Figure 4.2: Obtaining total conditions at the compressor outlet – Iterative method

The above process was repeated until convergence of the static temperature at the outlet of the compressor (T_{s3}) was reached. Following that, the total pressure at the outlet of the compressor was computed using Equation 4.10.

$$p_{t3} = \frac{p_{s3}}{\left[1 + \left(\frac{\gamma_3 - 1}{2}\right) {Ma_3}^2\right]^{\frac{\gamma_3}{\gamma_3 - 1}}} \quad (4.10)$$

Once the total and static conditions at the inlet and outlet of the compressor were obtained, the total-total efficiency of the compressor could be computed using Equation 4.11.

$$\eta_{C,t-t} = \frac{\left({}^{p_{t3}}/_{p_{t0}}\right)^{\frac{\gamma}{\gamma-1}} - 1}{\left({}^{T_{t3}}/_{T_{t0}}\right) - 1} \tag{4.11}$$

The sample calculation for the performance of the compressor is presented in Appendix B.3

4.2.3 Turbine Performance

The turbine was used as a driver of the centrifugal compressor, therefore, it was not essential to generate well-defined performance curves for the turbine. However, in order to define the overall specification of the test bench, it was necessary to compute certain parameters from the data obtained from the tests. These parameters included the mass flow rate, total-static pressure ratio, and total-static efficiency of the turbine.

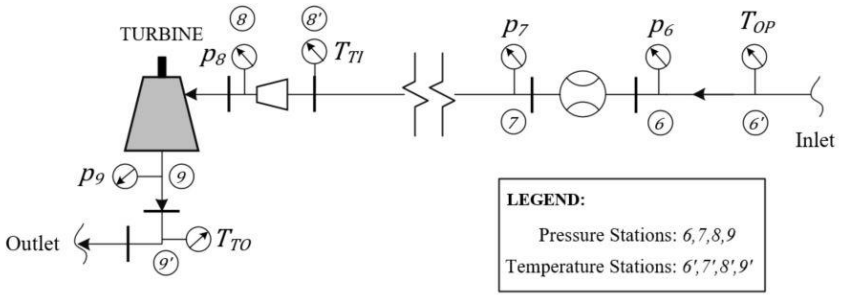

Figure 4.3: Turbine side – Pressure and temperature stations

The calculation of these parameters is explained with the help of a schematic of the turbine side shown in Figure 4.3. An iterative method (Figure 4.4) was used to determine the mass flow rate through the turbine. This method starts by setting the static pressure and temperature equal to the measured values at stations 6 and 6' respectively. These values were used to compute the static properties of air such as the density (ρ_6), specific heat at constant pressure (c_P), and specific heat ratio (γ) using the ideal gas law and Equation 4.9.

After this, an initial mass flow rate through the orifice plate ($\dot{m}_{OP}$) was computed with the assumed value of flow coefficient ($C_d = 0.6003$) and pressure drop across the orifice plate ($\Delta p_{OP} = p_6 - p_7$) using Equation 3.4.

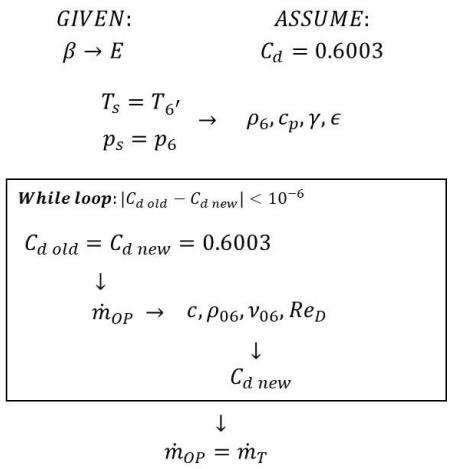

Figure 4.4: Turbine mass flow rate – Iterative method

The initial value of the mass flow rate was then used to obtain the dynamic properties of the air such as the velocity (c), total density (ρ_{06}), and kinematic viscosity (ν_{06}). These properties were then used to compute the Reynolds number (Re_{OP}), which in turn was used to compute a new value for C_d. This process was repeated until an acceptable convergence (10^{-6}) was reached for C_d. Thereafter, $\dot{m}_{OP}$ was computed and set equal to the mass flow rate through the turbine ($\dot{m}_T$).

The methodology followed to compute the total and static conditions at the inlet and outlet of the turbine were similar to those used for the compressor. These conditions were then used to compute the total-total efficiency of the turbine with the help of Equation 4.12.

$$\eta_{T,t-t} = \frac{1 - \left({}^{T_{t9}}/_{T_{t8}}\right)}{1 - \left({}^{p_{t9}}/_{p_{t8}}\right)^{\frac{\gamma-1}{\gamma}}} \tag{4.12}$$

5 Test Bench Simulations

5.1 Introduction

This chapter describes the modelling and simulation of the compressor test bench. The goal of the modelling was to reproduce the results which were obtained experimentally. In the future, the model can be used to observe the effects of proposed modifications before implementing it into the actual test bench. In order to accurately simulate the test bench, every component used in the test rig had to be modelled, along with its true size and characteristics. For this purpose, it was decided to perform a one-dimensional (1D) flow analysis on the test bench.

The 1D flow analysis was performed using the Flownex® Simulation Environment version 8.9.1. It is suited for the analysis of a system that is driven by a fluid. It allows the user to examine the effect a component will have on the whole system by altering its properties. Furthermore, it allows users to design and optimise the system according to their requirements.

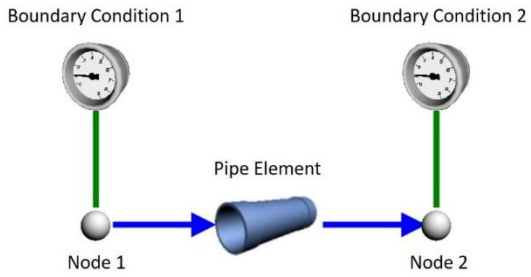

Figure 5.1: Basic Flownex® network (Flownex-FTM, 2018)

The governing equations of mass, momentum, and energy conservation are represented in terms of partial differential equations (PDEs) and some components are represented in terms of empirical formulas. Flownex® solves the PDEs along with the empirical formulas by implementing the implicit pressure correction method (IPCM), which is a solution algorithm to calculate the mass flow rate, pressure and temperature throughout the network (Flownex-FTM, 2018).

A thermo-fluid system is referred to as a network and it is composed of at least two boundary conditions (BCs) and one or many components which are known as elements (Figure 1). A point where two elements are connected to each other is referred to as a node. In order to obtain realistic results, it is imperative that the boundary conditions are realistic. For a transient simulation, the initial conditions need to be realistic, which is usually the steady-state solution of a network.

An example of empirical formulas used in Flownex® is the general empirical (GE) relationship element. It is commonly used to model pressure drop through experimental equipment, valves, and heat exchangers. For the validity of the GE model, it is assumed that no work is done on/by the fluid, the flow is quasi-steady, and the volume contribution of the GE is negligible compared to the volume of the system (Flownex-FTM, 2018). The total pressure drop Δp_0 through the GE relationship element is defined by Equation 5.1.

$$\Delta p_0 = C_k \rho^{\beta} Q^{\alpha} + \rho g \Delta z \tag{5.1}$$

where C_k, α and β are pressure drop constants and Δz is the change in elevation from inlet to outlet.

5.2 Methodology

This section describes the objectives of the simulations and the approach to accomplish those objectives. It further discusses the complications experienced throughout the simulation process and their solutions.

5.2.1 Simulation Objectives

The objectives of the simulation are as follows:

- Build a network in Flownex® which represents the compressor test bench.
- All the components should be modelled with their true size and characteristics to accurately represent the actual test bench.

- The operation of the network must be similar to the actual test bench in order to obtain a good comparison between results.
- Examine the performance of the network and compare it with the data obtained experimentally.

5.2.2 Approach

In order to simulate the test bench accurately, it was necessary to obtain the dimensions of all the components and most importantly the characteristics of components such as valves and turbomachinery used in the test bench.

Flownex® required the characteristic curves for elements such as valves, turbines, and compressors amongst others. This information was necessary to simulate the behavior of these components. All the required information for the components, except for the turbine, was available from the manufacturers.

The information for the specific turbine used on the test bench was unavailable. The manufacturers could only provide the turbine map for the turbine of a similar model, but it had a different serial number. Furthermore, the turbine map obtained from the manufacturers was incomplete as it does not specify the reference conditions at which the turbine was tested. There was only one speed curve available and it did not mention the corrected speed of the speed curve.

The unavailability of information for the turbine map made the turbine element a variable in the network. Therefore, it was decided to build a network without the turbine and validate it against the experimental results. Once a good comparison between the results was obtained, it ensured that all the hardware except the turbine and compressor were simulated accurately. The drawback of this approach is that the experimental results with the turbocharger cannot be compared with the simulation results. However, as mentioned previously the turbine is simply a component that is used to drive the compressor so the network can be validated by changing the current turbine in the test bench to a turbine, for which a turbine map is available.

5.3 Test Bench Modelling

This section describes the modelling of each component in the test bench along with its parameters. Furthermore, it briefly discusses the theory and assumptions which Flownex® takes into consideration to calculate the thermo-fluid properties.

The network was divided into two sections similar to the division of the pipeline system discussed in Section 3.2.1. The two sections, namely, compressed air supply connection and test bench were modelled separately. These sections were connected together by simply having a common node. This node represents the end of the compressed air supply connection and the start of the test bench section.

5.3.1 Compressed Air Supply Connection

The compressed air supply connection section of the network can be seen in Figure 5.2. As discussed previously, this section was composed of a tank, a shut-off valve, and a 12 m length of pipe that led to the laboratory. The number of elements used to model the compressed air supply connection is listed in Table 5.1.

Table 5.1: Elements used to model compressed air supply connection

Element Name	Number
Nodes	8
Pipe	4
Bend	3
Type C butterfly valve	1
Reservoir	1

To simulate the tank, a “reservoir” element was used. The reservoir element was basically a node component with restricted capability. It was subjected to the following assumptions (Flownex-FLM, 2018):

- The volume of the reservoir was completely filled with the fluid.
- Other than flow work and the effect of gravity, no work was done on the fluid in the reservoir.
- Static conditions were assumed for the fluid when a volume was assigned to a reservoir.

Struwig (2014) mentioned the tank capacity to be 88 m^3, which was specified as the volume of the reservoir element. This element was chosen as a datum level i.e. its elevation was set equal to 0. Static pressure and temperature boundary conditions (BCs) were implemented on this element. The pressure boundary condition was used for the transient analysis of the network, which is discussed in detail in subsequent sections. As there were no transducers attached to the tank, the temperature of the fluid in the tank had to be measured iteratively. The process of obtaining the tank temperature boundary condition is discussed in subsequent section.

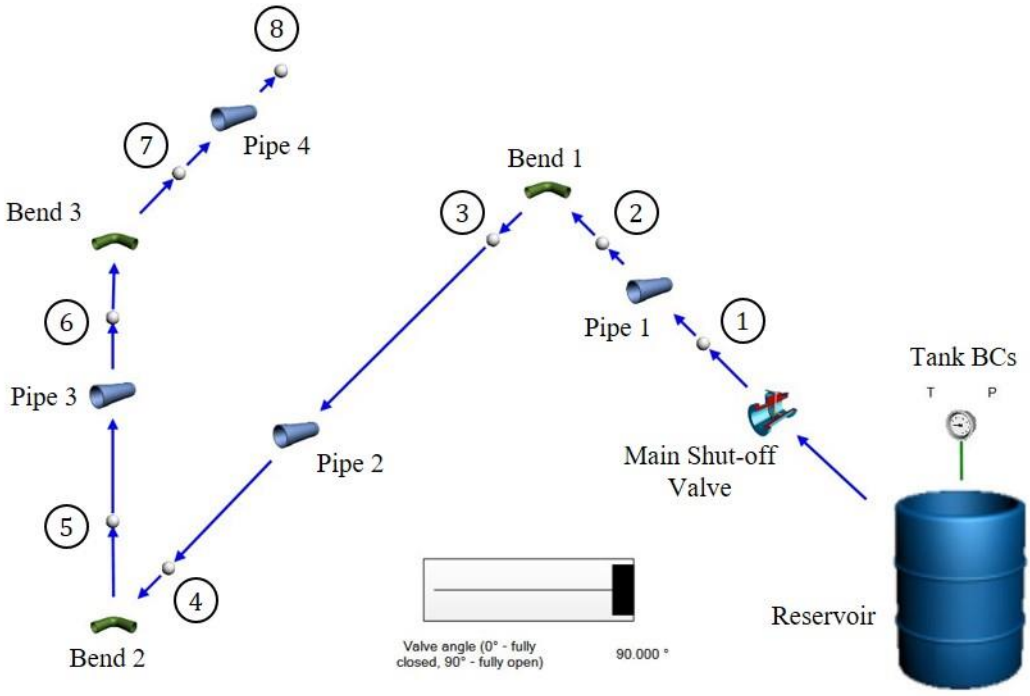

Figure 5.2: Compressed air supply connection network

The main shutoff valve was connected downstream of the tank and was represented by a Type C butterfly valve element in the network. There were three different types of butterfly valves in Flownex®, based on their disc shape (Figure 5.3). Type C best represents the main shutoff valve as well as all the other butterfly valves used in the test bench such as secondary and throttling valves.

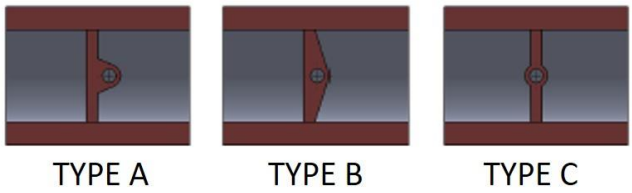

Figure 5.3: Butterfly valve disc types (Flownex Manual)

The butterfly valve element was subject to the following assumptions (Flownex-FLM, 2018):

- The GE relationship element (Section 5.1) is used for the butterfly valve.
- Choking cannot occur in this element.

The Type C butterfly valve required two inputs, namely a pipe diameter and the valve angle, which were set to 102.26 mm and 90º respectively. The diameter of the valve was similar to the upstream and downstream pipes and the valve was fully open during tests. The main shutoff valve was followed by a 12 m long pipeline system which was composed of four pipe sections and three 90º elbows. In order to represent these pipeline components, a pipe and bend element were used.

Pipe element was used to model friction and secondary losses and it was subject to the following assumptions (Flownex-FLM, 2018):

- The fluid was subsonic (Ma < 1) throughout the length of the pipe.
- Other than flow work and gravitation, no work was done on the fluid in the pipe.

- Ideal gasses with constant specific heat were used to relate total temperature to static temperature.
- The heat transfer through diffusion was disregarded.

The pipe element requires the geometry of the pipe, which was selected from the database as DN 100 and Schedule 40 which had a wall thickness and inner diameter of 6.02 mm and 102.26 mm respectively. The length of each pipe element, respective nodes and the orientation relative to the datum is summarized in Table 5.1. Furthermore, the roughness of the pipe was chosen from the database as "Seamless steel tubes – New, unused" which has a roughness (ϵ) of 60 μm.

Table 5.1: Length and orientation of the pipe elements

Pipe Elements	Length [m]	Node No.	Orientation
Pipe 1	0.788	1,2	Horizontal
Pipe 2	8.135	3,4	Horizontal
Pipe 3	2.370	5,6	Vertical
Pipe 4	1.500	7,8	Horizontal

The correlations for the bend element were derived from the theory of short circular arc bends (Figure 5.4). This element was subject to the following assumptions (Flownex-FLM, 2018):

- The flow was fully developed upstream and downstream of the element.
- Other than flow work and gravitation, no work was done on the fluid in the bend.
- The flow was considered adiabatic when using the empirical correlation to compute losses.

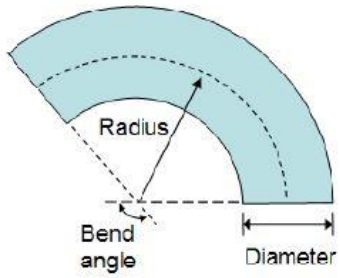

Figure 5.4: Geometry of circular arc bend (Flownex-FLM, 2018)

Similar to the pipe element, the geometry of the bend element was selected from the database as a "Long radius elbows" with DN 100 and Schedule 40. Therefore, the radius of the elbow was 152 mm and the wall thickness and wall roughness values were the same as for the rest of the system.

5.3.2 Test Bench

The test bench network without the test section can be seen in Figure 5.5. The number of elements used to model the test bench is listed in Table 5.2.

Table 5.2: List of elements used in the test bench network

Element Name	Number
Nodes	25
Pipe	13
Bend	2
Gradual pipe transition	4
British standard orifice	1
Restrictor with discharge coefficient	1
Type C butterfly valve	1
Ball valve	1
ANSI control valve	1

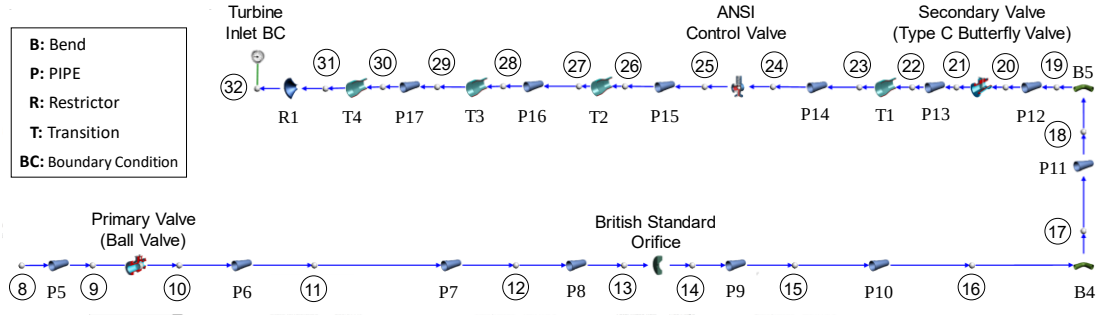

Figure 5.5: Test bench without the turbocharger

5.3.2.1 Pipeline System

The size of all the pipe elements was selected as DN 100 and Schedule 40 except pipe elements 13, 11 and 10. These pipe sizes were selected as DN 80 and Schedule 40 which had a thickness and inner diameter of 5.49 mm and 77.92 mm respectively. The length of each pipe element and the respective nodes is summarized in Table 5.1. Furthermore, the roughness of the pipe elements was chosen as before. The geometry of the bend element is the same as mentioned in Section 5.3.1.

Table 5.3: Length of pipe elements used in test bench network

Pipe Elements	Length [m]	Node No.	Geometry	Orientation
Pipe 5	0.5	8,9	DN 100, Sch 40	Horizontal
Pipe 6	0.6	10,11	DN 100, Sch 40	Horizontal
Pipe 7	2.3	11,12	DN 100, Sch 40	Horizontal
Pipe 8	0.1	12,13	DN 100, Sch 40	Horizontal
Pipe 9	0.05	14,15	DN 100, Sch 40	Horizontal
Pipe 10	1.45	15,16	DN 100, Sch 40	Horizontal
Pipe 11	0.48	17,18	DN 100, Sch 40	Vertical
Pipe 12	0.225	19,20	DN 100, Sch 40	Horizontal
Pipe 13	0.225	21,22	DN 100, Sch 40	Horizontal
Pipe 14	0.418	23,24	DN 80, Sch 40	Horizontal

Pipe Elements	Length [m]	Node No.	Geometry	Orientation
Pipe 15	0.418	25,26	DN 80, Sch 40	Horizontal
Pipe 16	0.928	27,28	DN 100, Sch 40	Horizontal
Pipe 17	0.092	29,30	DN 80, Sch 40	Horizontal

The reducers used in the test bench were modelled with a gradual pipe transition element, subject to the following assumptions:

- The GE relationship element (Section 5.2) was used for the gradual pipe transition element.
- It could not model choked flow.

The gradual pipe transition required geometric parameters such as the length of the transition, along with the upstream and downstream pipe diameters. The geometric inputs for all four elements are listed in Table 5.4. Transition elements 1 to 3 were used to model a reducer from 100 mm to 80 mm and vice versa. Transition 4 was used to model a turbine adapter which is further discussed later in this section.

Table 5.4: Transition element geometry parameters

Element No.	Length [mm]	Pipe Diameter [mm]	
		Upstream	Downstream
Transition 1	56	102.26	77.92
Transition 2	56	77.92	102.26
Transition 3	56	102.26	77.92
Transition 4	56	77.92	62.61

5.3.2.2 Valves

The primary and secondary valves were represented as a type C butterfly valve and ball valve element respectively. The pipe diameter and the valve angle for both of these valves were set to 102.26 mm and 90º.

The control valve used in the test bench was modelled with the ANSI control valve element. It was subjected to the following assumptions:

- The walls of the valve were considered to be adiabatic.
- Fluid mass and thermal inertia were negligible.
- The inlet and the outlet of the valve were situated two and six nominal pipe diameters upstream and downstream of the valve fitting.

The ANSI control valve required inputs such as the geometry, opening fraction and the flow characteristics of the valve. This information was provided by the manufacturer and the valve has a diameter of 80 mm. It must be noted that the valve diameter was different from the upstream and downstream pipe diameters and that the opening fraction of the valve varies with each simulation.

With regards to the flow characteristics, a valve flow coefficient (K_v) and pressure drop ratio factor (x_T) was required. The pressure drop ratio factor is defined as the pressure ratio at which the compressible flow will start to choke in the vena contracta (Flownex-FLM, 2018). Both of the flow parameters were inserted as a curve that was provided by SAMSON.

5.3.2.3 Orifice Plate

The orifice plate was represented as a British Standard orifice element that required the pipe inner diameter, orifice diameter, and the pressure tapping configuration. The pipe and orifice diameter were inserted as 102.26 mm and 38.4 mm respectively. The pressure tappings configuration was set to “D and D/2 tappings”.

5.3.2.4 Adapter

As discussed in Section 3.1.1, an adapter was used to convert the circular pipe cross-section to a rectangular turbine cross-section. There was no element available in Flownex which could represent this transition. Therefore, a gradual pipe transition element with outlet diameter as a hydraulic diameter (D_h) of 48.83 mm was used. All the elements used to represent the adapter along with its dimensions are listed in Table 5.5.

Table 5.5: Elements used to represent adapter

Element No.	Length [mm]	Pipe Diameter [mm]	
		Upstream	Downstream
Transition 3	56	102.26	77.92
Pipe 17	92	77.92	
Transition 4	56	77.92	48.83

5.3.2.5 Restrictor

A restrictor with a discharge coefficient was used at the end of the adapter when the turbine was not attached to the model. The outlet discharged air into the atmosphere, which implied that the recovery of static pressure was not required. For this reason, a restrictor with a discharge coefficient of 1 was used. It had a similar diameter to the outlet diameter of the adapter.

5.4 Transient Simulation

The functionality of the test bench had to be simulated using a transient event. In this case, the pressure in the tank dictated the operation of the test bench. The time it took for the tank to discharge fully was dependent on the percentage opening of the control valve. As the percentage opening of the control valve increases the discharge time decreases. For the same reason, it was not considered practical to obtain a curve that

represented the rate of change of pressure at different valve opening. Therefore, one transient event was defined for all the simulation runs.

The setup of the transient event was such that the pressure boundary condition of the tank was removed at a trigger point of 0. This resulted in a decrease in pressure over time starting at 0 s. The time step for the simulation was set to 10 ms and run mode as "Fast as possible". This was followed by preliminary simulation runs which led to the modification of the model. It must be noted that it was not possible to define constant boundary conditions for the reservoir element as the ambient conditions did not stay constant. Therefore, it was necessary to change the boundary condition for each simulation run.

5.4.1 Preliminary Simulation Runs

The preliminary simulation runs were performed to establish a method for the operation of the model such that the experimental and simulation results could be comparable. Additionally, it assisted in determining the accuracy of the model and identifying the modifications which could be implemented to further improve the accuracy of the model. The method followed to obtain the simulation results were similar to the operation of the test bench namely, opening the control valve at a certain percentage and allowing the compressed air tank to discharge.

It is important to note that there were no measurements taken at the compressed air tank, which implied that the exact conditions at the tank were unknown. However, the pressure and temperature measurement upstream of the orifice plate could be used to compute the boundary conditions (BCs) at the tank. This was done via a designer tool in Flownex® which allowed automatic calculation of components to obtain the desired operating condition of the system (Flownex®-GUM, 2018). Furthermore, as discussed previously, the operating conditions during the test did not stay constant, therefore an average value per test was used as a BC for a respective simulation run.

5.4.1.1 Control Valve Opening (5 – 100%)

Referring to the explanation in Section 4.1.1 this test was discontinuous. This implied that the boundary conditions after each interruption were inherently different. These BCs are tabulated in Table 5.6.

Table 5.6: Boundary conditions for CV (5 – 100%) preliminary simulations

CV (5 – 100%)	Tank – BCs		Turbine Inlet – BCs
Test Range	**Temp. [K]**	**Press. [kPa]**	**Press. [kPa]**
05 – 50 %	287.337	1150	102.572
55 – 80 %	288.197	1150	102.584
85 – 100 %	288.849	1150	102.482

5.4.1.2 Control Valve Opening (40 – 90%)

Based on the explanation in Section 4.1.1 two tests were performed which were referred to as Up and Down. The overall boundary conditions of the system are listed in Table 5.7.

Table 5.7: Boundary conditions for CV (40 – 90%) preliminary simulations

CV (40 – 90%)	Tank – BCs		Turbine Inlet – BCs
Test Name	**Temp. [K]**	**Press. [kPa]**	**Press [kPa]**
Up	286.418	1120	103.743
Down	286.285	1100	103.925

5.4.2 Modification of the Model

The accuracy of the model was based on parameters such as differential pressure over the orifice plate, mass flow rate, and the turbine inlet pressure. From the results of the preliminary simulation runs, it was noticed that the model predicted the same trend as the experimental results. However, the differential pressure over the orifice plate was

under-predicted which resulted in an underprediction of the mass flow rate, whereas the turbine inlet pressure was over predicted.

Various approaches could be considered for modification of the model to achieve the desired results. However, it was decided that the operation of the model should not be altered and to limit changes to the dimensions of the components. From the preliminary simulation runs, it was identified that quantities such as the flow coefficient (K_v) of the control valve and the adapter outlet diameter resulted in a considerable change in the above-mentioned parameters. Therefore, these quantities were altered to modify the model with the help of a designer tool.

The approach adopted to alter these quantities is explained with the help of the flow diagram shown in Figure 5.6. It started with the actual model and a control valve percentage opening of 90 %. The boundary conditions at the tank were then obtained. Thereafter, the valve coefficient was computed to acquire the desired mass flow rate. The required turbine inlet pressure was then used to compute the outlet diameter of the adapter. This resulted in two different pressures because of the restrictor. The difference in this pressure was then used to find the outlet diameter of the adapter without the restrictor.

Following the modification of the model, the final simulation runs were conducted in order to validate the model against the experimental results. The changes made to the model are summarized in Table 5.8.

Table 5.8: Actual and modified model quantities

Quantities	Units	Model	
		Actual	Modified
K_v	$[m^3/\sqrt{bar}.h]$	100.00	144.25
$d_{out,adpt}$	[mm]	48.83	70.50

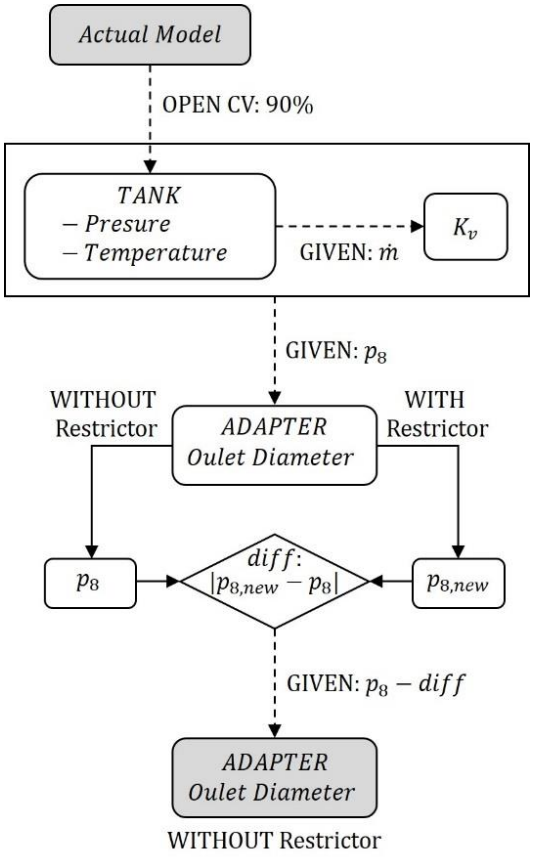

Figure 5.6: Procedure for modification of the model

The boundary conditions for the final simulations using modified model are same as the preliminary simulations. For the control valve opening (5 – 100 %) and (40 – 90 %) tests the BCs are listed in Table 5.6 and Table 5.7 respectively.

6 Results and Discussion

This section discusses the experimental and simulation results separately. The simulation results of the actual and modified models are then compared. Thereafter, the experimental results are compared to the simulation results of the modified model.

6.1 Experimental Results

6.1.1 Control Valve Opening (5-100%)

The mass flow rate and the turbine inlet pressure at varying control valve percentage openings are shown in Figure 6.1 (a) and (b). The dotted line between 5-50 %, 55-80 %, and 85-100 % represents discontinuities in the testing process. The trend of the graph shows that the test bench reached a maximum flow rate at 75% control valve opening. Further increasing the control valve opening to 80% caused the flow rate to decrease as the discharge flow was higher than the inlet flow of the compressed air tank. For the same reason the flow rate decreases drastically between 85 to 90% control valve opening.

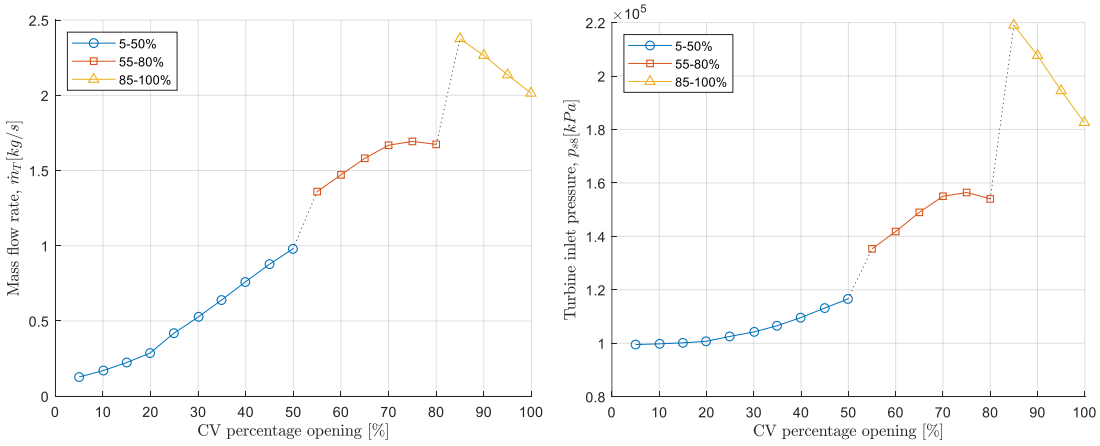

(a) (b)

Figure 6.1: CV 5-100% (a) Mass flow rate (b) Turbine inlet pressure

A similar trend was noticed in the turbine inlet pressure (Figure 6.1 (b)). The opening of the control valve resulted in a lower pressure drop across the valve, hence an increase in the static pressure at the turbine inlet. After reaching 75 % control valve opening, the supply pressure was not enough to compensate for the pressure drop over the control valve, which resulted in a decrease in the static pressure at the turbine inlet.

6.1.2 Control Valve Opening (40-90 %)

The fact that the test bench approached its maximum flow rate at 75 % control valve opening was also observed for the continuous test performed for 40-90 % (Up). The results of the tests are shown in Figure 6.2 (a and b). Ideally, the mass flow rate and the turbine inlet pressure should follow a similar trend for both up and down tests. However, due to the limited air supply, these trends were different. It was found that a higher mass flow rate and turbine inlet pressure could be achieved by closing the control valve from 90 % (down). This was due to the fact that the supply pressure at 90% for the down test was at its maximum which was higher than the up test.

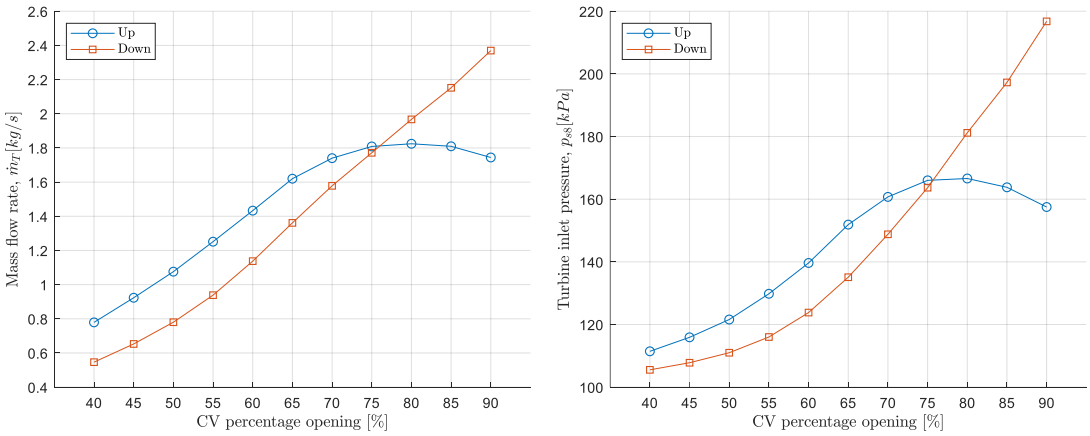

(a) (b)

Figure 6.2: CV 40-90 % (a) Mass flow rate (b) Turbine inlet pressure

6.1.3 Final Test

The measurements for the final tests were first analysed for the stability. This was done by calculating the fluctuations using Equation 4.4 and comparing it to the tolerance

listed in Table 4.1. The stability results for the measurement of three test points, namely onset of surge, highest efficiency, and choke are summarized in Table 6.1. The fluctuations were found to be low for the inlet conditions and high for the outlet conditions, but still within the tolerance provided by both criteria. The speed was the only parameter which exceeded the limit by a significant amount. This was attributed to the positioning of the sensor.

Ideally, the sensor should be placed such that it faces the outer face of the impeller as shown in Figure 6.3. This slot is usually cast into the volute. However, for this installation, a special installation point had to be machined into the casing, with a subsequent reduction in measurement precision (Figure 3.12 (a)).

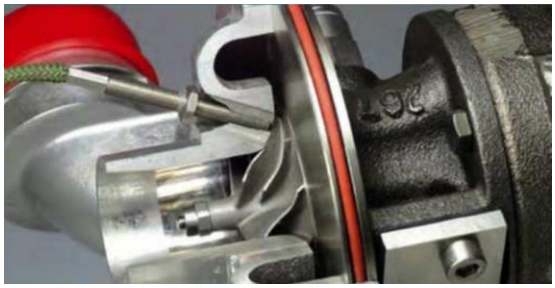

Figure 6.3: Prescribed positioning of the speed sensor (Micro-Epsilon, 2014)

Table 6.1: Stability results for the measurements of the compressor test bench

Speed [rpm]		**60 000**		**80 000**		**100 000**	
Criteria		ASME	Brun	ASME	Brun	ASME	Brun
Surge	Inlet temperature	0.1 %	0.2 ℃	0.1 %	0.2 ℃	0.2 %	0.4 ℃
	Outlet temperature	0.2 %	0.2 ℃	0.2 %	0.2 ℃	0.2 %	0.2 ℃
	Inlet pressure	0.3 %	0.2 %	0.4 %	0.2 %	0.4 %	0.3 %
	Outlet pressure	0.8 %	0.6 %	0.4 %	0.3 %	0.8 %	0.5 %
	Speed	1.4 %	842 rpm	1.7 %	1337 rpm	1.0 %	1043 rpm
	Mass flow rate	0.5 %	0.4 %	0.4 %	0.3 %	0.5 %	0.4 %

Speed [rpm]		**60 000**		**80 000**		**100 000**	
Criteria		ASME	Brun	ASME	Brun	ASME	Brun
Highest Efficiency	Inlet temperature	0.1 %	0.2 ℃	0.1 %	0.2 ℃	0.2 %	0.4 ℃
	Outlet temperature	0.2 %	0.2 ℃	0.2 %	0.2 ℃	0.2 %	0.2 ℃
	Inlet pressure	0.4 %	0.2 %	0.3 %	0.2 %	0.3 %	0.2 %
	Outlet pressure	0.5 %	0.4 %	0.6 %	0.4 %	0.7 %	0.6 %
	Speed	1.5 %	917 rpm	1.4 %	1095 rpm	0.9 %	928 rpm
	Mass flow rate	0.3 %	0.2 %	0.4 %	0.3 %	0.4 %	0.3 %
Choke	Inlet temperature	0.1 %	0.2 ℃	0.1 %	0.2 ℃	0.1 %	0.2 ℃
	Outlet temperature	0.2 %	0.2 ℃	0.2 %	0.2 ℃	0.5 %	0.7 ℃
	Inlet pressure	0.3 %	0.2 %	0.3 %	0.2 %	0.4 %	0.2 %
	Outlet pressure	0.8 %	0.6 %	0.8 %	0.6 %	0.7 %	0.5 %
	Speed	1.3 %	765 rpm	1.2 %	982 rpm	1.0 %	1020 rpm
	Mass flow rate	0.3 %	0.2 %	0.3 %	0.2 %	0.2 %	0.1 %

The test bench was then analysed for repeatability over three independent tests per speed. These three tests per speed were conducted on different days. This resulted in different ambient conditions for each speed, which are summarized in Table 6.2. The results presented in Figure 6.4 to Figure 6.7 are the averaged values of three tests per speed along with the 99% confidence interval. Ideally, all the speed curves must have similar ambient conditions in order to be plotted in one graph. However, it was ignored because of the slight variation in ambient conditions.

Table 6.2: Ambient conditions for each speed

Speed [rpm]	Ambient Conditions		Corrected Speed $[N/\sqrt{T_{t0}}]$
	Temperature [K]	Pressure [kPa]	
60 712.07	294.55	100.76	3537.47
80 710.39	297.32	99.66	4680.77
100 855.73	299.36	99.10	5829.10

Three test speeds along with a confidence interval of 99 % for each test can be seen in Figure 6.4. The overall speed remained constant and the confidence interval was narrow, which suggested that the tests were repeatable. The speeds of 60 000 rpm and 80 000 rpm had the highest confidence interval of $\pm$ 222 rpm and $\pm$ 144 rpm respectively at test point 2. For 100 000 rpm the highest confidence interval was $\pm$ 480 rpm at test point 4.

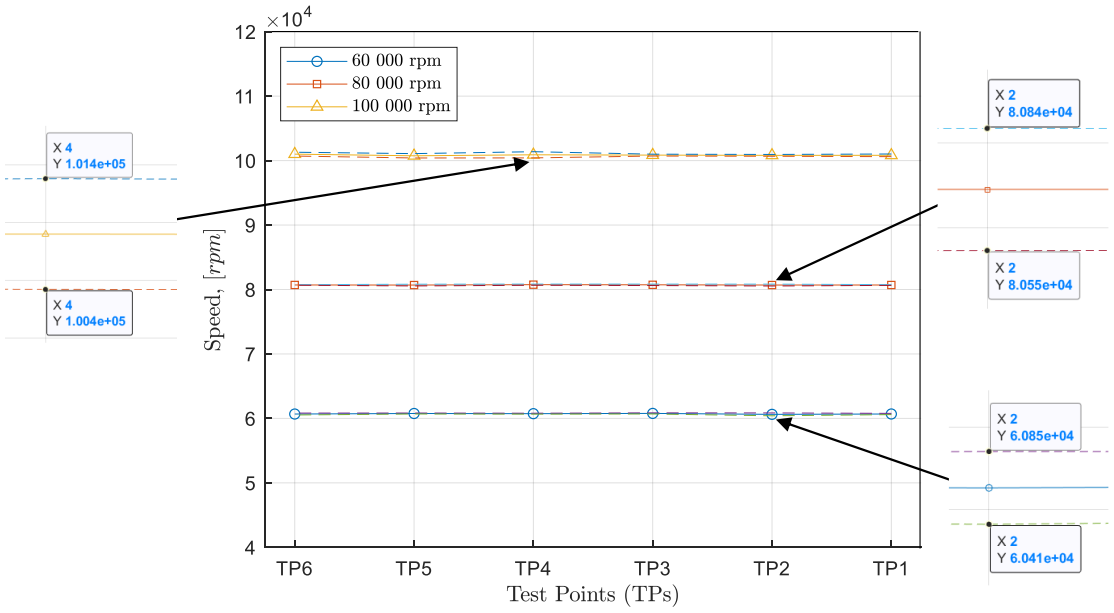

Figure 6.4: Operating speeds for the tests

The total to static (t-s) pressure ratio over the compressor was plotted against the corrected mass flow rate in Figure 6.5. The graph also shows a 99% confidence interval for each speed. This interval was small for 60 000 rpm and 80 000 rpm. For 100 000 rpm, the interval reached the highest value of 0.018 towards surge. It must be noted that the variation was very small, therefore it was neglected and overall the results for the pressure ratios were deemed repeatable.

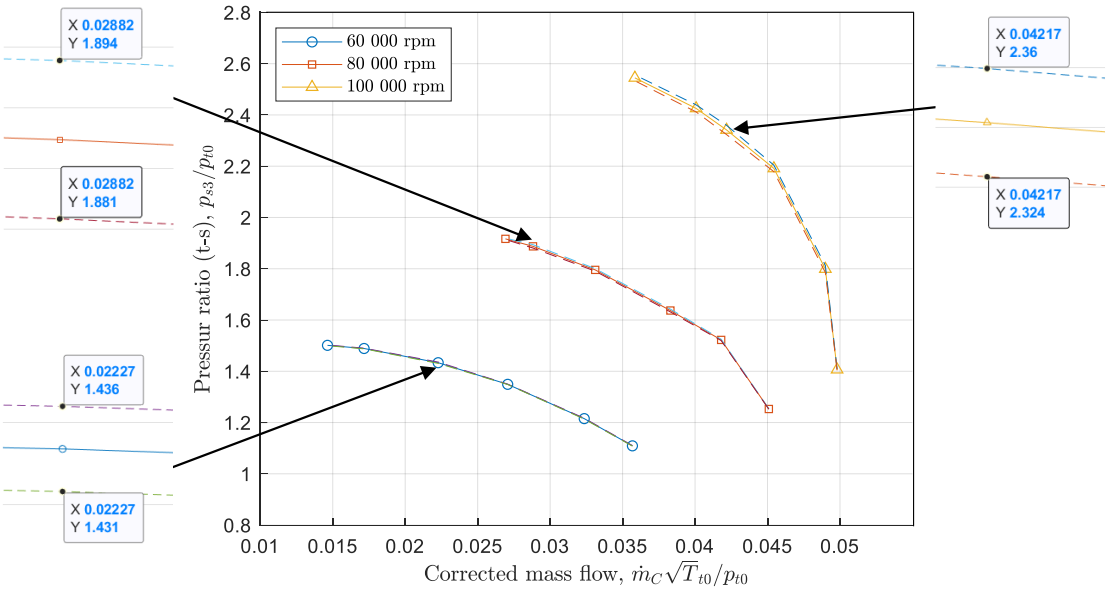

Figure 6.5: Total to static (t-s) pressure ratio over the compressor

Similarly, the total to total (t-t) temperature ratio versus corrected mass flow rate is shown in Figure 6.6. The confidence interval was small, as it reached its highest value of 0.0062 at 100 000 rpm. The total to total (t-t) efficiency is presented in Figure 6.7. For 60 000 rpm and 80 000 rpm, the compressor had a maximum efficiency of 0.80. At 100 000 rpm, the maximum efficiency was 0.77.

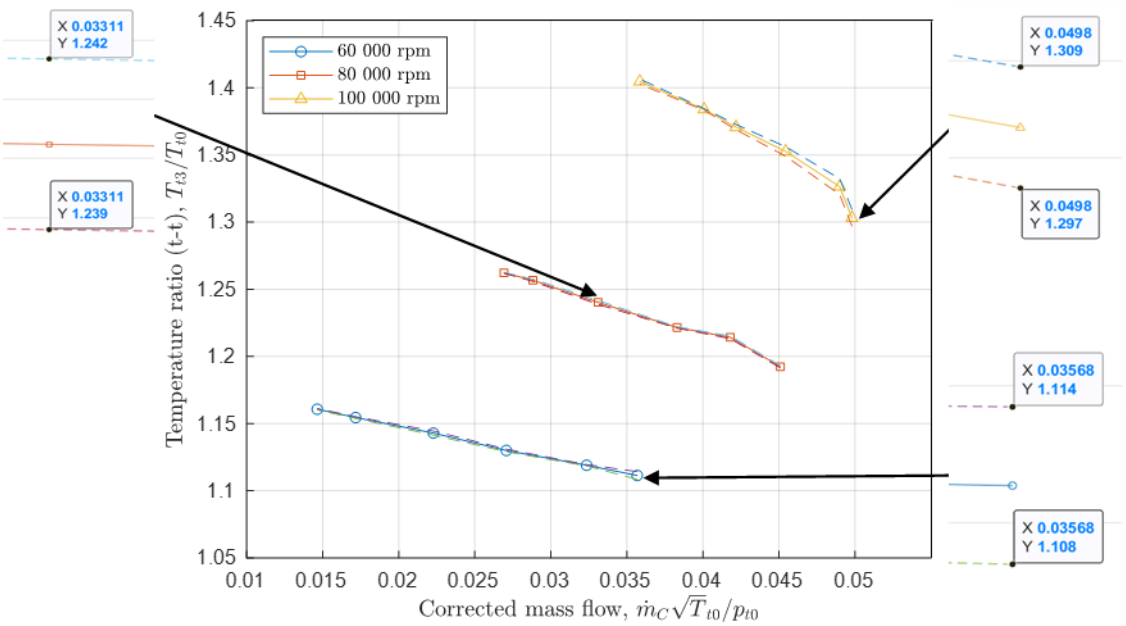

Figure 6.6: Total to total (t-t) temperature ratio over the compressor

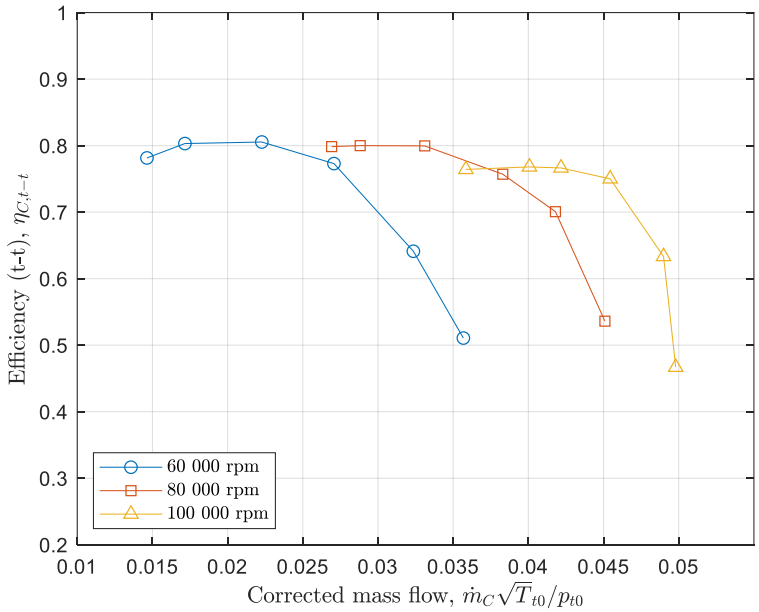

Figure 6.7: Total to total (t-t) efficiency of the compressor

6.2 Simulation Results

Only the simulation results of the continuous test for the actual and modified models are discussed, as a similar trend was observed for the discontinuous test simulation.

The simulation results for both the control valve percentage opening 40-90 % (Up) and (Down) tests are shown in Figure 6.8 and Figure 6.9. The increase in valve coefficient (K_v) resulted in an increase in the mass flow rate for the test bench. The original model over predicted the turbine inlet pressure when using a hydraulic diameter of 48.83 mm for the turbine inlet diameter. This was resolved by increasing the diameter to 70.50 mm.

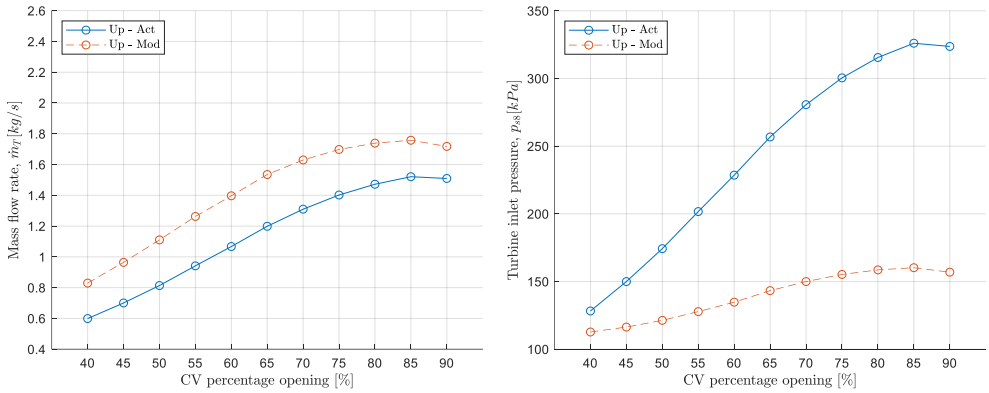

(a) (b)

Figure 6.8: CV 40-90 % - Up (a) Mass flow rate (b) Turbine inlet pressure

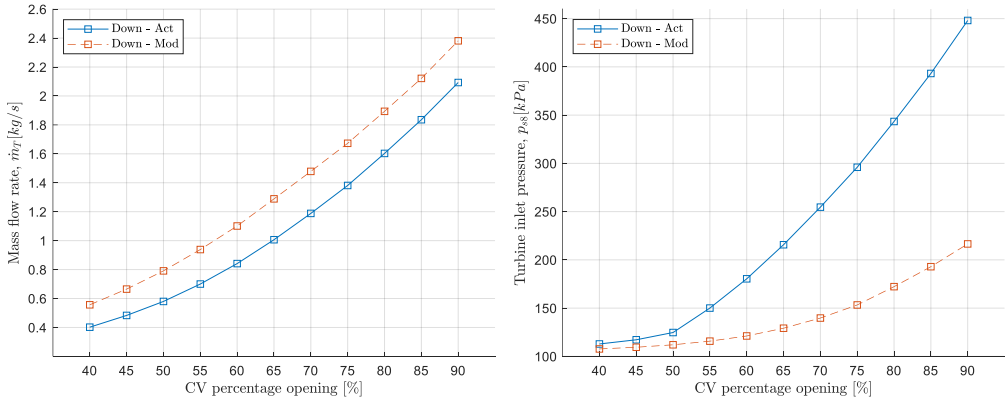

(a) (b)

Figure 6.9: CV 40-90 % - Down (a) Mass flow rate (b) Turbine inlet pressure

6.3 Results Comparison

In this section, the experimental results are compared to the simulation results of the control valve opening 40-90 % (Up and Down) simulations. For the comparison, only the results of the modified model were considered as it represents the test bench accurately.

Figure 6.10 (a) and (b) present the mass flow rate and turbine inlet pressure comparison for the CV opening 40-90 % - Up test. It was found that there was a good agreement with regard to the trend of the curve. The modified model represented the test bench very accurately at CV percentage openings lower than 60%. An interesting pattern was observed between 60-90 % CV opening for both the mass flow rate and the turbine inlet pressure. For the mass flow rate, the 2.5 % difference in values at 60 % CV opening increased and reached a maximum of 6.3 % at 70 % CV opening. It then decreased to 1.5 % at 90 % CV opening. The turbine inlet pressure showed a difference in values of 4.92 % at 60 % CV opening, which then increased to reach a maximum of 6.7 % at 70 % CV opening and decreased to 0.4 % at 90 % CV opening.

Possible reasons of the deviation encountered between 65 and 80% are the fluid conditions and valve area. The mass flow rate is dependent on the fluid conditions which implies that the air temperature in the simulations needs to be similar to the experimental values throughout the course of the simulation. This was difficult to achieve as the temperature variation experienced during the test was not linear. Furthermore, during the simulation, choked flow at the ANSI CV element was observed between 65 and 80 % CV valve opening. This was likely due to the x_T values used for the simulation as those were valid for the valve with the K_v=100.

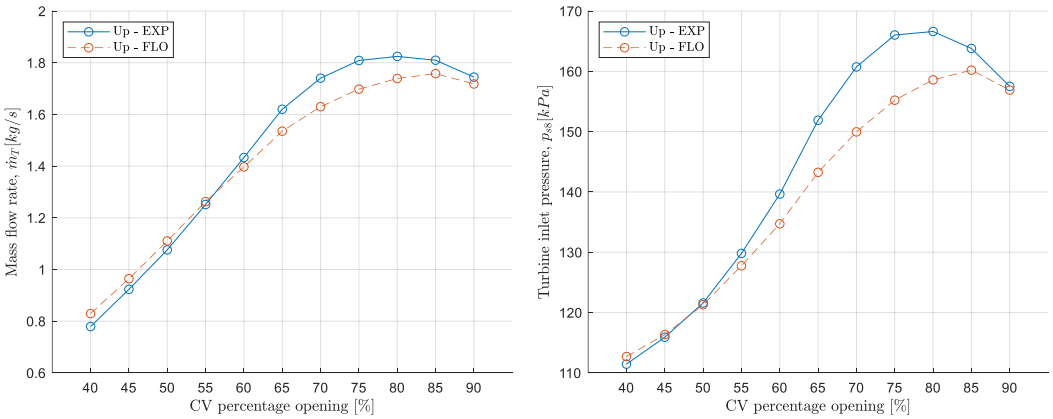

(a) (b)

Figure 6.10: Comparison of experimental and simulation results for CV 40-90 % - Up (a) Mass flow rate (b) Turbine inlet pressure

A similar pattern was observed for the mass flow rate and turbine inlet pressure comparison for the CV opening 40-90 % - Down test (Figure 6.11 (a) and (b)). For the mass flow rate, the difference in values of 3.2 % at 60 % CV opening increased and reached a maximum of 6.3 % at 70 % CV opening. It then decreased to 0.5 % at 90 % CV opening. The turbine inlet pressure showed a difference of 2.2 % at 60 % CV opening, which increased to reach a maximum of 6.4 % at 70 % CV opening, and later decreased to 0.1 % at 90 % CV opening.

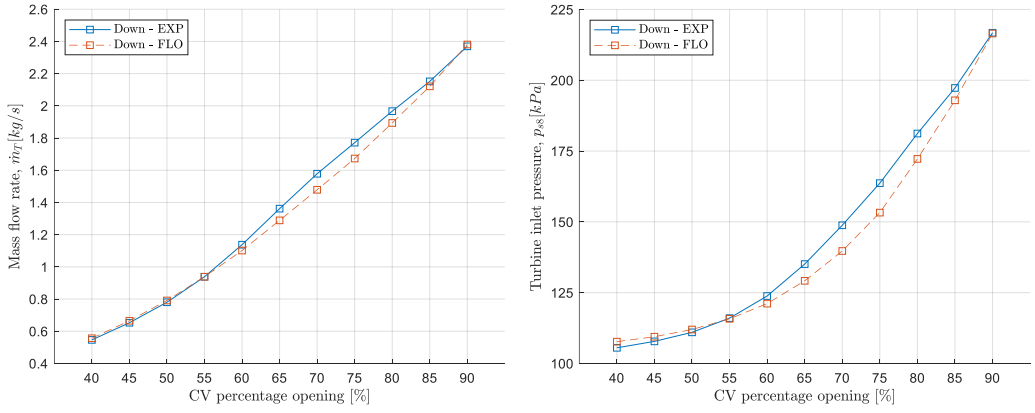

(a) (b)

Figure 6.11: Comparison of experimental and simulation results for CV 40-90 % - Down (a) Mass flow rate (b) Turbine inlet pressure

7 Conclusion and Recommendations

7.1 Conclusion

The project was set out to design a test bench for the centrifugal compressors used in micro gas turbines. The purpose of the test bench was to characterize the newly designed components by generating performance maps of the compressor. The operation of the test bench was proven by testing a KKK K27 compressor up to speeds of 100 000 rpm. The high discharge rate of the compressed air tank limited the operation at higher speeds.

National Instruments™ high-speed modules in conjunction with LabVIEW™ software were used as a data acquisition system for the test bench. The speed of the compressor was controlled with the help of a control valve coupled with a pneumatic actuator and a positioner. The control was achieved with the help of a PI controller. The mass flow rate through the compressor was regulated using a throttling valve which was coupled to an electric actuator and a positioner. A secondary valve was also installed on the test bench which acted as a safety valve and it was coupled to a pneumatic actuator coupled with a solenoid valve with open and close configuration.

A model of the test bench was created using Flownex® SE. The turbine map for the turbocharger was unavailable, therefore the model was simulated without the turbocharger. The actual model had to be modified by altering two parameters, namely the control valve coefficient (K_v) and the outlet diameter of the adapter. These parameters were changed to 144.25 $m^3/\sqrt{bar}$.h and 70.50 mm respectively to obtain better accuracy.

A comparison between the experimental and the simulation results was made for control valve opening of 40 % to 90 % (Up and Down) tests. It must be noted that these tests and simulations were conducted without the attachment of the turbocharger. An excellent agreement was observed between the two results for both of the tests. There were slight deviations noticed between 60 % - 90 % control valve opening. The

difference reached a maximum of 6.3 % and 6.7 % for the mass flow rate and turbine inlet pressure respectively, at 70 % control valve opening for the Up test. Similarly, the maximum difference of 6.3 % and 6.4 % was observed for the Down test. This

The pipeline system was designed with the safety factor of 18 for both 100 and 80 mm pipe. The welds and bolt connection were tested for strength and leaks by hydraulic testing at 1.5 times the operating pressure. Furthermore, all the valves used in the test bench were rated at least 2 times the operating pressure. The abovementioned design consideration ensured the durability of the test bench.

The modularity of the test bench was ensured by avoiding use of one continuous pipe. A series of pipe sections were bolted together, which will assist in the installation of components such as combustor (heating system). This can be done by simply bolting it between two flanges and shifting the test section. It must be noted that the test section base can be slotted and moved by at least 1.8 m which will provide ample space to install variety of components in line with the test section. Furthermore, control valve can withstand temperature in excess of 560 °C which allows the installation of heating system without replacing existing components. Above mentioned points regarding the durability and the modularity have been added to the thesis where applicable.

Overall, the project achieved all of its objectives. It is unfortunate that the simulation results with the turbocharger could not be obtained. However, a turbine with turbine maps can be used in the test bench to validate the model which includes the turbocharger.

7.2 Recommendations

Throughout the project several concerns related to the experimental work, post processing, and simulations were identified. Following are the recommendations for future work:

- Compressed air tank must be equipped with the temperature and pressure transducers to obtain air inlet conditions. This will assist in improving the 1D model of the test bench.
- Test bench should be equipped with a dedicated mass flow meter for the turbine in order to obtain more accurate measurement of the mass flow rate and to avoid its computation during post-processing.
- Two pressure transducers must be installed upstream and downstream of the control valve to evaluate the pressure drop across the valve. This will assist in troubleshooting the 1D model and simulation process in broader sense.
- It is recommended to install instruments such as Kiel probes which can measure total conditions at the inlet and outlet of the compressor. This will decrease the errors which are usually incurred during post-processing of experimental data.
- A feedback control must be implemented for the throttling valve to obtain better control of the compressor mass flow rate.
- It is recommended that two separate control loops must be designed in the LabVIEW for both the speed and mass flow rate feedback control to unify the system.
- The control valve and throttling valve opening percentage must be incorporated in the LabVIEW so that its data can be logged along with all the measurements.
- The current turbocharger must be replaced with a different turbocharger.
    - The turbocharger should have complete turbine and compressor maps so that the compressor test bench model with the turbocharger can be completed.

    - A provision for a speed sensor must be available in order for a stable speed measurement.
- The adapter component of the test bench should be further analyzed using computational fluid dynamics (CFD) to better understand the discrepancies between actual and modified model.
- The outlet pipe of the compressor must be altered by removing the 90° elbow and letting the air discharge into the chimney.

Future work on these matters will further improve the operation of the test bench, stability of the measurements, and usability of the simulation model.

Appendices

A Instrumentation Calibration

A.1 Temperature Calibration

Figure A.1 to Figure A.4 presents the calibration curves for all the thermocouples installed on the test bench. The calibration curve equations for these thermocouples are listed in Table A.1.

Table A.1: Thermocouples calibration curve equations

Thermocouple	No.	Equation	R^2
Bellmouth (BM)	1	$y = 1.0067787x - 1.8126414$	0.999
	2	$y = 1.0049000x - 1.3221025$	0.999
	3	$y = 0.9900644x + 2.9730367$	0.999
	4	$y = 1.0036263x - 1.0885260$	0.999
Compressor Outlet (CO)	1	$y = 0.9821228x + 5.1430339$	0.999
	2	$y = 0.9758425x + 6.9800672$	0.999
	3	$y = 0.9804876x + 5.5850118$	0.999
	4	$y = 0.9765366x + 6.7476860$	0.999
Turbine Inlet (TI)	1	$y = 0.9758450x + 6.9900550$	0.999
	2	$y = 0.9816181x + 5.3954365$	0.999
	3	$y = 0.9809132x + 5.5401585$	0.999
	4	$y = 0.9823812x + 5.0585862$	0.999
Turbine Outlet (TO)	1	$y = 0.9692210x + 8.6662250$	0.999
Orifice Plate Upstream (US)	1	$y = 0.9987855x + 0.0778472$	0.999

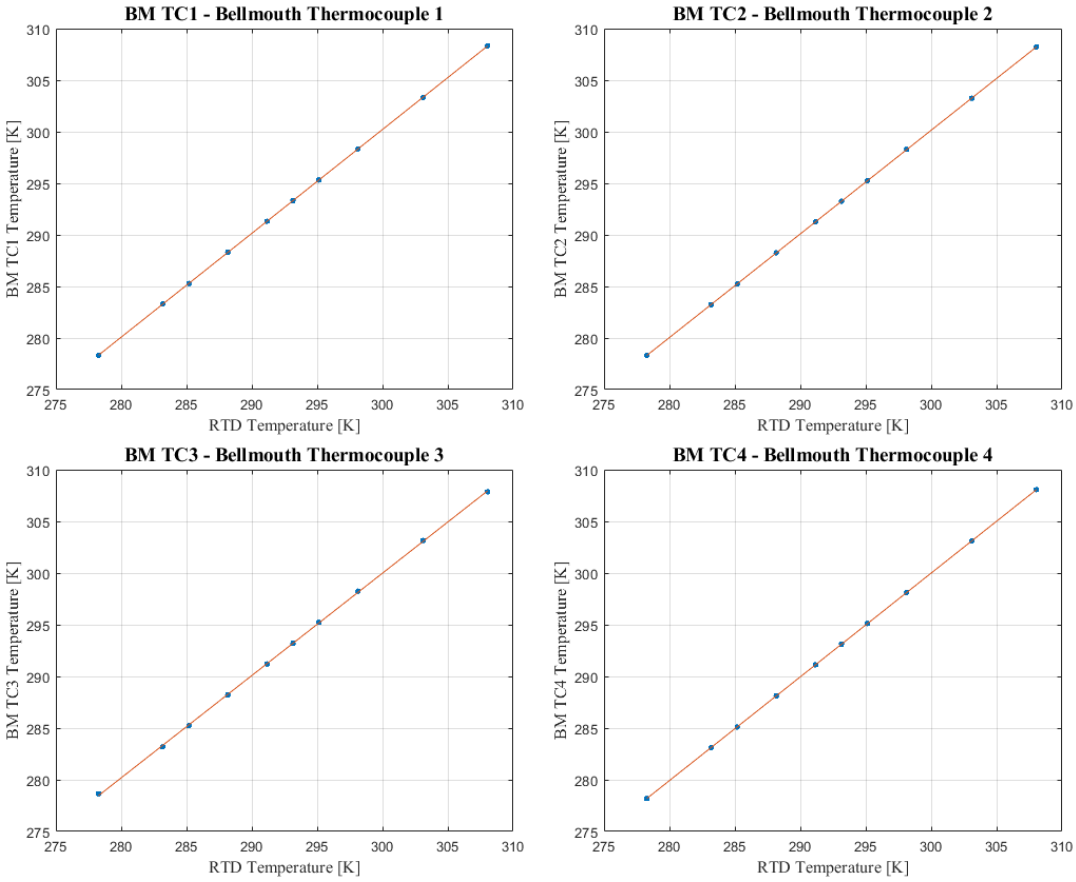

Figure A.1: Bellmouth (BM) thermocouple calibration curves

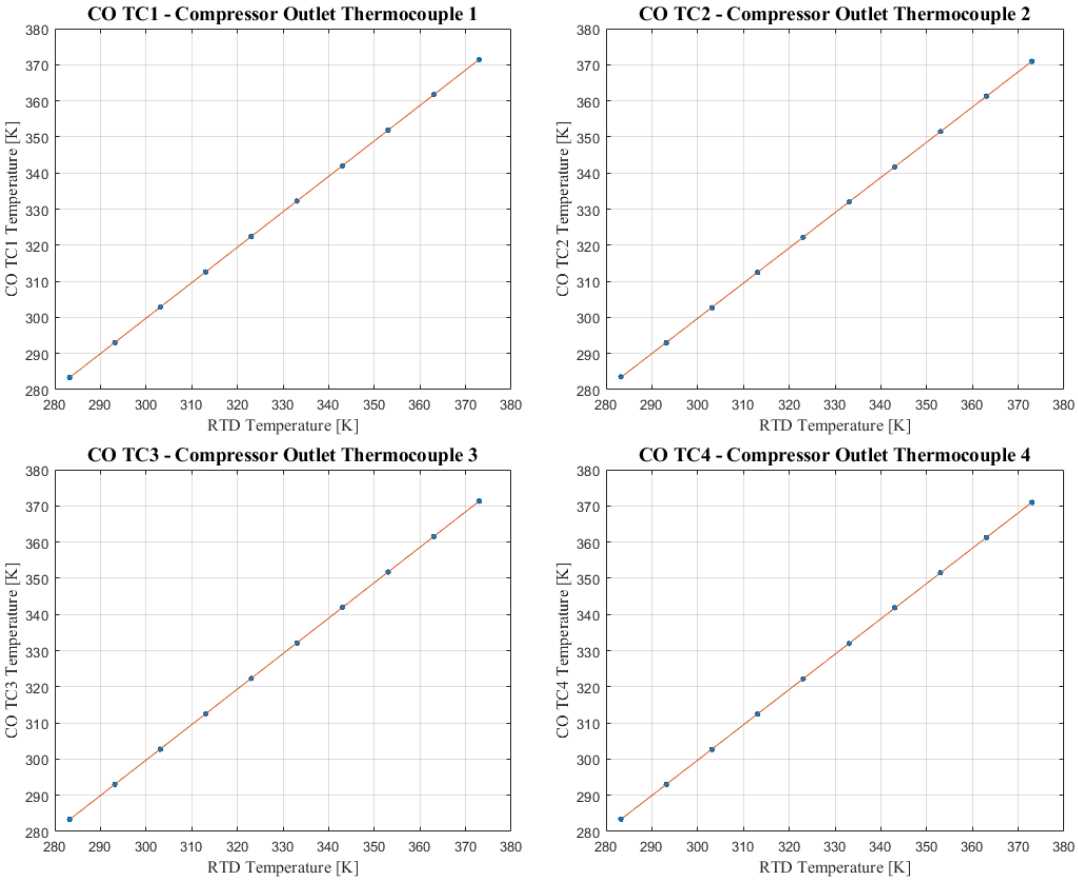

Figure A.2: Compressor outlet (CO) thermocouple calibration curves

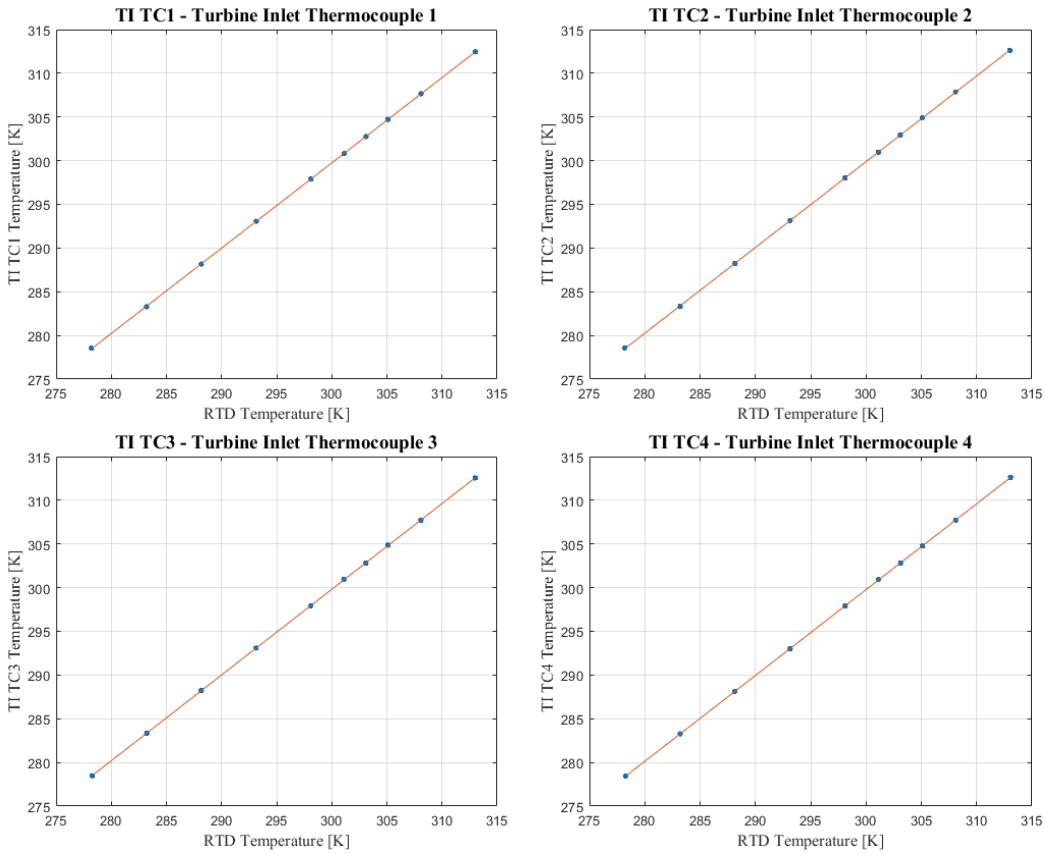

Figure A.3: Turbine inlet (TI) thermocouple calibration curves

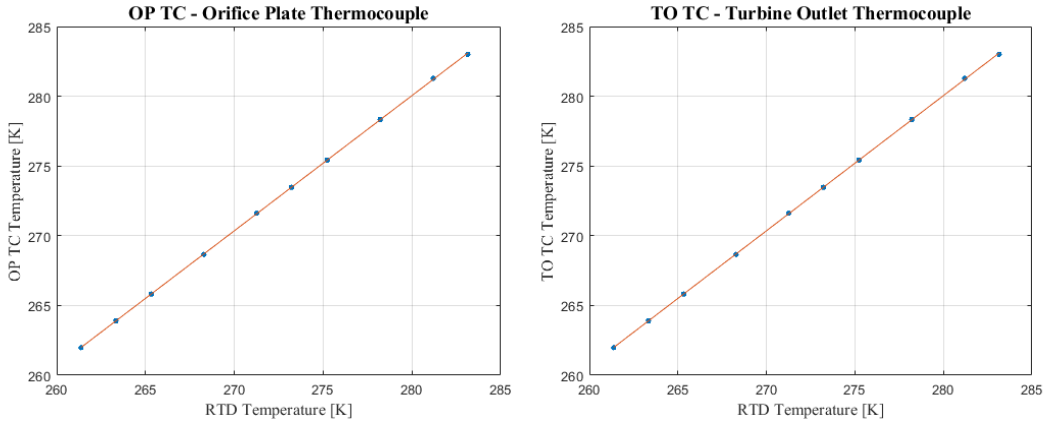

Figure A.4: Orifice plate (OP) and turbine outlet (TO) thermocouple calibration curves

A.2 Pressure Calibration

Figure A.5 to Figure A.9 presents the calibration curves for all the pressure transducers installed on the test bench. The calibration curve equations for these pressure transducers are listed in Table A.2.

Table A.2: Pressure transducer calibration curve equations

Placement	No.	Equation	R^2
Bellmouth	dp	$y = 0.9997859x + 0.0153029$	0.999
Compressor Inlet	0	$y = 19.639793x + 4.7748158$	0.999
Impeller Outlet	1	$y = 50.357535x - 5.3401679$	0.999
Diffuser Outlet	2	$y = 49.958552x + 13.532428$	0.999
Compressor Outlet	3	$y = 50.249401x - 3.2716762$	0.999
Orifice Inlet	4	$y = 109.62575x + 3.4701742$	0.999
Orifice Outlet	5	$y = 107.92591x + 20.887734$	0.999
Turbine Inlet	6	$y = 60.694844x - 6.6283831$	0.999
Turbine Outlet	7	$y = 60.204463x - 2.2401059$	0.999
Lubrication Oil	8	$y = 91.665613x - 15.616828$	0.999
Atmospheric	9	$y = 72.110894x - 378.96453$	0.999

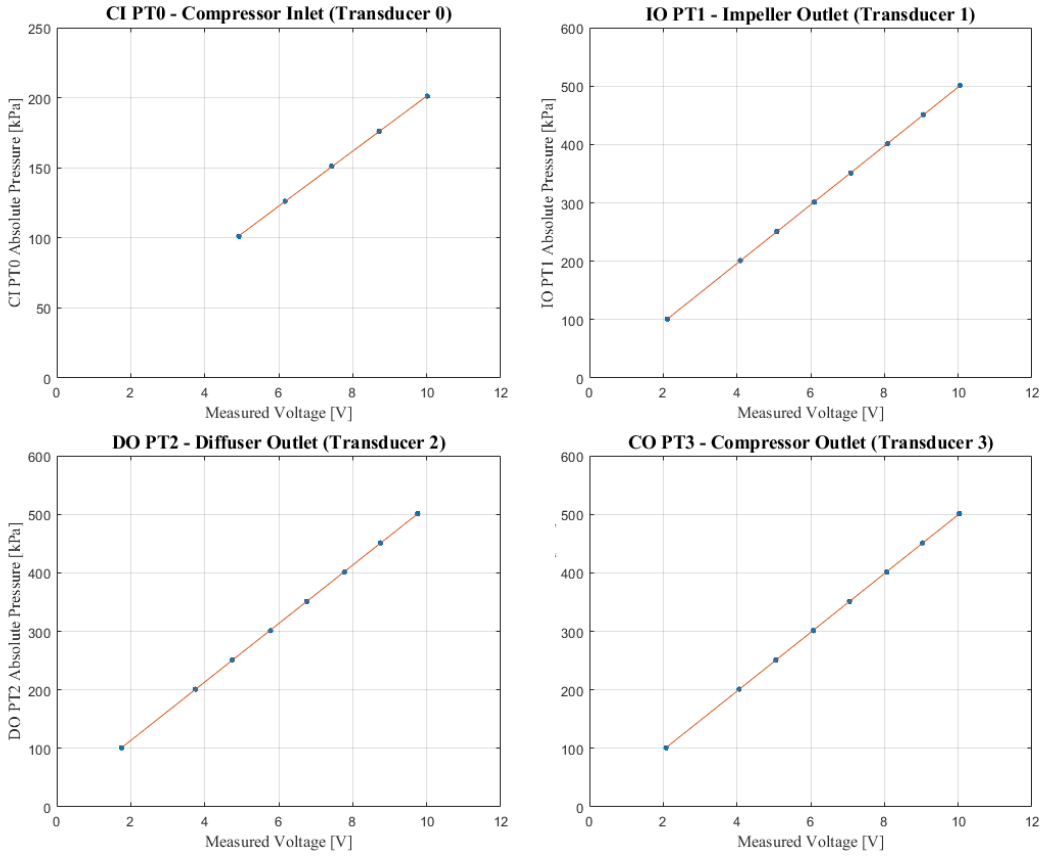

Figure A.5: Calibration curves of pressure transducers (0 – 3) on the compressor

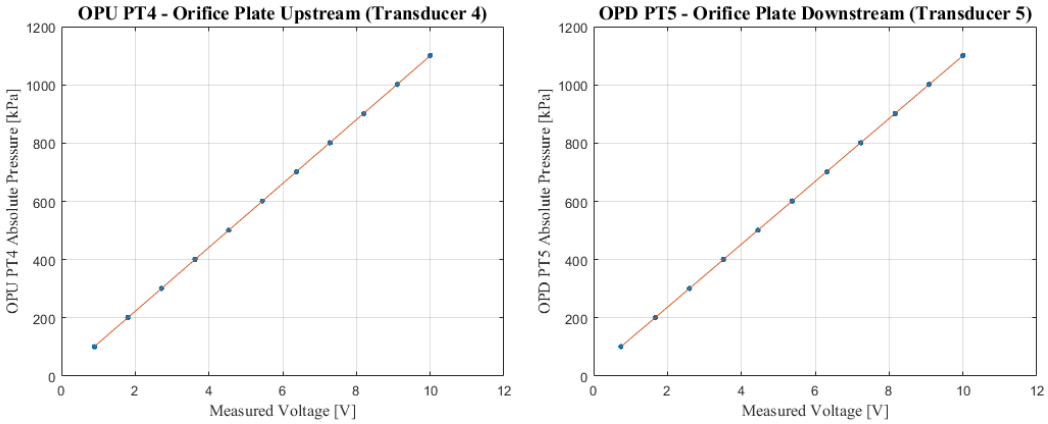

Figure A.6: Calibration curves of pressure transducers (4 and 5) on the orifice plate

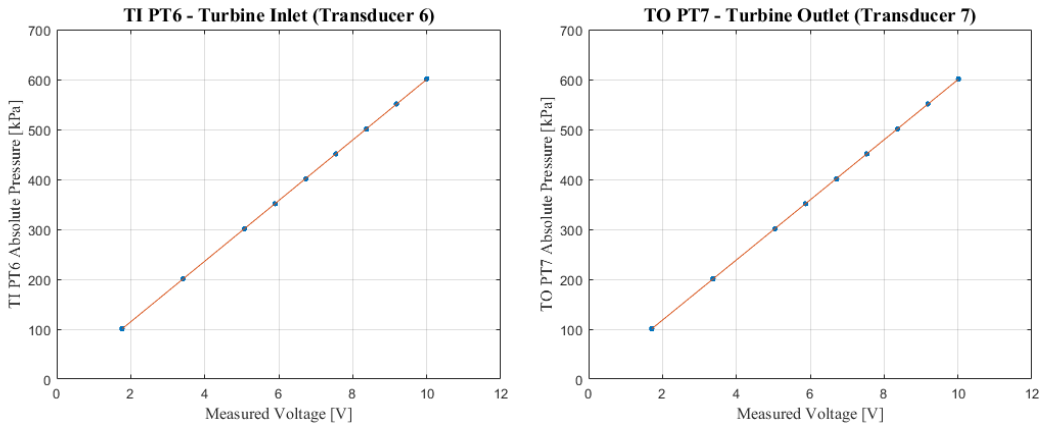

Figure A.7: Calibration curves of pressure transducers (6 and 7) on the turbine

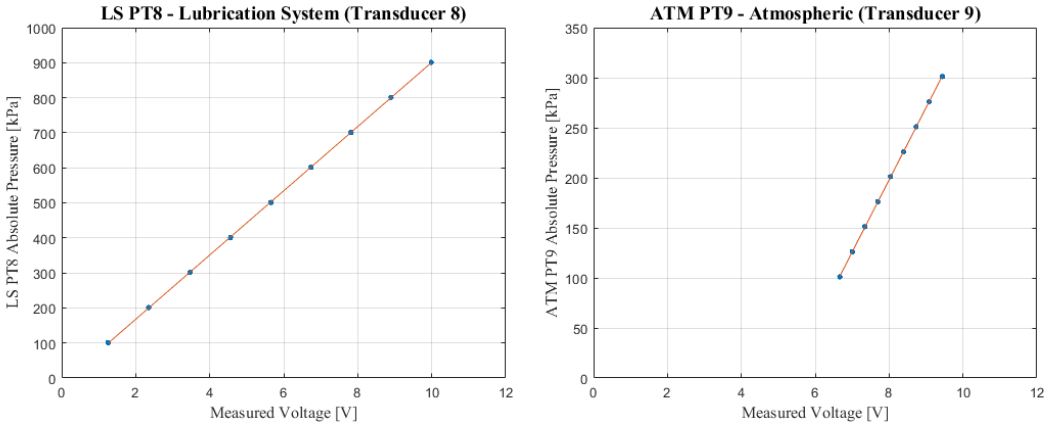

Figure A.8: Calibration curves of pressure transducers (8 and 9)

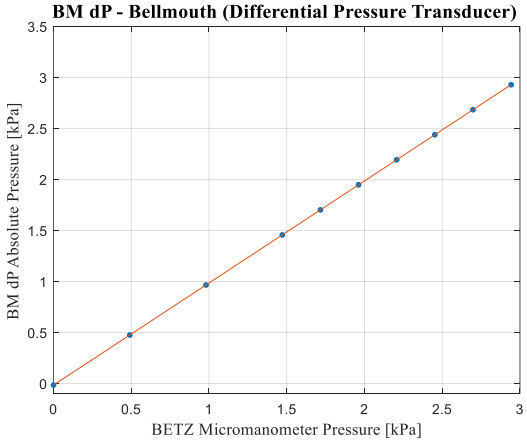

Figure A.9: Calibration curves of differential pressure transducer on bellmouth

A.3 Throttling Valve Calibration

Figure A.10 shows a curve which relates the voltage input to the percentage opening of the throttling valve represented by Equation 3.7. The curve was obtained by supplying a voltage through NI-9263 output module. The voltage signal was then converted to current signal (4-20 mA) using ACDC voltage converter which opens or closes the throttling valve. The percentage opening value displayed on the positioner was recorded along with the voltage input value for voltage values ranging between 2 to 9 V.

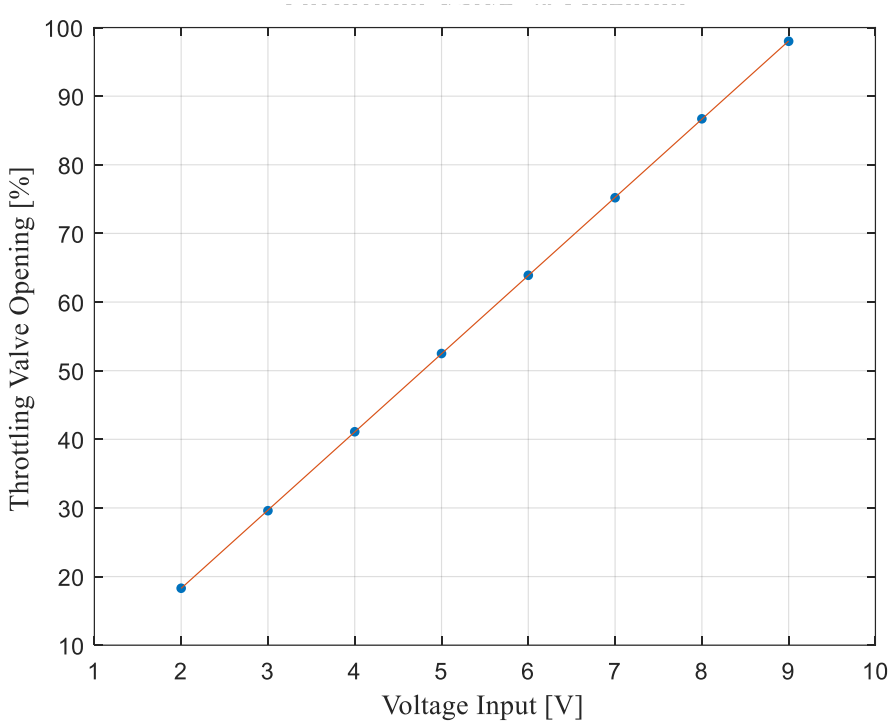

Figure A.10: Throttling valve percentage opening

B Sample Calculation

This section provides the sample calculations for the minimum pipe thickness, orifice plate design, and a single test point of the compressor.

B.1 Minimum Pipe Thickness of the Pipeline System

This section provides the calculations for the design of the pipeline system. The objective is to find the minimum pipe thickness of the pipes which has a nominal outside diameter (D) of 114.3 mm. So that the pipeline system can withstand the operating pressure of 1100 kPa. The minimum pipe thickness is calculated using Equation 3.13 which is manipulated to make thickness (t) as a subject of the formula (Equation B.1.1).

$$t = \frac{pD}{2S\,FET} \tag{B.1.1}$$

All the constants used in Equation B.1.1 were obtained from the respective tables in ASME B31.8-2003. A list of these constants along with the values and the table number is as follows:

Design pressure	p	=	159.54 psi	
Nominal outside diameter	D	=	4.50 $inch$	
Specified minimum yield strength	S	=	35 000 psi	(Table D1)
Design factor	F	=	0.80	(Table 841.114A)
Longitudinal joint factor	E	=	1	(Table 841.115A)
Temperature derating factor	T	=	0.967	(Table 841.116A)

Substituting above values in Equation B1.1,

$$t = \frac{159.54 \times 4.50}{2 \times 35000 \times 0.80 \times 1 \times 0.967}$$
$$= 0.0133\ inch$$

Therefore, the minimum thickness of the pipe needs to be approximately 0.34 mm. Similarly, the minimum thickness of the pipe with the nominal outer diameter of 88.9 mm is calculated to be 0.26 mm.

B.2 Orifice Plate Design

Following is the list of constants which were used to deign the orifice plate as well as for the computation of single test point of the compressor:

Molar mass of dry air	M	= 28.96×10^{-3} kg/mol
Universal gas constant of dry air	R	= 287 J/kg · K
Sutherland temperature for air	S	= 110.40 K
Viscosity of air at 20°C	μ	= 1.80×10^{-5} kg/s · m
Reference temperature of air	T_{ref}	= 273.15 K
Reference viscosity of air	μ_{ref}	= 1.71×10^{-5} kg/s · m
Specific heat at constant pressure	c_p	= 1005 J/kg · K
Specific heat ratio	γ	= 1.4
Dynamic correction factor	K	= 0.96
Discharge coefficient parameters	L_1, L_2	= 1, 0.47

The orifice plate design is based on the assumption of the following design parameters:

Maximum pressure supply (10 bar)	p_{supply}	= 1 MPa
Supply air total temperature (15℃)	$T_{supply,t}$	= 288.15 K
Mass flow rate	$\dot{m}$	= 0.5 kg/s
Design pressure drop	Δp	= 20 kPa
Inner dimeter of the pipe	D_i	= 102.26 mm
Internal cross-sectional area of the pipe	A_c	= 8212.993 mm^2

The air velocity upstream of the orifice plate was determined iteratively for the given design parameters. Assume the static temperature is equal to the measured supply temperature:

$$T_s = T_{supply,t} = 288.15 \text{ K} \tag{B.2.1}$$

The initial static density is determined as follows:

$$\rho_s = \frac{p_s}{RT_s} = \frac{1 \times 10^6}{(287)(288.15)} = 12.09 \text{ kg/m}^3 \tag{B.2.2}$$

The initial flow velocity is determined by:

$$V = \frac{\dot{m}}{A_c \rho_s} = \frac{0.5}{(8212.99 \times 10^{-6})(12.09)} = 5.03 \text{ m/s} \tag{B.2.3}$$

A new static temperature is then determined:

$$T_{s,new} = T_{supply,t} - \frac{V^2}{2c_p} = 288.15 - \frac{5.03^2}{2(1005)} = 288.14 \text{ K} \tag{B.2.4}$$

This new static temperature (Equation B.2.4) is used to calculate new density (Equation B.2.2) and then new velocity (Equation B.2.3). The process is repeated until a convergence is reached between the velocity values i.e. change in velocity is less than 1×10^{-6} m/s.

Total conditions upstream of the orifice plate were required to compute the design Reynolds number (Re_D). This was done by using isentropic relations:

$$
\begin{aligned}
p_t &= p_{supply}\left(\frac{T_{supply,t}}{T_s}\right)^{\frac{\gamma}{\gamma-1}} \\
&= 1\times10^{6}\left(\frac{288.1374}{288.15}\right)^{\frac{1.4}{1.4-1}} \\
&= 1\,000\,153.19\ Pa
\end{aligned}
\tag{B.2.5}
$$

$$
\begin{aligned}
\rho_t &= \rho_s\left(\frac{T_{supply,t}}{T_s}\right)^{\frac{\gamma}{\gamma-1}} \\
&= 12.09\left(\frac{288.1374}{288.15}\right)^{\frac{1.4}{1.4-1}} \\
&= 12.0939\ kg/m^3
\end{aligned}
\tag{B.2.6}
$$

Viscosity of the air was calculated using the Sutherland equation (Equation B.2.7):

$$
\begin{aligned}
\mu_t &\approx \mu_{ref}\left(\frac{T_{suply,t}}{T_{ref}}\right)^{\frac{3}{2}}\left(\frac{T_{ref}+S}{T_{supply,t}+S}\right) \\
&\approx 1.71\times10^{-5}\left(\frac{288.1374}{273.15}\right)^{\frac{3}{2}}\left(\frac{273.15+110.04}{288.1374+110.04}\right) \\
&\approx 1.789\times10^{-5} kg/s\cdot m
\end{aligned}
\tag{B.2.7}
$$

$$
\begin{aligned}
v_t &= \frac{\mu_t}{\rho_t} \\
&= \frac{1.789\times10^{-5}}{12.0939} \\
&= 1.48\times10^{-6}\ m^2/s
\end{aligned}
\tag{B.2.8}
$$

The design Reynolds number (Re_D) was then determined as follows:

$$
\begin{aligned}
Re_D &= \frac{VD}{v_t} = \frac{(5.03)(102.26\times10^{-3})}{1.47961\times10^{-6}} \\
&\approx 3.48\times10^{5}
\end{aligned}
\tag{B.2.9}
$$

The diameter ratio (β) was computed iteratively by assuming the value of $\beta = 0.5$. This was used to compute the discharge coefficient (C_d) from the correlation provided in BSI (1998). Furthemore, initial values for the velocity approach factor (E), the expansion factor (ϵ) and the flow coefficient (α) were calculated.

$$\begin{aligned} C_d &= 0.5959 + 0.0312\beta^{2.1} - 0.1840\beta^8 + 91.7061\beta^{2.5}Re_D^{-0.75} \\ &\quad + \frac{0.09L_1\beta^4}{1-\beta^4} - 0.0337\beta^3 L_2 \\ &= 0.5959 + 0.0312(0.5)^{2.1} - 0.1840(0.5)^8 \\ &\quad + 91.7061(0.5)^{2.5}(3.4794 \times 10^5)^{-0.75} \\ &\quad + \frac{0.09(1)(0.5)^4}{1-(0.5)^4} - 0.0337(0.5)^3(0.47) \\ &= 0.6041 \end{aligned} \tag{B.2.10}$$

$$\begin{aligned} E &= (1-\beta^4)^{-0.5} = (1-0.5^4)^{-0.5} \\ &= 1.0328 \end{aligned} \tag{B.2.11}$$

$$\begin{aligned} \epsilon &= 1 - (0.41 + 0.35\beta^4)\frac{\Delta p}{\gamma p_{supply}} \\ &= 1 - (0.41 + 0.35(0.5)^4)\frac{20 \times 10^3}{(1.4)(1 \times 10^6)} \\ &= 0.9938 \end{aligned} \tag{B.2.12}$$

A new value for β is then determined from:

$$\begin{aligned} \beta &= \frac{V^2\rho_s}{\sqrt{\alpha^2(2\Delta p)}} = \frac{(5.03)^2(12.09)}{\sqrt{(0.63)^2(2(20 \times 10^3))}} \\ &= 0.3757 \end{aligned} \tag{B.2.13}$$

Therefore, the final value for the diameter ratio of the orifice plate with the design mass flow rate of 0.5 kg/s is:

$$\beta = 0.376$$

B.3 Compressor Performance Calculation

A sample calculation for a single test point is provided in this section. It corresponds to the $\dot{m}$ = 0.193 kg/s at 80 000 rpm, which is the point of the highest efficiency at given speed. In order to proceed with the calculations, the averaged quantities were obtained from the experiments which are given below:

Ambient temperature	T_{amb}	= 297.46 K
Ambient pressure	p_{amb}	= 99 629.53 Pa
Bellmouth differential pressure	Δp	= 737.17 Pa
Compressor inlet total temperature	T_{t0}	= 297.46 K
Compressor outlet probe temperature	T_{p3}	= 370.34 K
Compressor inlet static pressure	p_{s0}	= 100431 Pa
Compressor outlet static pressure	p_{s3}	= 178525 Pa

Bellmouth dimensions listed as follows:

Inlet diameter	D	$\gg d$
Outlet diameter	d	= 77.3×10^{-3} m

Following are the dimensions of the pipes at the compressor outlet where the static pressure measurement was obtained:

Pipe internal diameter (Outlet)	d_3	= 40.9×10^{-3} m
Pipe internal cross-sectional area (Outlet)	$A_{c,3}$	= 1.31×10^{-3} m^2

The ambient air density is determined by:

$$\rho_{amb} = \frac{p_{amb}}{RT_{amb}} = \frac{99\,629.53}{(287)(297.46)} = 1.167\ kg/m^3 \quad \text{(B.3.1)}$$

The bellmouth velocity (V_{bm}) is calculated using Equation 4.5, where the term $\beta^4 = 0$, as well as the Reynolds number is determined:

$$V_{bm} \approx \sqrt{\left(\frac{2\Delta p}{\rho_{amb}(1 - d^4/D^4)}\right)}$$
$$\approx \sqrt{\left(\frac{2(737.17)}{(1.167)(1-0)}\right)} \tag{B.3.2}$$
$$\approx 35.544\ m/s$$

$$Re_{bm} = \frac{V_{bm}\rho_{bm}d}{\mu}$$
$$= \frac{(35.483)(1.171)(0.0773)}{1.8 \times 10^{-5}} \tag{B.3.3}$$
$$= 178\ 130$$

The discharge coefficient is determined from the bellmouth calibration curve (Equation 4.6):

$$C_d = e^{-\frac{1500}{Re_{bm}}}$$
$$= e^{-\frac{1500}{178\ 420}} \tag{B.3.4}$$
$$= 0.992$$

The mass flow can now be determined by:

$$\dot{m} = C_d E \epsilon \frac{\pi}{4} d^2 \sqrt{2\Delta p \rho_1}$$
$$= (0.992)(1)(1)\left(\frac{\pi}{4}\right)(0.0773)^2\sqrt{2(737.17)(1.167)} \tag{B.3.5}$$
$$= 0.193\ kg/s$$

where $E = 1$ and $\epsilon = 1$.

The total pressure at the inlet of the compressor is calculated using Equation 4.7.

$$p_{t0} = p_{s0} + \rho_{amb}\frac{{V_{bm}}^2}{2}$$
$$= 100\ 431 + 1.167\frac{35.544^2}{2} = 101\ 170\ Pa \tag{B.3.6}$$

The initial static temperature is approximated as the measured probe temperature in order to determine the total-to-static (t-s) pressure ratio and the total-to-total (t-t) efficiency:

$$T_{s3} = T_{p3} = 370.34\ \text{K} \tag{B.3.7}$$

Furthermore, the initial static conditions are determined at the pressure measurement station:

The specific heat at constant pressure is calculated using Equation 4.9, where the coefficients of each term are represented as a, b, c, and d.

$$\begin{aligned} c_{p,s3} &= \frac{a + bT_{s3} + cT_{s3}^2 + dT_{s3}^3}{M} \\ &= \frac{a + b(370.34) + c(370.34)^2 + d(370.34)^3}{28.96 \times 10^{-3}} \\ &= 1011.69 \frac{J}{kg} \cdot K \end{aligned} \tag{B.3.8}$$

$$\begin{aligned} \rho_3 &= \frac{p_{s3}}{RT_{s3}} \\ &= \frac{178\,525}{(287)(370.34)} \\ &= 1.68\ kg/m^3 \end{aligned} \tag{B.3.9}$$

$$\begin{aligned} \gamma_3 &= \frac{c_{p,s3}}{c_{p,s3} - R} \\ &= \frac{1011.69}{1011.69 - 287} \\ &= 1.396 \end{aligned} \tag{B.3.10}$$

The absolute gas velocity is determined, followed by the Mach number:

$$c_3 = \frac{\dot{m}}{\rho_{s3} A_3}$$
$$= \frac{0.193}{(1.68)(1.31 \times 10^{-3})} \quad \text{(B.3.11)}$$
$$= 87.73\ m/s$$

$$Ma_3 = \frac{c_3}{\sqrt{\gamma_3 T_{s3} R}}$$
$$= \frac{87.73}{\sqrt{(1.396)(370.34)(287)}} \quad \text{(B.3.12)}$$
$$= 0.228$$

The total temperature is determined by:

$$T_{t3} = T_{p3} + \frac{(1-K)c_3^2}{2c_{p,s3}}$$
$$= 370.34 + \frac{(1-0.96)(87.729)^2}{2(1011.687)} \quad \text{(B.3.13)}$$
$$= 370.49\ K$$

The new static temperature is then determined by:

$$T_{s3,new} = \frac{T_{t3}}{1 + \frac{(\gamma_3 - 1)Ma_3^2}{2}}$$
$$= \frac{370.49}{1 + \frac{(1.396-1)(0.228)^2}{2}} \quad \text{(B.3.14)}$$
$$= 366.73\ K$$

A comparison is then made between the static temperatures from Equation B.3.14 and B.3.7. If the absolute difference between the two static temperatures (ΔT_{s3}) exceed 1×10^{-6}, the static temperature from Equation B.3.14 is substituted back into B.3.8 and iterated until the convergence is reached:

$$\Delta T_{s3} = \left| T_{s3} - T_{s3,new} \right| \quad \text{(B.3.15)}$$

$$= |370.34 - 366.73|$$
$$= 3.614 \gg 1 \times 10^{-6}$$

The process is repeated again by repeating Equation B.3.7 to B.3.15 until the absolute temperature difference is less than 1×10^{-6}. The total pressure can then be determined as follows:

$$p_{t3} = p_{s3}\left(1 + \frac{(\gamma_3 - 1)Ma_3^2}{2}\right)^{\frac{\gamma_3}{\gamma_3 - 1}}$$
$$= 178\,525\left(1 + \frac{(1.396 - 1)(0.228)^2}{2}\right)^{\frac{1.396}{1.396-1}} \quad \text{(B.3.16)}$$
$$= 185\,070\ Pa$$

Using the static and total conditions the total to static (t-s) pressure ratio, total-total (t-t) efficiency is calculated:

$$\Pi_{t-s} = \frac{p_{s3}}{p_{t0}}$$
$$= \frac{178\,525}{101\,170} \quad \text{(B.3.17)}$$
$$= 1.78$$

$$\eta_{t-t} = \left[\left(\frac{p_{t3}}{p_{t0}}\right)^{\frac{(\gamma-1)}{\gamma}} - 1\right]\left[\frac{T_{t0}}{T_{t3} - T_{t0}}\right]$$
$$= \left[\left(\frac{185\,070}{101\,170}\right)^{\frac{(1.396-1)}{1.396}} - 1\right]\left[\frac{297.46}{370.49 - 297.46}\right] \quad \text{(B.3.18)}$$
$$= 0.79$$

C Data acquisition (DAQ) Programming

The data flow and manipulation of the measured quantities is briefly discussed in this section. It must be noted that the program created by Struwig (2014) was modified to make it suitable for the new test bench. Therefore, it is recommended to refer to his report for further explanation.

C.1 Temperature Measurement

The field-programmable gate array (FPGA) chip scales the raw temperature measurements which was then scaled via a real-time processor. The block diagram for temperature measurement scaling is similar to the one presented by Struwig (2014) as there was no modification made to this section of the code (Figure C.1).

It must be noted that the raw measured data was in micro-volts (μV) which was then scaled to Kelvin (K) using Equation C.1.1 to C.1.3 in Struwig (2014). These equations correspond to a specific type of thermocouple and were included as standard in the LabVIEW™ software.

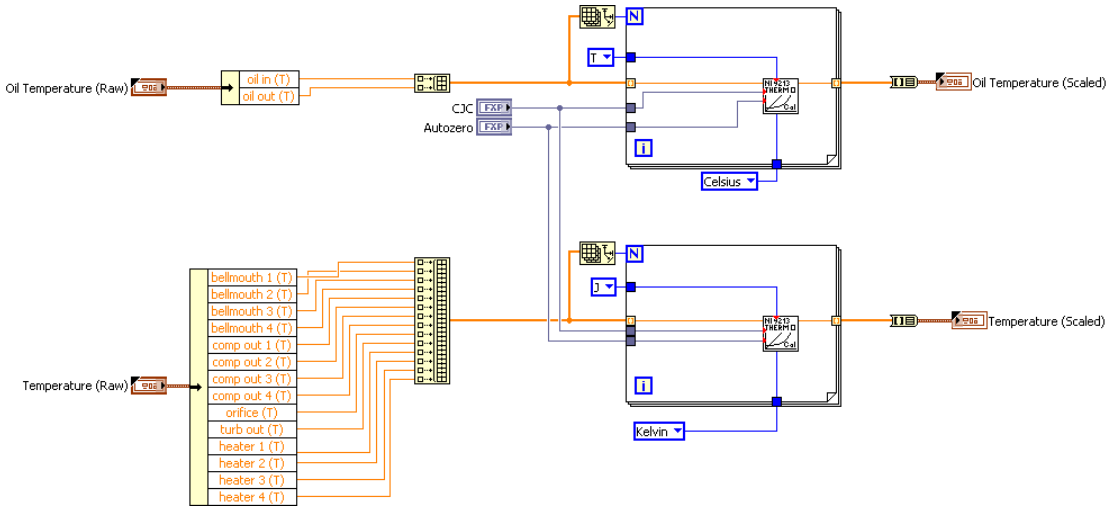

Figure C.1: Temperature measurement scaling – Block diagram (Struwig, 2014)

C.2 Pressure Measurement

For the pressure measurements the raw data in volts (V) was obtained and scaled to Kilo-Pascal (kPa) using the calibration curves of the pressure transducers (Appendix A.2). There calibration curves were implemented in LabVIEW and can be seen in Figure C.2.

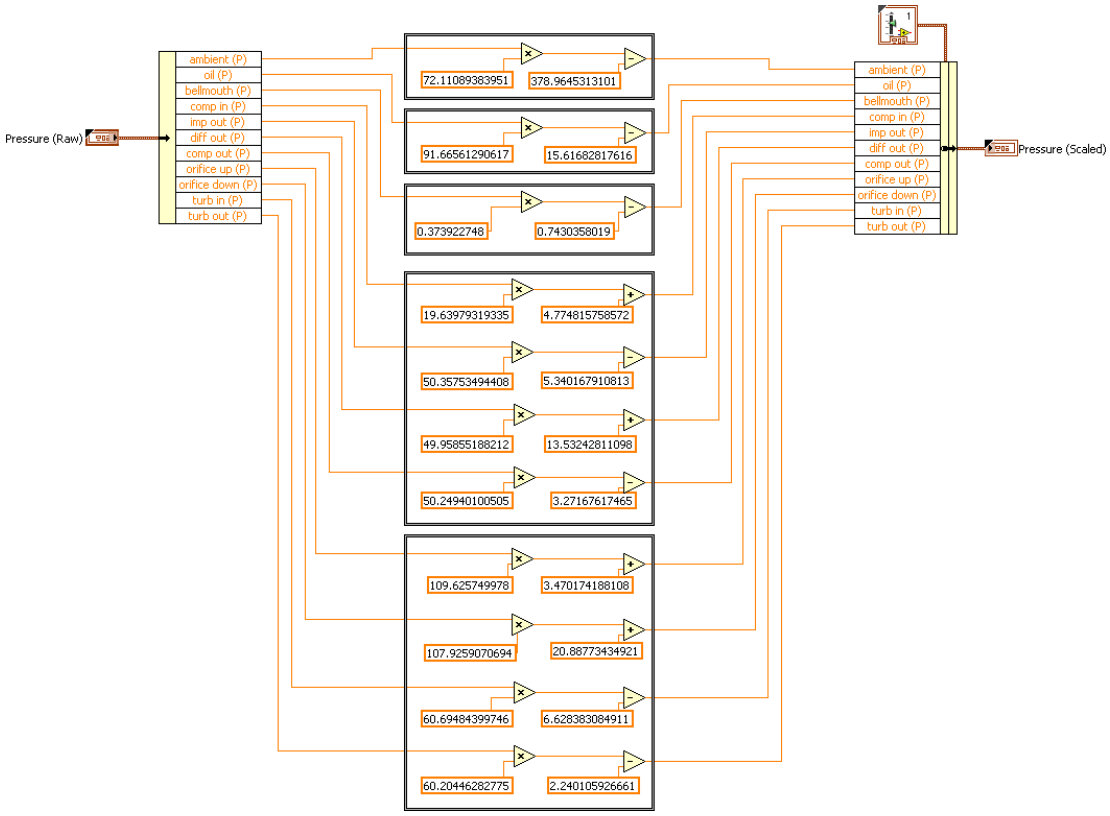

Figure C.2: Pressure measurement scaling – Block diagram

C.3 Speed Measurement

The raw measured data for speed was in volts which was scaled to revolutions per minute (rpm) using Equation 3.18. The block diagram for the scaling of speed measurement can be seen in Figure C.3.

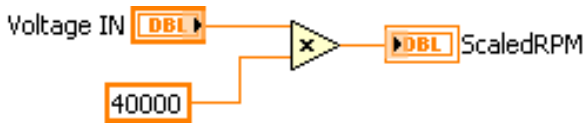

Figure C.3: Speed measurement scaling – Block diagram

C.4 Mass Flow Rate Measurement

The mass flow rate measurement procedure was slightly modified from the Struwig's (2014) procedure. This was to incorporate calibration curves for the thermocouples (Figure C.4). The scaled temperature measurements were first corrected and then used to compute the mass flow rate via an iterative process explained earlier.

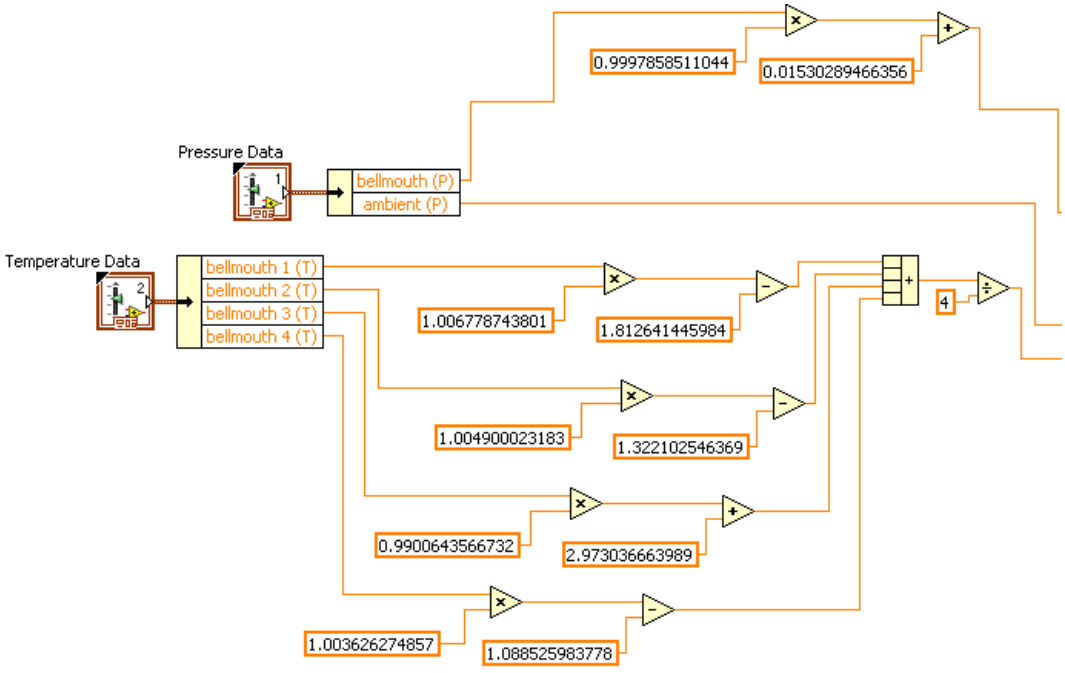

Figure C.4: Mass flow rate measurement – Block diagram

C.5 Throttling Valve Percentage Opening

The percentage opening of the throttling valve was incorporated by implementing the calibration curve (Equation 3.17) in LabVIEW™. This is shown in Figure C.5. It must be noted that the Equation 3.17 was manipulated to make voltage as a subject of the formula and then was used in the block diagram.

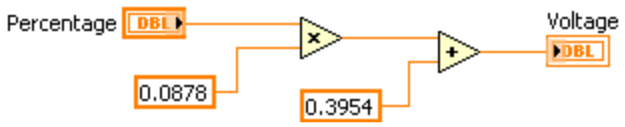

Figure C.5: Throttling valve percentage opening – Block diagram

D Operating Procedure

The commissioning process was followed by preliminary tests in order to compile an operating procedure for the test bench. This operating procedure was strictly followed every time a test run was conducted to ensure the safety of the operator and the equipment installed in the test bench.

The following set of instructions must be followed by an operator to ensure a safe operation of the centrifugal compressor test bench:

Test Briefing

1. Ensure that all the warning signs (Test in Progress, High Noise Level, etc.) are pasted on the laboratory entrance door.
2. Ensure that the ear protection is worn for the duration of the test procedure.
3. Ensure the wire and tube connectivity for all the instruments and the equipment.
4. Ensure that the control valve controller is connected to the PC.
    a. This can be done by connecting the infrared connector to the controller and plugging the USB cable to the PC.
    b. Check the connection port and ensure the connectivity – This can be done from “Administrative Tools” which device is connected at which port of the PC.
    c. Check the connectivity by switching the controller to manual mode on the controller and switching it back to automatic from the PC.
5. Switch on the data acquisition system.
    a. Ensure that all of the instruments are connected and the displayed readings are reasonable.
    b. Small fluctuations in the reading are normal.
6. Switch on the lubrication system
    a. Ensure that the bypass valve is open to bypass the turbocharger.
    b. Set the thermostat to 45 °C.

   c. Set the pressure on the lubrication system to 450 kPa. Make sure that the reading on the pressure gauge at the turbocharger is 450 kPa.
   d. Observe the oil pressure and temperature on the display.
7. Once oil temperature has stabilized to set value, close the bypass valve to allow the oil to pass through the bearing housing of the turbocharger.
8. Ensure that the throttling valve is set to 100 %.
   a. This can be done by typing 100 at the throttling valve percentage opening box on front display.
   b. Physically check if the throttling valve is fully open.
9. Ensure that the control valve is fully closed.
   a. This can be done by switching the controller to manual mode.
   b. Close the valve to 0 %
10. Open the primary valve (manually).
11. The operator should be in the control area.
12. Open the secondary valve by switching the button which is placed on the desk.
13. Gradually increase the speed to 20 000 rpm in increments of 5 000 rpm.
14. Idle the compressor at 20 000 rpm for 3 minutes.
   a. Ensure all the components are working correctly.
   b. Ensure that the measurements are reasonable and the instruments are functioning correctly.
15. Increase the speed to 40 000 rpm and idle it for 5 minutes to ensure the integrity of the test bench and heat soak of thermocouples.
16. Decrease the speed to 0 rpm to allow compressed air tank to refill.
17. After the tank is replenished, increase the speed to 20 000 rpm for 1 minute.
18. Increase the speed to 40 000 rpm for 1 minute.
19. Increase the speed to required speed and commence testing.
20. Once the speed is stable log the data to obtain first testing point.
21. Close the throttling valve to certain percentage to decrease the compressor flow rate.

a. Wait for 1 minute for the speed to stabilize and obtain second test point.
b. Repeat the Step 21 in order to obtain 5 to 6 test points per speed.

22. Decrease the speed once 5 to 6 points are taken or if the compressed air tank has reached 600 to 500 kPa
23. Allow the compressed air tank to replenish and continue with the other testing speeds.

Test Debriefing

1. Fully open the throttling valve.
2. Decrease the speed to 20 000 and let the compressor idle for 2-3 minutes.
3. Shut the secondary valve by switching off the switch on the operator's desk.
4. Close the primary valve manually.
5. Allow the remainder of air to leave the system by opening the secondary valve.
6. Once all the air has left the system close the control valve fully and close the secondary valve.
7. Open the bypass valve to bypass the compressor.
8. Turn the thermostat back to 0 °C.
9. Switch off the lubrication system.
10. Ensure that the data samples are correct and reasonable.
11. Switch off the DAQ system.
12. Check the test bench and observe the condition.

NOTE:

- It is recommended to conduct preliminary tests to get the throttling valve percentage opening which corresponds to the desired test points.
- Always increase the speed with the increments of 5 000 rpm to avoid overshoot.

E Test Facility CAD Model

Figure E.1 to Figure E.4 presents the computer-aided design (CAD) model of the compressor test bench. Figure E.1 shows the top and side view and Figure E.2 shows the isomertric view of the test bench. The test bench along with the main supply connection can be seen in Figure E.4.

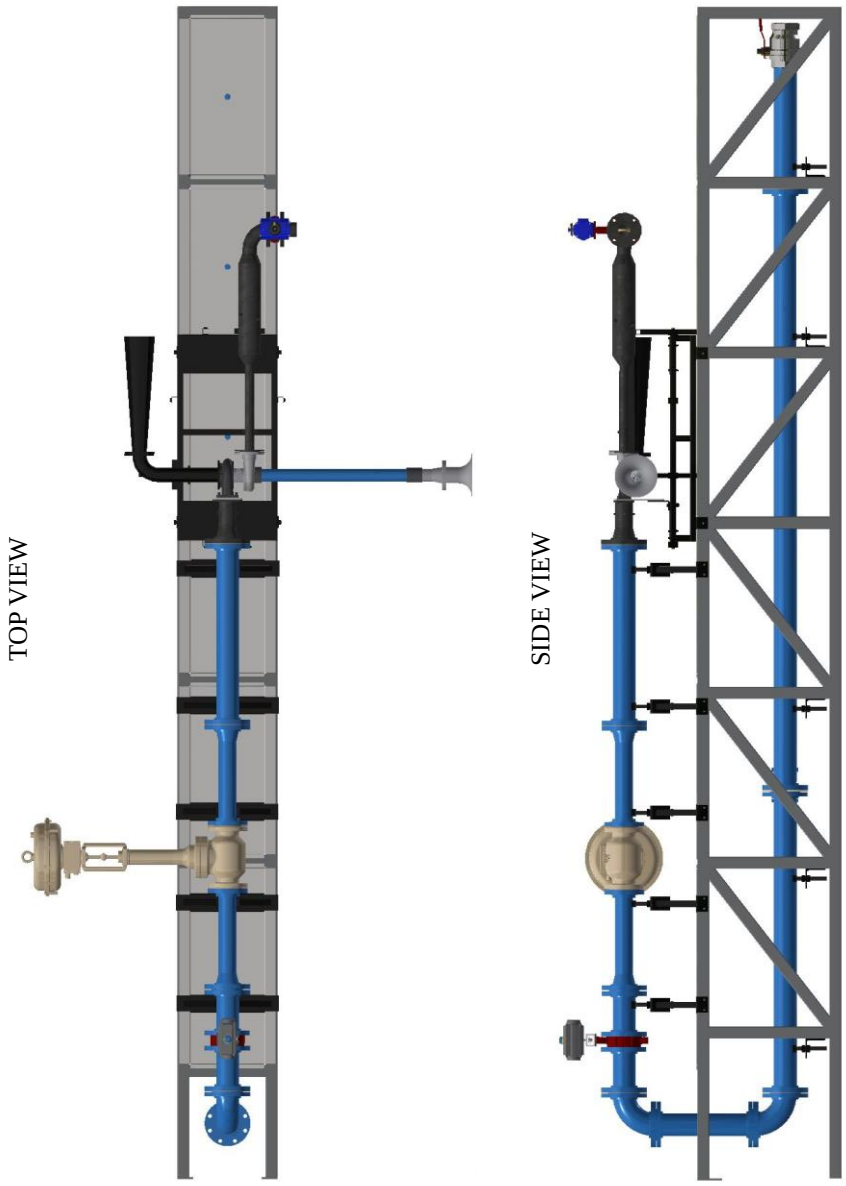

Figure E.1: Top and side view of the test bench

Figure E.2: Isometric view of the test bench

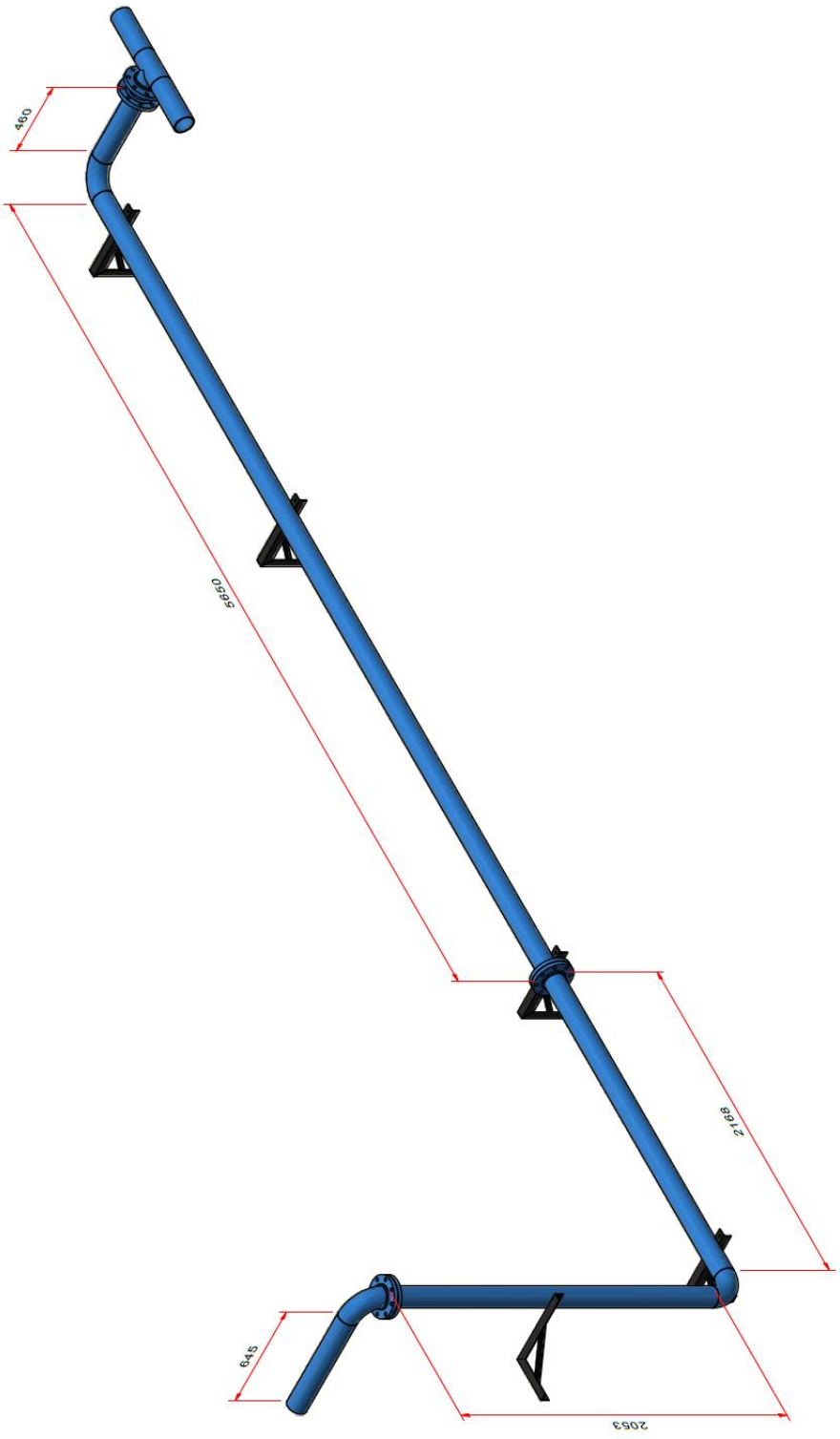

Figure E.3: Main supply connection

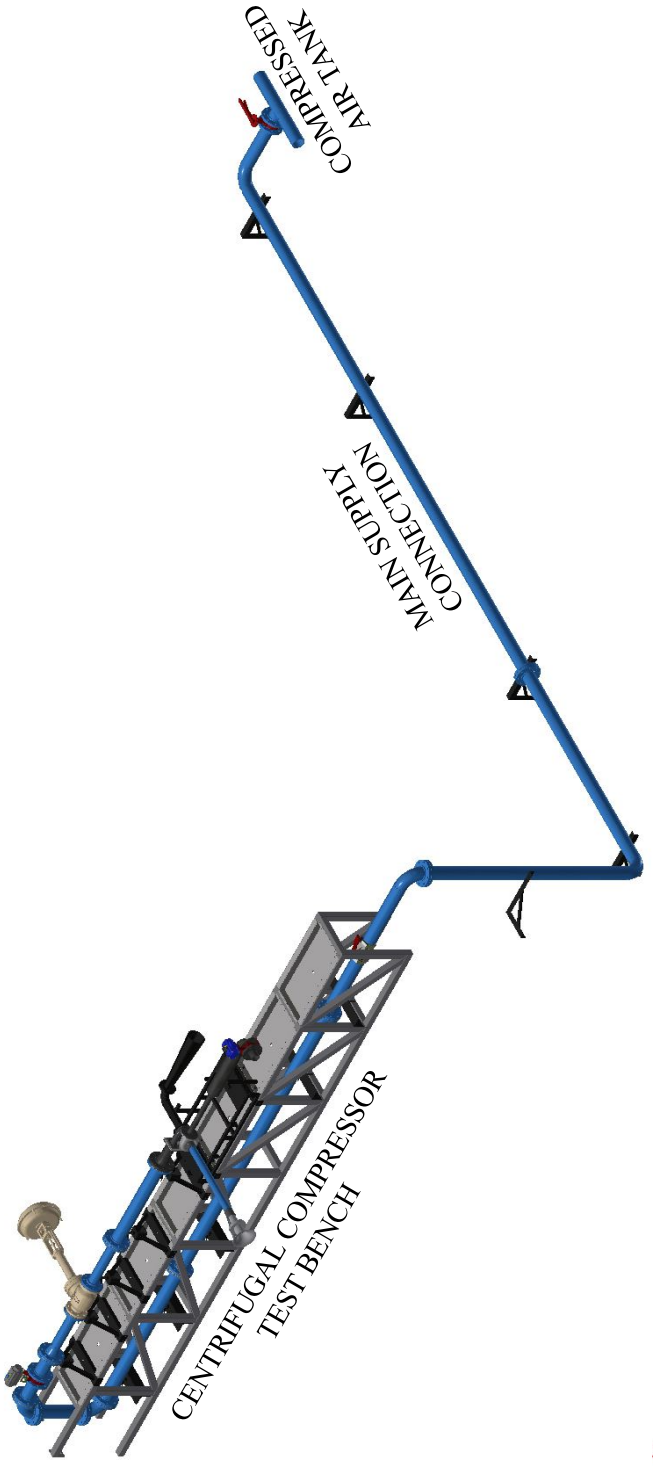

Figure E.4: Compressor test bench and main supply connection

F Pipeline Design Procedure

The design of the pipeline adheres to SANS 347:2012 as mentioned in Section 3.2. A pressure vessel is defined as any enclosure which contains fluid at a pressure of 50 kPa or greater. The compressed air for the test bench was supplied at a pressure of 1 MPa, therefore the pipeline system transferring the compressed air was considered to be a pressure vessel.

According to Table 1 in SANS 347:2012 (Figure F.1), pipe sections that conveys a non-dangerous gas should be evaluated according to Figure 7 of SANS 347:2012 (Figure F.2). Examining Figure F.2, in order to stay in the standard engineering practice (SEP) category at the design pressure of 1000 kPa, the maximum diameter should be 100 mm. It must be noted that the design point lying on the category separator "red line" represents the category below the line. For this reason, a nominal diameter of 100 mm was chosen for the pipeline system.

1	2	3	4	5	6	7	8	9	10	11	12	13	14
Equipment type	**Pressure vessels**				**Steam generator**	**Piping**				**Transportable pressure equipment**			
State of contents	**Gas**		**Liquid[b]**			**Gas**		**Liquid[b]**		**Gas**		**Liquid[b]**	
Fluid group[c]	1	2	1	2		1	2	1	2	1	2	1	2
Refer to figure	1	2	3	4	5	6	7	8	9	10	2[a]	10	4[a]
NOTE For two-phase flow, the equipment should be categorized to the higher risk.													
[a] For categorization of transportable pressure equipment figures 2 or 7 and 4 or 9 may be used as appropriate. Pressure accessories for equipment associated with figure 10 shall also be assessed with figure 10. Valves having an internal volume less than 0,1 L shall be deemed to be equal to 0,1 L for the purpose of defining the hazard category in relation to figure 10.													
[b] No pockets of gas may form above the liquid in the equipment, including steam.													
[c] Fluid group 1 = dangerous; fluid group 2 = not dangerous (see 4.3.1).													

Figure F.1: Product classifications and relevant figures (SANS 347:2012)

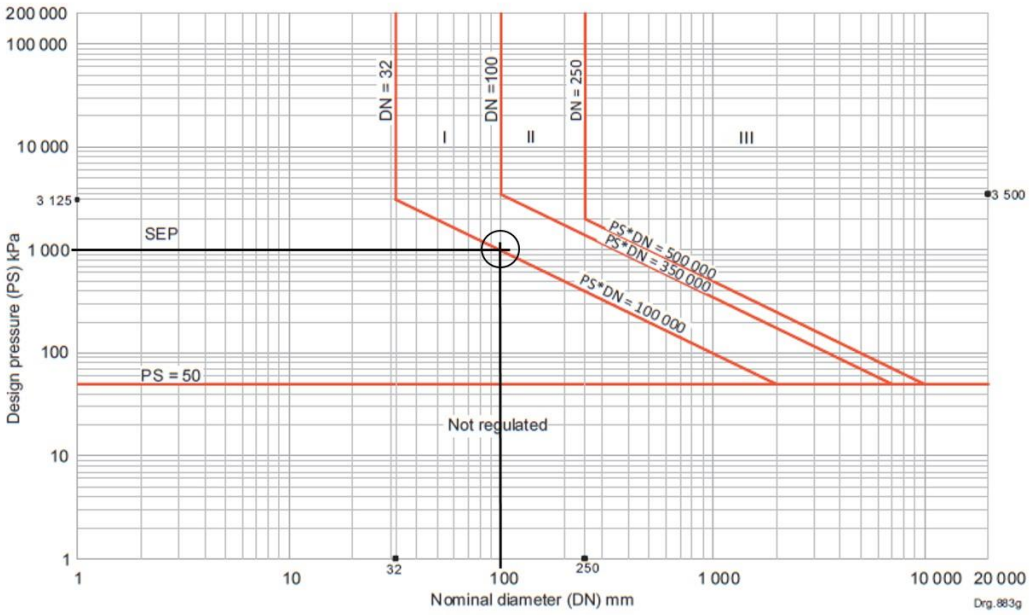

Figure F.2: Graph for piping of non-dangerous gas (SANS 347:2012)

List of References

Antônio, M., Do Nascimento, R., De, L., Rodrigues, O., Cruz, E., Santos, D., Eber, E., Gomes, B., et al. 2014. *Micro Gas Turbine Engine: A Review*. Progress in gas turbine performance, pp. 107-141.

ASME. 1997. *ASME PTC 10 - 1997: Performance Test Code on Compressors and Exhausters*. New York.

Aungier, R.H. 2000. *Centrifugal Compressors : A Strategy for Aerodynamic Design and Analysis*. New York, N.Y.: American Society of Mechanical Engineers (ASME) Press.

Aus der Wiesche, S. 2012. A mobile test rig for micro gas turbines based on a thermal power measurement approach. *Journal of Engineering for Gas Turbines and Power*. 134(11):112301.

Benedict, R.P. 1977. *Fundamentals of temperature, pressure, and flow measurements*. 2nd ed. ed. New York: Wiley.

Benini, E. & Giacometti, S. 2007. Design, manufacturing and operation of a small turbojet-engine for research purposes. *Applied Energy*. 84(11):1102–1116.

Bianchini, A., Carnevale, E.A., Biliotti, D., Altamore, M., Cangemi, E., Giachi, M., Rubino, D.T., Tapinassi, L., et al. 2015. Development of a research test rig for advanced analyses in centrifugal compressors. *Energy Procedia*. 82:230–236.

Brun, K. & Nored, M.G. 2006. *Guideline for Field Testing of Gas Turbine and Centrifugal Compressor Performance*.

Çengel, Y.A. & Cimbala, J.M. 2008. *Essentials of fluid mechanics : fundamentals and applications*. (McGraw-Hill series in mechanical engineering). Boston: McGraw-Hill Higher Education.

Chernov, M. 2013. Design of a Test Stand for a Centrifugal Compressor. Lappeenranta:

Lappeenranta University of Technology.

Diener, O.H.F. 2016. Development of a mixed-flow compressor impeller for micro gas turbine application. Master of Engineering thesis, Dept. of Mechanical Engineering, University of Stellenbosch, Stellenbosch.

Dixon, S.L. & Hall, C. 2014. *Fluid mechanics and thermodynamics of turbomachinery*. 7th ed. Butterworth-Heinemann.

Esper, A., Lenzen, C. & Wirsum, M. 2017. Commissioning of a Test Stand for Turbocharger Investigations at Constant Turbine Inlet Temperatures. In *Proceedings of the 17th International Symposium on Transport Phenomena and Dynamics of Rotating Machinery (ISROMAC-17)*.

Figliola, R.S. (Richard S.. & Beasley, D.E. (Donald E.. 2015. *Theory and design for mechanical measurements*. 6th ed., I ed. Hoboken, NJ: John Wiley.

Flownex-FLM. 2018. *Flownex Simulation Software version 8.9.1.3598 - Flownex Library Manual*.

Flownex-FTM. 2018. Flownex Simulation Software version 8.9.1.3598 - Flownex Theory Manual.

Flownex-GUM. 2018. *Flownex Simulation Software version 8.9.1.3598 - General User Manual*.

Galindo, J., Serrano, J.R., Guardiola, C. & Cervelló, C. 2006. Surge limit definition in a specific test bench for the characterization of automotive turbochargers. *Experimental Thermal and Fluid Science*. 30(5):449–462.

Garrett. 2019. *Compressor Map*. [Online], Available: https://www.garrettmotion.com/racing-and-performance/performance-catalog/turbo/g-series-g25-550/.

Hagelstein, D., Hillewaert, K., van den Braembussche, R.A., Engeda, A., Keiper, R. &

Rautenberg, M. 2000. Experimental and numerical investigation of the flow in a centrifugal compressor volute. *ASME*. 122(1):22–31.

Jain, S., Roy, S., Aggarwal, A., Gupta, D., Kumar, V. & Kumar, N. 2015. Study on the Parameters Influencing Efficiency of Micro-gas Turbines—A Review. In Vol. 28 *Proceedings of the ASME 2015 Power Conference, San Diego, CA, USA*. V001T09A006.

Japikse, D. & Baines, N. 1994. *Introduction to turbomachinery*. NREC

Kock, M.P. 2017. Design of a cross-over diffuser for a mixed-flow compressor impeller. Master of Engineering Thesis, Dept. of Mechanical Engineering, University of Stellenbosch, Stellenbosch.

Krige, D.S. 2013. Performance evaluation of a micro gas turbine centrifugal compressor diffuser. Master of Engineering Thesis, Dept. of Mechanical Engineering, University of Stellenbosch, Stellenbosch.

Lim, K.T., Yoon, S.Y., Goyne, C.P., Lin, Z. & Allaire, P.E. 2011. Design and characterization of a centrifugal compressor surge test rig. *International Journal of Rotating Machinery*. 2011.

Micro-Epsilon. 2014. [Online], Available: https://www.micro-epsilon.com/download/manuals/man--turboSPEED-DZ140--en.pdf.

Micro-Epsilon. 2016. [Online], Available: https://www.micro-epsilon.com/press/publication/pub-en--2016-03--Speed-measurement.pdf.

NI. 2003. [Online], Available: https://www.ni.com/pdf/manuals/320999e.pdf.

NI. 2009. [Online], Available: http://www.ni.com/pdf/manuals/372499b.pdf.

Olivero, M. 2012. Evolution of a centrifugal compressor: From turbocharger to micro gas turbine applications. Thesis, Delft University of Technology, Delft

Pilavachi, P.A. 2002. Mini-and micro-gas turbines for combined heat and power. *Applied thermal engineering*. 22(18):2003–2014.

Saravanamuttoo, H.I.H., Rogers, G.F.C., Cohen, H., Straznicky, P.V. & Nix, A.C. 2017. *Gas turbine theory*. 7th ed. Pearson Education.

Simon, T.W. & Jiang, N. 2003. Micro-or small-gas turbines. In *Proceedings of the International Gas Turbine Congress (IGTC'03), Tokyo, Japan, November*. 2–7.

Struwig, D.J. 2014. The development and verification of a centrifugal compressor test bench. Master of Engineering thesis, Dept. of Mechanical Engineering, University of Stellenbosch, Stellenbosch.

Swanepoel, P.C. 2018. The Experimental evaluation of a mixed-flow compressor impeller and cross-over diffuser. Master of Engineering thesis, Dept. of Mechanical Engineering, University of Stellenbosch, Stellenbosch.

Van den Braembussche, R.A. 2005. Micro Gas Turbines—A Short Survey of Design Problems. *Micro Gas Turbines*. 1.

Van der Merwe, B.B. 2012. Design of a centrifugal compressor impeller for micro gas turbine application. Master of Engineering Thesis, Dept. of Mechanical Engineering, University of Stellenbosch, Stellenbosch.

Venson, G.G., Barros, J. & Mautone, E. 2008. Turbocharger performance maps building using a hot gas test stand. In *ASME Turbo Expo 2008: Power for Land, Sea, and Air*. 777–785.

Whitfield, A. & Baines, N.C. 1990. *Design of radial turbomachines*. Harlow, Essex: Longman Scientific and Technical.